THE DEVELOPMENT OF MICROMANIPULATOR SYSTEMS UTILIZING LIQUID

CRYSTALS

A Thesis

by

Jose Eduardo MEJIA

A dissertation submitted to the
Engineering Course, Department of Engineering,
Graduate School of Engineering,
Kochi University of Technology,
Kochi, Japan
For the degree of

DOCTOR OF PHILOSOPHY

Chair of Committee,   Prof. Tomohiro Tsuji
Co-Chairs of Committee,   Prof. Shigeomi Chono
                           Prof. Kazuhiro Kusukawa
Committee Members,   Associate Prof. Sadao Momota
                           Associate Prof. Yasunori Matsumoto

March 2021

Major Subject: Mechanical Engineering

ABSTRACT

In recent years, with the miniaturization of mechanical devices and objects, micromanipulators capable of high-precise control of micro to nanoscale objects have been required for the applicability of biomedical applications and MEMS. In respond to this demand, research on the development of various micromanipulator and microactuator systems have actively been conducted. Focusing on the phase interface existing at the boundary between the isotropic and liquid crystal phases, West *et al.* proposed a micromanipulator system that takes advantage of the phase interface and physical characteristics of a nematic liquid crystalline material. This micromanipulator can create a phase interface between the nematic liquid crystal and isotropic phases through temperature distribution, in which the phase interface of the nematic liquid crystals is capable of capturing and dragging microscale particles from one place to another.

When the particles are on the phase interface, they are subjected to a force whose direction is perpendicular to the phase interface and toward the isotropic phase region. Then, the interfacial force arises from the disturbance of the molecular orientational field inside the nematic liquid crystal phase, and the nematic phase region acts to exclude the microscale objects into the isotropic phase region. That is, it is possible to develop a micromanipulator system capable of controlling the position of objects by utilizing the interfacial force generated at the phase interface as a driving source in thermotropic liquid crystals. Therefore, this micromanipulator is a mechanical device that can be carried out as thermal and kinetic energy through the phase change in thermotropic liquid crystals. Previously, Tsuji and Chono proposed a manipulator system to measure the nematic-isotropic phase interfacial force of a 4-cyano-4'-pentylbiphenly liquid crystal (where the phase interface of a nematic liquid crystal drags a polystyrene particle with diameter of 30μm and density of 1.19 g/cm^3), and they found that the force is about 1.4nN.

To further explain, thermotropic liquid crystals are the only material that possess two distinctive fluid phases, where the spatial coexistence of two fluid phases (liquid crystal and isotropic phases) depends on the temperature distribution. It is noted that both the liquid crystal and isotropic phases

ii

are capable of infinite deformation, and the volume change and heat transition associated with the phase change is relatively unchanged. From the physics perspective, the nematic liquid crystals exhibit a high degree of long-range orientational order of molecules in the molecular orientation field, such that the rod-like (or disk-like) molecules have orientational order, but no translational order. However, in the isotropic phase of thermotropic liquid crystals (i.e. nematic liquid crystals), molecules in the molecular configuration lacks both orientational and translational order. In other words, the order of the molecular configuration differs between the nematic and isotropic phases, where the molecules are orientationally ordered only in the nematic phase. On the other hand, the molecular configuration of smectic liquid crystals exhibit the layer structure (i.e., possess translational order) in addition to the orientational order, and the deviation of the orientational order and the layered structure from their equilibrium state may cause the greater phase interfacial force than that for the nematic liquid crystal materials.

In the first part of this work, we have chosen three distinctive thermotropic liquid crystal materials, which are the 5CB 4-cyano-4'-pentylbiphenyl, 8CB 4-cyano-4'-octylbiphenyl and 12CB 4-cyano-4'-dodecybiphenyl liquid crystals. The 5CB liquid crystal provides the phase interface between the nematic and isotropic phases at $T = 35.2\,^\circ$C. The 8CB liquid crystal possesses phases of nematic and isotropic phases, and nematic and smectic phases. The 8CB liquid crystal provides the phase interface between the nematic and isotropic phases at $T = 40.5\,^\circ$C and the phase interface between the nematic and smectic phases at $T = 33.5\,^\circ$C. Lastly, the 12CB liquid crystal, having a higher layered structure of molecules in the molecular orientation field, provides a phase interface between the smectic and isotropic phases at $T = 58.5\,^\circ$C. The liquid crystal materials are individually enclosed between two rectangular glass plates treated with a homeotropic alignment treatment. When a temperature distribution is applied through the ends of the liquid crystal cell, two phases appears in which are separated by a phase interface. Therefore, the stable phase interfaces are created by controlling the temperature distribution of the encapsulated liquid crystal material, and the interfacial force is evaluated by tracking and trapping microscale particles, which fall from a higher temperature phase into a lower temperature phase between the liquid crystal

and isotropic phase interface. We have found that the 12CB liquid crystal provides the highest interfacial force when trapping a tungsten carbide particle of density of 15.63 g/cm^3 and diameter of 100μm. This interfacial force was estimated to be 76nN, which is more than 13 times stronger than that of the nematic-isotropic phase interfacial forces of 5CB and 8CB. From these results, the application of a greater interfacial force can be achieved by utilizing the phase interface in smectic liquid crystals for better micromanipulator systems. In addition, it is reported that the liquid crystal interfacial forces depend on the size of a spherical particle. A theoretical discussion on the stress acting on the surfaces of spherical particles is considered for generalizing our results. Lastly, the capturing of spherical particles utilizing the phase interfacial forces of the 6CB, 7CB, 9CB and 11CB is attempted, respectively.

Secondly, another liquid crystal mechanical device has been proposed by utilizing the elasticity of the molecular orientation field in nematic liquid crystals. In nematic liquid crystals, when there is a spatial distortion in the director field of the molecules, the local energy density can be represented by the Frank elastic energy density. Some of the factors to create a distorted director field may consist of orientational anchoring at the solid boundary of a container, electric or magnetic fields, and flow. By using the energy when the molecular orientation field of a nematic liquid crystal filled between two small circular glass plates is distorted by the anchoring condition, the rotation of an upper glass plate is achieved. Our experimental results confirm that an upper glass plates rotates 90° counterclockwise with the relaxation of the director field, so the development of unique mechanical elements can be expected for future liquid crystal applications. A theoretical approach was attempted through the use of the Frank's energy theory and Leslie-Ericksen elasticity theory to quantify a physical description of the anchoring condition between the lower and upper circular glass plates.

NOMENCLATURE

K_1	Frank elastic constant: splay
K_2	Frank elastic constant: twist
K_3	Frank elastic constant: bend
n	Director
Θ	Angle of the rotational upper glass plate
ω	Angular velocity
R	Radius
H	Gap between glass plates
A	Rate of strain tensor
α	Viscosities
η	Miesowicz coefficients
I	Inertia
N	Nematic
Sm	Smectic
I	Isotropic
F_i	Phase interfacial force
F_g	Gravity
F_b	Buoyancy
F_d	Drag force
m	Mass of particle
v_p	Velocity of the particle
ρ_p	Density of the particle

ρ	Density of the liquid crystal material
dv_p/dt	Acceleration of the particle
τ	Elastic stress of the liquid crystal
P	Stress acting on the particle

TABLE OF CONTENTS

LIST OF FIGURES

xiii

LIST OF TABLES

1. INTRODUCTION

1.1 Background

In recent years, the miniaturization of mechanical systems applicable for MEMS has led to the demand for micromanipulators capable of high-precise control of micro to nanoscale objects, such as the manipulation of biological cells [2, 3, 4] and micro-beads [5, 6]. A micromanipulator is defined as a mechanical system capable of transporting small objects from one location to another under a microscope, and it is indispensable for observing and handling them without the use of a microscopic observation instrument. However, in conventional micromanipulator systems, its mainstream is to utilize a needle-like metal probe at the tip of a robotic arm to manipulate a microscopic object [7], which may damage the object during the manipulation process. Besides, this micromanipulator system can become enlarged in size and complicated since a high-precision control mechanism is required. For attempt of this issue, it has been proposed in the past that the use of a moving nematic-isotropic phase interface allows the soft manipulation of microscale particles [8, 9].

It is known that there is an interfacial force at the interface of two different phases, such as solid-liquid and liquid-air. The thermotropic liquid crystals are the only materials that can create a liquid-liquid phase interface, in which an interface is formed between the liquid crystal and isotropic phase. Furthermore, thermotropic liquid crystals are classified into nematic and smectic liquid crystals depending on the orientational and translational order of the rod-like molecules [10, 11]. The nematic liquid crystals have molecular orientational order but no translational order, while the smectic liquid crystals have both alignment order and one-dimensional translational order. However, in the case of the isotropic phase, there is neither orientational nor translational order. The spatial coexistence of the liquid crystal phase and isotropic phase depends on the temperature distribution. Figure 1.1 shows the chemical structures of liquid crystalline materials and their phase transition temperatures.

1

4'-n-Pentyl-4-cyanobiphenyl
n —— C_5H_{11}

CN

solid $\xleftrightarrow{24.0\ ^\circ C}$ nematic $\xleftrightarrow{35.2\ ^\circ C}$ isotropic

4'-n-Octyl-4-cyanobiphenyl
n —— C_8H_{17}

CN

solid $\xleftrightarrow{21.5\ ^\circ C}$ smectic A $\xleftrightarrow{34\ ^\circ C}$ nematic $\xleftrightarrow{40.5\ ^\circ C}$ isotropic

4'-n-dodecyl-4-cyanobiphenyl
n —— $C_{12}H_{25}$

CN

solid $\xleftrightarrow{48\ ^\circ C}$ smectic $\xleftrightarrow{58.5\ ^\circ C}$ isotropic
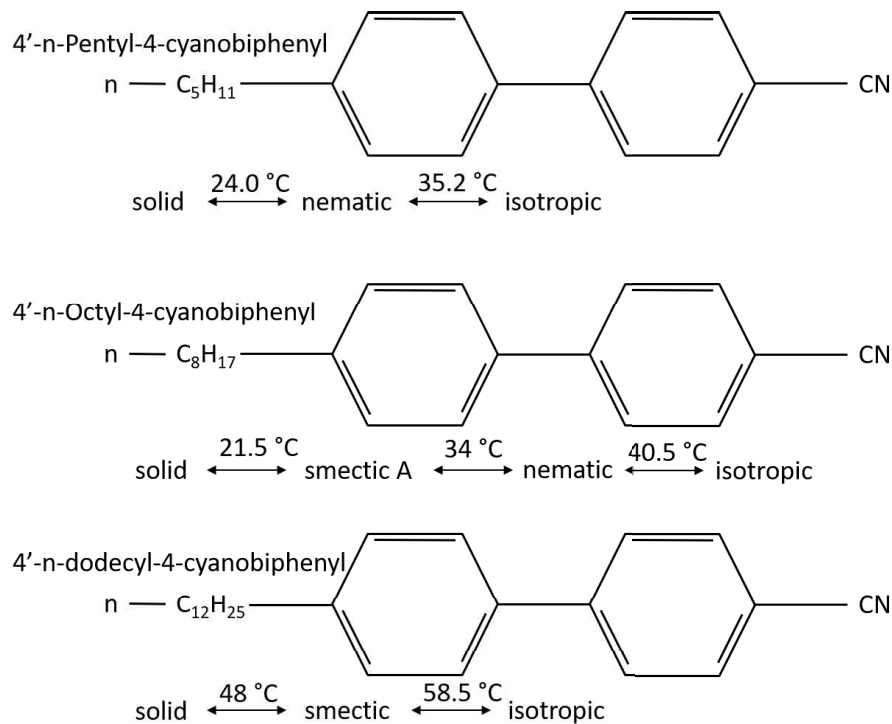
Figure 1.1: Schematics of the thermotropic liquid crystal compounds with respect to the phase transition temperature.

An interfacial force is generated at the liquid crystal-isotropic phase interface, and can softly actuate or manipulate the objects within an encapsulated liquid crystal cell. Figure 1.2 represents the future image of the liquid crystalline micromanipulator system. The liquid crystalline material is encapsulated between two glass plates, and high resistance electrodes are used to heat the material. By controlling the temperature of the liquid crystalline material, a phase interface is created and displaced to actuate objects. This actuator device can be miniaturized and be used for transferring and handling microscale objects, such as micro-beads or biological cells.

Recently, Kamei *et al.* [12] attempted to utilize the interfacial force between the nematic liquid crystal and isotropic phases to trap and manipulate a microscale object (spherical polystyrene particles of diameter 30μm and density of 1.19 g/cm^3). Their experimental setup and experimental results are shown in Figure 1.3. When the particle makes contact at the phase interface, the nematic molecular orientation field is disturbed; thus, the energy of the molecular orientation field

2

(a)　(b)　(c)
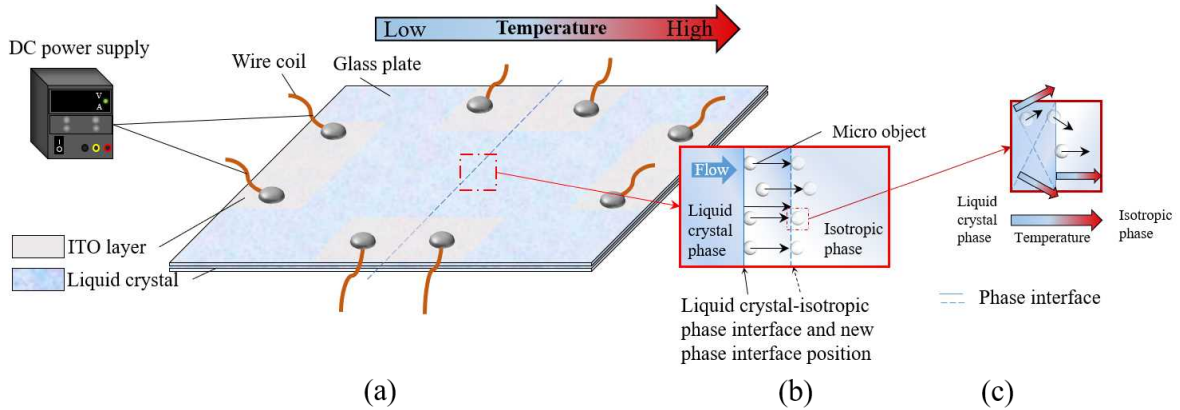
Figure 1.2: A possible case for creating a temperature distribution is by supplying electric currents to the ITO layer that will partly heat the liquid crystal material to generate a phase interface between the liquid crystal-isotropic phases. The schematic shows (a) a proposed actuator device suitable for MEMS that can be miniaturized, (b) can drive objects by the liquid crystal-isotropic phase interface when controlling the temperature distribution, (c) and can change the driving direction of the microscale object.

(a)　(b)　(c)
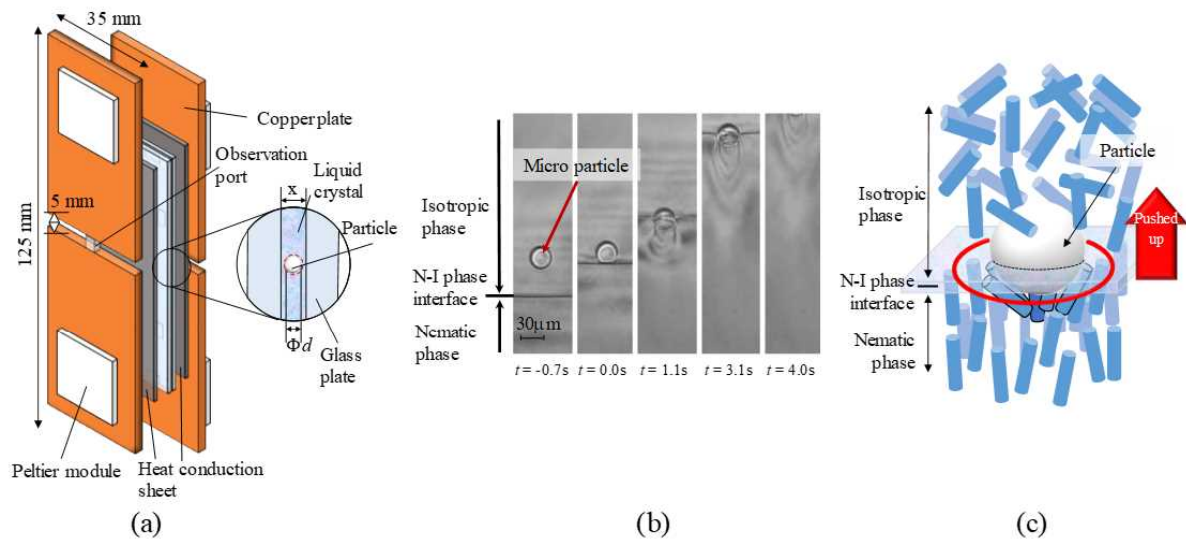
Figure 1.3: (a) The overall schematic diagram of the micromanipulator system. (b) A sequence of microscopic images of the moving nematic-isotropic phase interface in a time interval t; the nematic-isotropic phase interfacial force to drive a polystyrene particle has been estimated to be 1.4nN. (c) When the particle invades the nematic region, the molecular alignment field of the liquid crystal is disturbed (thus, it increases the molecular orientation field energy,) and creates a force to push the particle into the isotropic phase.

3

increases, creates a force and pushes the particle up to the isotropic phase. Therefore, for the motivation of this research is to develop a liquid crystal micromanipulator, which can softly move objects at any specific direction. For the application of the micromanipulator, it is essential to measure the phase interfacial forces of various thermotropic liquid crystal phases. If this device is realized, it will be possible to move biological cells freely in pathological examinations without damaging them, which is expected to lead to more accurate diagnosis in the biomedical field.

1.2 Objectives

The interfacial force between the nematic and isotropic phases is just 1.4nN, and it is not strong enough for lab-on-a-chip devices or micromanipulators. We propose the use of the smectic liquid crystal, which has a higher alignment order of molecules than that for the nematic liquid crystal and may generate a stronger interfacial force. Therefore, the objective of this research is to measure the interfacial forces of the cyanobiphenyl liquid crystalline materials. The phase interfacial force of a 5CB, 8CB and 12CB has been evaluated, respectively. The capturing of a polystyrene particle utilizing the nematic-isotropic phase interfaces of a 6CB, 7CB, 9CB has been attempted. In addition, the capturing of a tungsten carbide particle utilizing the smectic-isotropic phase interface of the 11CB liquid crystal is attempted. It is found that the force of the smectic-isotropic phase interface is much stronger than that of the other phase interfaces.

1.3 Thesis organization

The thesis will be organized as follows. In chapter 2, a background of current microactuator and micromanipulator devices and the properties of thermotropic liquid crystalline materials will be discussed. We will describe the interaction between the rod-like molecules in liquid crystals, the short-range order (microscopic) and long-range order (macroscopic) of the molecular orientation field. The particle driven mechanism will be described from the Frank elastic energy density. In chapter 3, we will focus on the interfacial force between the liquid crystal and isotropic phases of three distinctive thermotropic liquid crystalline materials. The experimental methods and results will be discussed. A brief discussion on the stresses acting on the surface of a particle will be

4

presented to generalize our results. In chapter 4, the elasticity of the molecular orientation field of a nematic liquid crystal will be discussed. Lastly, in chapter 5 and chapter 6, conclusions and future work will be presented.

2. BACKGROUND

2.1   Introduction to micromanipulators

The manufacturing of micromanipulators capable of precise manipulation of microscale objects has been revolutionized in the past decades. The purpose of a micromanipulator is to miniaturize the instrument so it can be utilized in a laboratory environment. An example of a micromanipulator is an electrostatic microelectromechanical system gripper [13]. The scale of the microgripper ranges closely to the scale of microscopic objects. First, spherical particles are suspended in a fluid, and the spherical particles are aligned through an ultrasonic field. Then, the microgripper is inserted inside the fluid and a microsphere particle is gripped and placed on a dry glass plate. Another micromanipulation technique is by utilizing the Bessel light beam technique. This technique has demonstrated that microscale objects can be moved or separated with the Bessel light beams [14]. Moreover, the Bessel light beam can be used as a tweezers without the need of any apparatus. The particle velocity during the manipulation process using the Bessel light beams have been reported to be ranging between 5 to 10 μm/s.

The manipulation of microscale particles using a moving nematic-isotropic phase interface has been proposed as a future option of a micromanipulator technique [8, 9]. When a particle contacts the nematic liquid crystal phase, the molecular orientation field is disturbed; thus, the energy is increased. That increased energy creates a force that allows the drag of microscale particles. Previously, it was found that the maximum interfacial force of a 5CB liquid crystal can transfer a 30 μm low density particle (polystyrene) at a moving phase interface velocity of 70 μm/s [12]. However, that interfacial force limits the capability of dragging or transferring heavier microscale objects. Therefore, it has been proposed that the use of the smectic liquid crystals can allow the transferring of not only of light weight particles, but heavy weight particles as well. The following section will discuss the background of the physics of liquid crystals.

2.2 Background of liquid crystals

Over the past decades, the liquid crystalline materials have become a great interest of study due to their optical [15], electromagnetic [16], mechanical anisotropic [17, 18] and flow properties [19, 20]. Specifically, liquid crystals have been used in the development of flat panel visual display devices, liquid crystal displays, biological membranes (e.g. lamellar liquid crystals) and drug delivery. Liquid crystals are a state of matter that occurs between the solid crystal state and the isotropic liquid state, as shown in Figure 2.1. Liquid crystals have been known to be an anisotropic structure because the liquid crystals exhibit different physical properties in different locations throughout the medium. Liquid crystals were discovered by Reinitzer in 1888, where he discovered that a typical fluid material had two melting points. When the sample was heated to a melting point transition, the fluidity of the sample was showing cloudy-based liquid, then the sample appeared to have another melting point where the cloudy liquid became a pure liquid at higher temperatures. Because of this discovery, the liquid crystals were further studied, which nowadays the applications of the liquid crystals have expanded from biomedical to industrial applications.

Generally, liquid crystals are composed of lyotropic liquid crystals, a phase change of concentration in a solvent, and thermotropic liquid crystals, phase change in temperature dependency. Particularly, liquid crystals consist of elongated rod-like molecules where the preferred local direction of the liquid crystal molecules is called the director field, **n**. Therefore, the director field of the liquid crystal molecules is defined as the unit vector that describes the average molecular configuration and alignment in liquid crystals [10, 11]. It is noted that the nematic phase is uniaxial, the uniaxial symmetry of the molecules has no polarity.

As shown in Figure 2.2, the thermotropic liquid crystals are classified into the nematic, the smectic A, the smectic C and the cholesteric liquid crystal depending on the order of alignment and arrangement of the rod-like molecules. To describe each liquid crystal, the nematic liquid crystals possess of long axes of constituent molecules, and the molecules tend to align parallel to each other along the anisotropic axis. Also, the nematic liquid crystals possess the molecular orientation order, but lack translational order. Smectic liquid crystals are commonly classified depending on

7
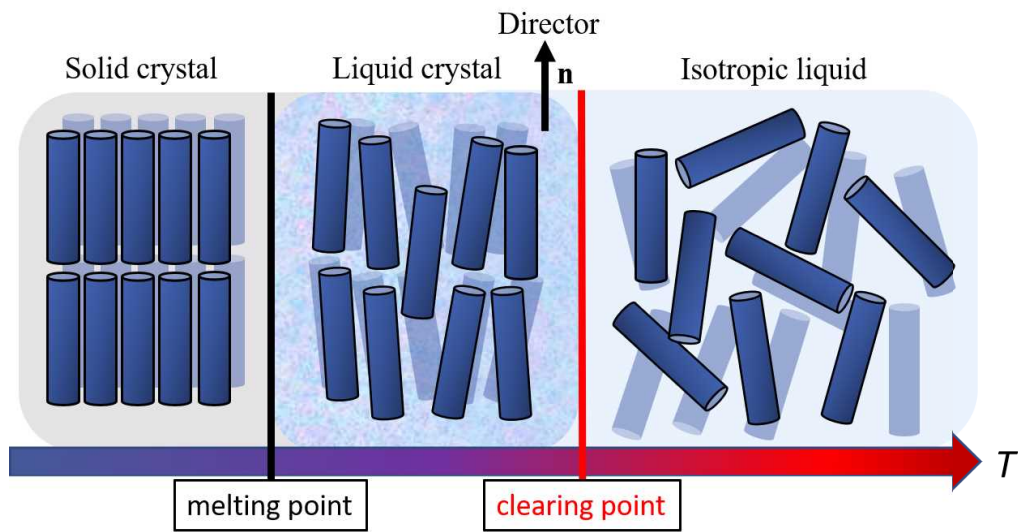
Figure 2.1: Schematic representation of the molecular order in the crystal, liquid crystal and isotropic phases with temperature distribution in the liquid crystalline material. The liquid crystals are the only materials that can create a liquid-liquid phase interface, where an interface is formed between the liquid crystal and isotropic phases.
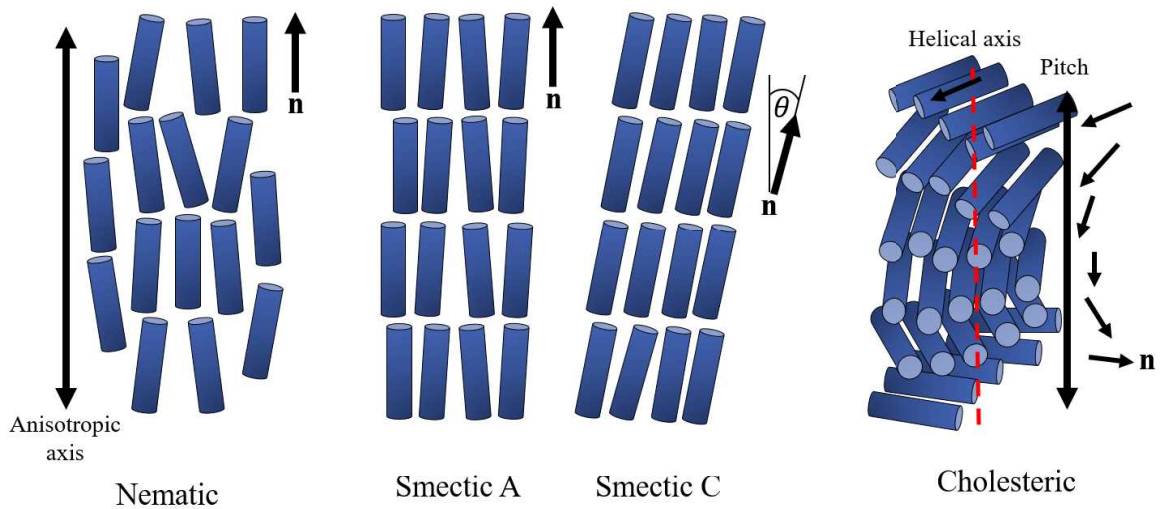
Figure 2.2: Thermotropic liquid crystals are classified into nematic liquid crystal, smectic liquid crystal, and cholesteric liquid crystal depending on the order of alignment and arrangement of the rod-like molecules in the molecular orientation field.
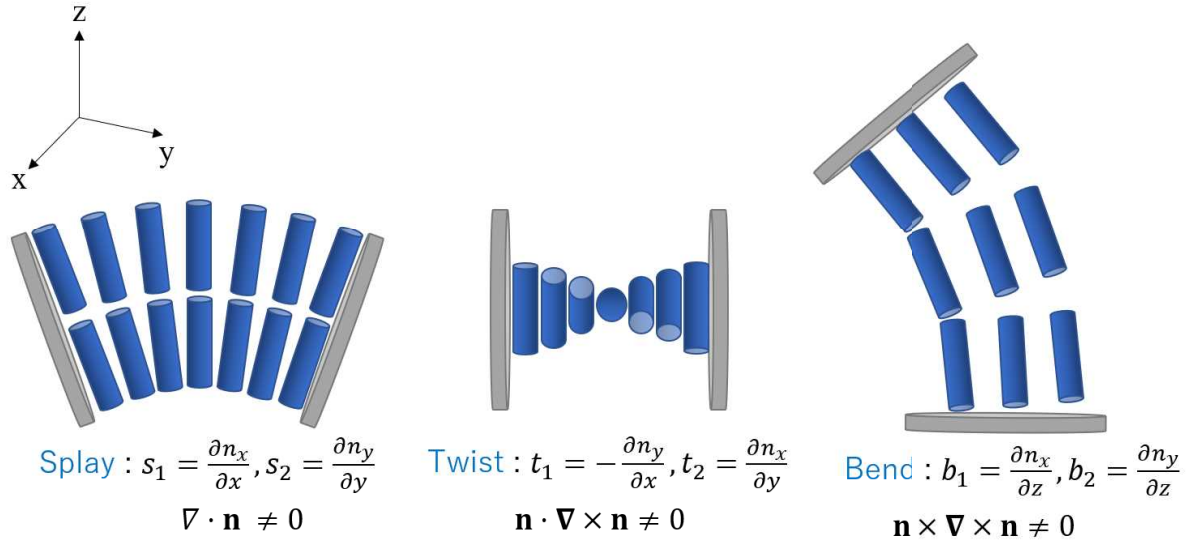
Figure 2.3: The three types of deformation at the molecular configuration in a nematic liquid crystalline material

the alignment of the molecules. In addition, the smectic liquid crystals are highly-layered structures having a well-defined interlayer distance between the molecules. The most commonly used smectic liquid crystals are the Smectic-A and Smectic-C liquid crystals. The preferred averaged direction of the molecules in the smectic-A liquid crystals are aligned perpendicular to the layers and the molecules are parallel positioned normal to the layered structure. In smectic-C liquid crystals, the average director field of the molecules is tilted to an angle normal to the layered structure. The tilted angle of the smectic molecules usually depends on the temperature distribution of the material. Unlike the nematic liquid crystals, the smectic liquid crystals possess molecular orientational order and a 1-dimensional translational order. Cholesteric liquid crystals possess similar physical properties to the nematic liquid crystals, except that the molecular orientation structure shows a preferred configuration that is helical structured. Therefore, the director field of the molecules is not fixed uniformly, but rotates along the helical axis. The director alignment varies throughout the liquid crystal phase with a periodicity of $P/2$, where P is the pitch of the helix.

The static theory of nematic liquid crystals employs the director **n** that describes the mean molecular alignment at a given point *x* in the medium or volume sample. Therefore, the director

9

field $\mathbf{n}$ is defined as $\mathbf{n} = \mathbf{n}(x)$ at a point x, where the $\mathbf{n} \cdot \mathbf{n} = 1$. It is noted that the nematic liquid crystals lack polarity, meaning that $\mathbf{n}$ and $-\mathbf{n}$ are indistinguishable. The deformation of the director field are considered as the splay, twist and bend curvature strains, where the distribution of the director $\mathbf{n}$ is represented in Figure 2.3.

Oseen and Frank considered an integrand that was quadratic in the gradients of the director field [10]. They postulated the free energy density per unit volume for the deformation of the director field as

$$W = \frac{1}{2}(K_1(\nabla \cdot \mathbf{n})^2 + \frac{1}{2}K_2(\mathbf{n} \cdot \nabla \times \mathbf{n})^2 + \frac{1}{2}K_3(\mathbf{n} \times \nabla \times \mathbf{n})^2. \tag{2.1}$$

As explained before, the smectic liquid crystals have some degree of orientational order and positional order. In the smectic-A liquid crystals, the molecules are arranged perpendicular to the layer structures. The molecules in the smectic liquid crystals are in the direction normal to the layers in a 2-dimensional configuration. However, the velocity of the molecules and the layers may not have the same velocity even though they are in the same spatial direction. A nonlinear continuum theory for the smectic-A liquid crystals have been established [21]. In the case of the smectic A liquid crystals, the molecules prefer to be normal to the layers with the direction of $\mathbf{n} = \nabla \phi$, and a free-energy functional is considered as

$$f_1 = \frac{1}{2}(\mathbf{n} - \nabla \phi)^T B(\mathbf{n} - \nabla \phi), \tag{2.2}$$

where $\mathbf{B} = B_\perp \mathbf{I} + (B_\parallel - B_\perp)\mathbf{nn}$. Therefore the total free energy for the smectic A liquid crystals is represented as

$$W = \frac{1}{2}(K_1(\nabla \cdot \mathbf{n})^2 + \frac{1}{2}K_2(\mathbf{n} \cdot \nabla \times \mathbf{n})^2 + \frac{1}{2}K_3(\mathbf{n} \times \nabla \times \mathbf{n})^2 + \frac{1}{2}(\mathbf{n} - \nabla \phi)^T B(\mathbf{n} - \nabla \phi). \tag{2.3}$$

2.3 The mechanism of the drive of particle by a phase interface

The interplay between colloidal particles and the phase interface of nematic liquid crystals have played an important role in the applications of the liquid crystals [22, 23, 24]. A specific

10

example is the topological defects occurring in nematic liquid crystals caused by a suspended particle inside the liquid crystal material, which is known as the Saturn ring of disclination [25]. As a result, researchers examined the energy and stability of the interaction between the particle and liquid crystal through experimental and simulation from this topological defect [26]. In addition, analytical expressions for the director field around colloidal particles with anchoring on the surface of the particle have been studied in the past [27].

Figure 2.4 shows a spherical particle surrounded with the rod-like molecules. In the isotropic phase region, there is no order regarding the molecular orientation, the distortion energy does not increase even with the presence of the particles inside the region. Figure (b) shows the particle appearing in the nematic phase region, where the particle invades the molecular orientation order. In (c), when the particles tries to invade the liquid crystal region, the distortion energy of the molecular field increases because of the directional order in the liquid crystal molecules. When the particle is in contact with the phase interface between the liquid crystal and isotropic phases, the energy is not increased above the particle, but the distortion energy increases below the particle. Hence, an upward force acts upon the particle. Therefore, the energy generated at the phase interface is experimentally demonstrated, and it is considered that the particle prefers to exist in a state above the liquid crystal bulk region. Taking note that the size of the liquid crystal molecules is about 10^6 smaller compared to the particle size in μm. Similarly in the smectic liquid crystals, molecules are aligned normal to the layers, which exerts a higher force compared to the nematic liquid crystals. When the particle tries to invade the high-layered structures of the smectic liquid crystals, as shown in Figure 2.5, molecules in the smectic phase are disturbed, and it generates a strong force in the smectic-isotropic phase interface. Therefore, micromanipulators with strong force can be developed using the smectic-isotropic phase interface.

2.4 Elasticity in the molecular orientation field of nematic liquid crystals

The distortion in the molecular orientation field of the liquid crystal molecules have played an important role in the applications of liquid crystals. Some factors to create a distorted director field may consist of orientation anchoring at the solid boundary of a substrate [28], electric or
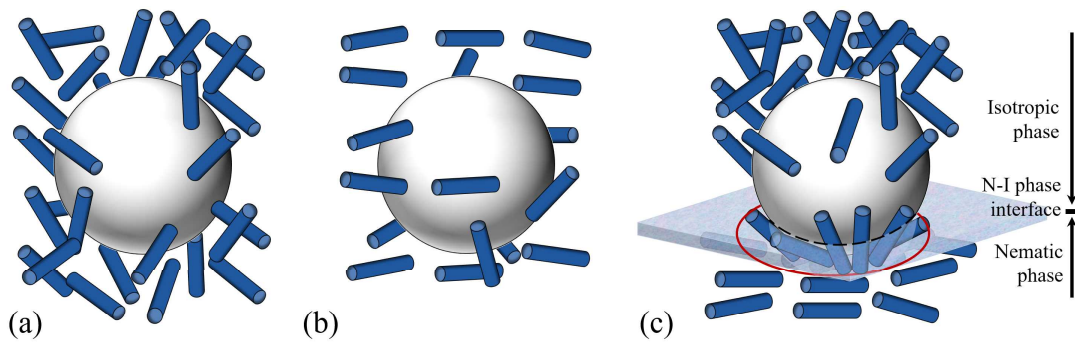
Figure 2.4: The schematics of the molecular orientation field around a spherical particle in nematic liquid crystals. The schematic is described as follows: (a) spherical particle in the isotropic phase region, (b) spherical particle in the nematic phase region, and (c) spherical particle trapped in the nematic-isotropic phase interface.
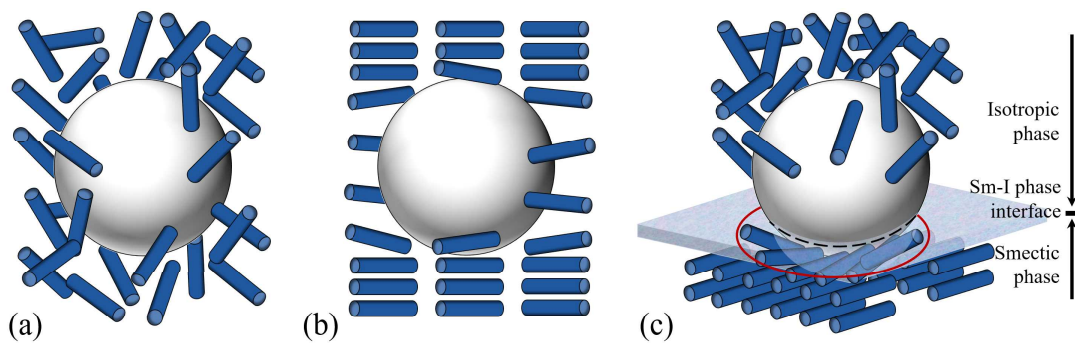
Figure 2.5: The schematics of the molecular orientation field around a spherical particle in smectic liquid crystals. The schematic is described as follows: (a) spherical particle in the isotropic phase region, (b) spherical particle in the smectic phase region, and (c) spherical particle trapped in the smectic-isotropic phase interface.

magnetic fields, and flow [8, 29, 30, 31, 32, 33]. By changing the orientation structure of the liquid crystal molecules by applying an electric field and the viscous force due to the flow of the liquid crystal, so called backflow, has been investigated to move an object in contact with the liquid crystal. Therefore, by changing the orientation direction of the liquid crystal molecules, a device can convert electrical energy into kinetic energy, so the development of unique mechanical elements can be expected for future liquid crystal applications.

3.   Capture of micro-scale objects utilizing the smectic-isotropic phase interfacial force for the development of soft-manipulation devices

3.1   Introduction

The precise manipulation of biological cells and microscopic particles has become an important interest of study for the new development of micromanipulator systems suitable for MEMS and μ-TAS modern technologies. The manufacturing of electrostatic microgrippers [13], bessel light-beam and light-driven optical micromanipulation [14, 34], laser-scanning micromanipulation [35], non-contact ultrasound particle micromanipulation [36, 37, 38] are just few widely potential examples of a micromanipulator technique.

The manipulation of particles utilizing the phase interface between the nematic liquid crystal and isotropic phases has been proposed as one option for future micromanipulator systems [8, 9]. The proposed liquid crystal micromanipulator system is characterized by its simple structure and small number of components in the system, mainly because it consists of a liquid crystal material, a container to encapsulate liquid crystals and a heat source to control the temperature of the liquid crystal. The nematic-isotropic phase interface emerges under the inhomogeneous temperature condition or during a phase transition process. When microscale objects are captured on the nematic-isotropic phase interface, they are subjected to a force whose direction is perpendicular to the phase interface and toward the isotropic phase region. The phase interfacial force arises from the disturbance of the molecular orientation field in the nematic phase region, and the nematic phase region acts to exclude the microscale objects to the isotropic phase region [12, 23]. That is, it is possible to develop a micromanipulator system capable of controlling the position of microscale objects by utilizing the interfacial force generated at the phase interface in liquid crystals as a driving source. Previously, authors have experimentally measured the nematic-isotropic phase interfacial force of a 4-cyano-4'-pentylbiphenyl (acting on a polystyrene particle with diameter of 30μm), and found that the phase interfacial force is about 1.4nN [12]. However, the phase interfa-

cial force of the nematic and isotropic phases is not strong enough for the development of future micromanipulator systems [12, 39].

The nematic liquid crystal focused in previous research studies exhibits the molecular configuration that the rod-like (or disk-like) molecules have orientational order, but no positional order. On the other hand, the molecular configuration of a smectic liquid crystal exhibits the layered structure (i.e., a part of a positional order) in addition to the orientational order [10, 11, 40], and deviation of the orientational order. Thus, the layered structure from the equilibrium state of the smectic liquid crystals may cause a greater interfacial force than that for the nematic liquid crystals. If we can obtain a stronger interfacial force compared to that of the nematic liquid crystals, the application of a liquid crystal micromanipulator system can become wider. We proposed the use of the phase interface of the 4-cyano-4'-dodecybiphenyl smectic liquid crystal, since the molecular orientation is highly ordered compared to that of the nematic liquid crystals, and a stronger interfacial force is expected.

In the first part of this work, we have chosen three distinctive thermotropic liquid crystal materials, as shown in Table 3.1, for the systematic investigation on various liquid crystal phase interfacial forces. The nematic-isotropic phase interface appears at temperature of $T = 35.2\,^\circ\text{C}$ in 5CB and $T = 40.5\,^\circ\text{C}$ in 8CB, the nematic-smectic phase interface at $T = 33.5\,^\circ\text{C}$ in 8CB, and the smectic-isotropic phase interface at $T = 58.5\,^\circ\text{C}$ in 12CB. The stabled phase interfaces are created by controlling the temperature distribution of the liquid crystal material, and the phase interfacial forces are evaluated by tracking the microspherical objects which fall from the higher temperature phase region to the lower temperature phase region across the interface between the phases. It is noted that both liquid crystal phases are capable of infinite deformation, and the volume change and heat transition associated with the phase change is relatively small. It is reported that the liquid crystal interfacial forces depend on the size of spherical objects [12, 39]. The theoretical discussion on the stress acting on the surface of the spherical objects will be presented for generalizing our results. Finally, the capturing of spherical particles on the phase interfaces of the 6CB, 7CB, 9CB, and 11CB will be discussed in the second part of the phase interfacial work.

Table 3.1: Summary of the thermotropic liquid crystal phases with a phase transition temperature

Thermotropic liquid crystals	Phase transitions [°C]			
4-cyano-4'-pentylbiphenyl (5CB)	Crystal		$\xrightarrow{24.0}$ Nematic	$\xrightarrow{35.2}$ Isotropic
4-cyano-4'-octylbiphenyl (8CB)	Crystal	$\xrightarrow{21.5}$ Smectic	$\xrightarrow{33.5}$ Nematic	$\xrightarrow{40.5}$ Isotropic
4-cyano-4'-dodecybiphenyl (12CB)	Crystal	$\xrightarrow{48.0}$ Smectic		$\xrightarrow{58.5}$ Isotropic

3.2 Experimental Methods

This section will describe the research process for the development of our micromanipulator system. A brief description of system, the calibration of the system, and the position of the phase interfaces of the thermotropic liquid crystals with temperature distribution will be discussed. It has been demonstrated a good reliability and stability of our developed micromanipulator system with minimal fluctuations of $\pm 0.01°C$. In addition, the experimental procedures in measuring the phase interfacial force utilizing spherical particles mixed in the liquid crystal will be discussed as well.

3.2.1 Development of the micromanipulator system

A schematic representation of the micromanipulator (liquid crystalline) system is shown in Figure 3.1. The experimental micromanipulator system is designed through SolidWorks and manufactured in the precision machining room utilizing a cutting modeling machine (MDX-5000R). The micromanipulator system is made of an MDF material of low thermal conductivity of 0.05 W/m·K, which allows the system to maintain stable temperature conditions. Furthermore, for accurate measurements of the phase interfacial force, a high-precision temperature control system is required. Therefore, four high-conductive copper plates, with thermal conductivity of 385.0 W/m·K, are attached/sandwiched inside the system along with Peltier modules (VICS. Co. Ltd: Peltier element unithermal UT-2020CE-M). The specifications of the Peltier modules used for this micromanipulator are shown in Table 3.2. The entire system is sealed tightly to minimize temperature fluctuations.

The overall representation of the experimental setup is illustrated in Figure 3.2. The Peltier modules (4 Peltier modules attached on both ends of the copper plates), which are sandwiched
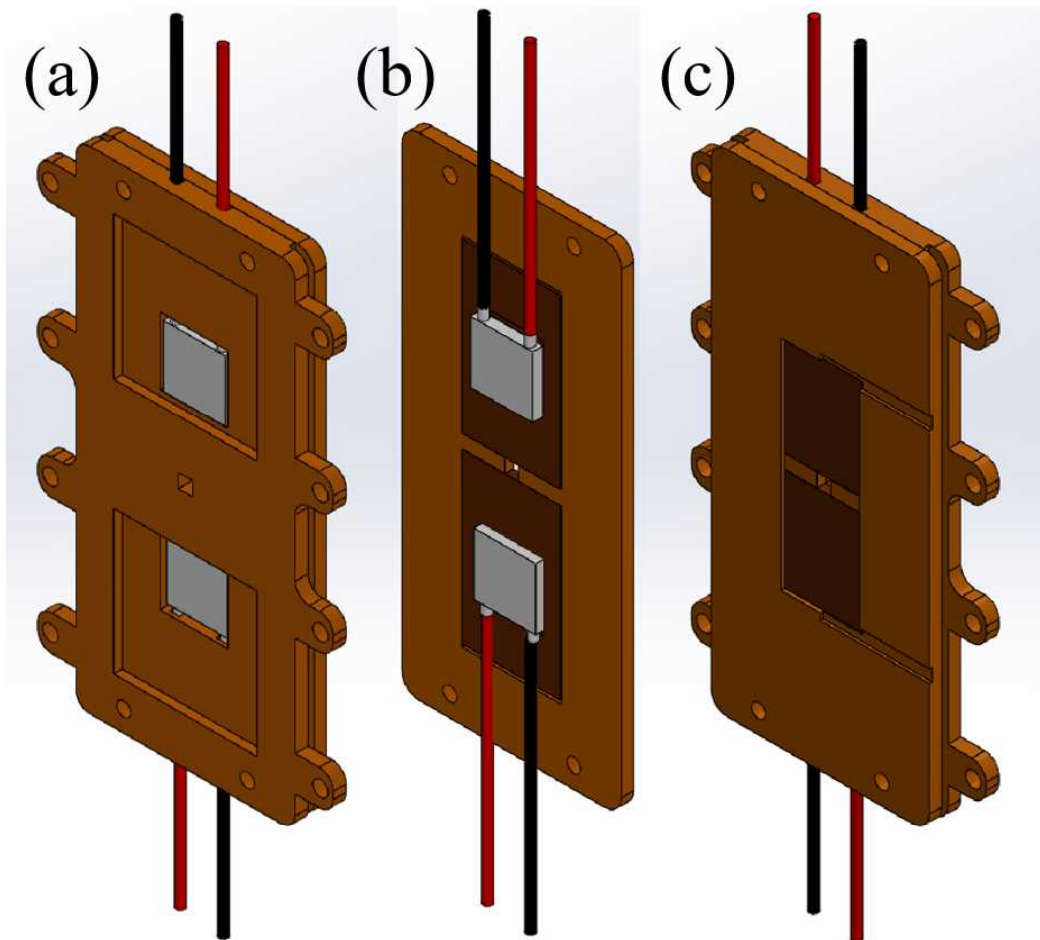
Figure 3.1: Schematic representation of the liquid crystalline device. (a) Front view of the liquid crystalline device, a cooling system is attached on the two rectangular spaces to cool down the Peltier modules during experimentation. (b) The interior of the liquid crystalline device, where the copper plates are separated by a 5 mm gap, and the Peltier modules are attached on the copper plates. The copper plates are connected to a PID controller to control the temperature distribution. (c) Back side of the liquid crystalline device, the liquid crystal glass cell is placed on top of the copper plates and thermocouples are used to measure the temperature applied from the PID controller.

Table 3.2: Peltier module specifications

Category	Specification
Maximum current	3.2 A
Maximum voltage	6.2 V(DC)
Maximum temperature difference	70.0 °C
Maximum heat absorption	13.0 W
Weight	8.0 g ± 10%
Size	22.0×22.0×3.73±0.10mm

inside the system, are connected to a PID controller (CELL System, Co. Ltd) with precision measurement of ±0.03 °C. Also, platinum thin-film RTD temperature sensor elements (Hayashi Kogyo Co. Ltd: CRZ-1632) are placed on the surface of the copper plates. The resistance temperature sensors are connected to a PID controller to give a signal to the PID and control the temperature of the Peltier modules. The temperature input is generated through a TDC-2000/4000 Test Program Software on PC. The experimental system has an observation port of 5×5mm and a microscope camera (IDS: UI-3360CP-C-HQ) equipped with an objective lens (Nikon Co. Ltd: M Plan-20X magnification/0.35) and a transmitted monochromatic light source (Edmund Optics: MI-150 High-Intensity Illuminator) are used to observe the behavior of the microscale particles along with the position of the liquid crystal phase interfaces. Both the camera and monochromatic light source are equipped with polarizing plates to reduce the diffraction from observations in the experiments.

To improve the thermal efficiency in our system, an exhaust cooling system is performed and added to the micromanipulator system, as shown in the schematic with the cooling system in Figure 3.2. An actual image of the cooling system attached to the manipulator is demonstrated in Figure 3.3. A cooling system allows the removal of excess heat from the Peltier modules and maintains the operating temperature more efficiently. A Peltier module is an element that transfers heat on a cooling side to a heat dissipation side, and a large amount of heat is generated at the heat dissipation side of the Peltier module. Thus, a heat sink on the heat dissipation side is required to dissipate the heat from the Peltier module. A liquid cooling method is used since the liquid cooling method transfers and dissipates heat more efficiently than the air-cooling method [41, 42]. Also,

18
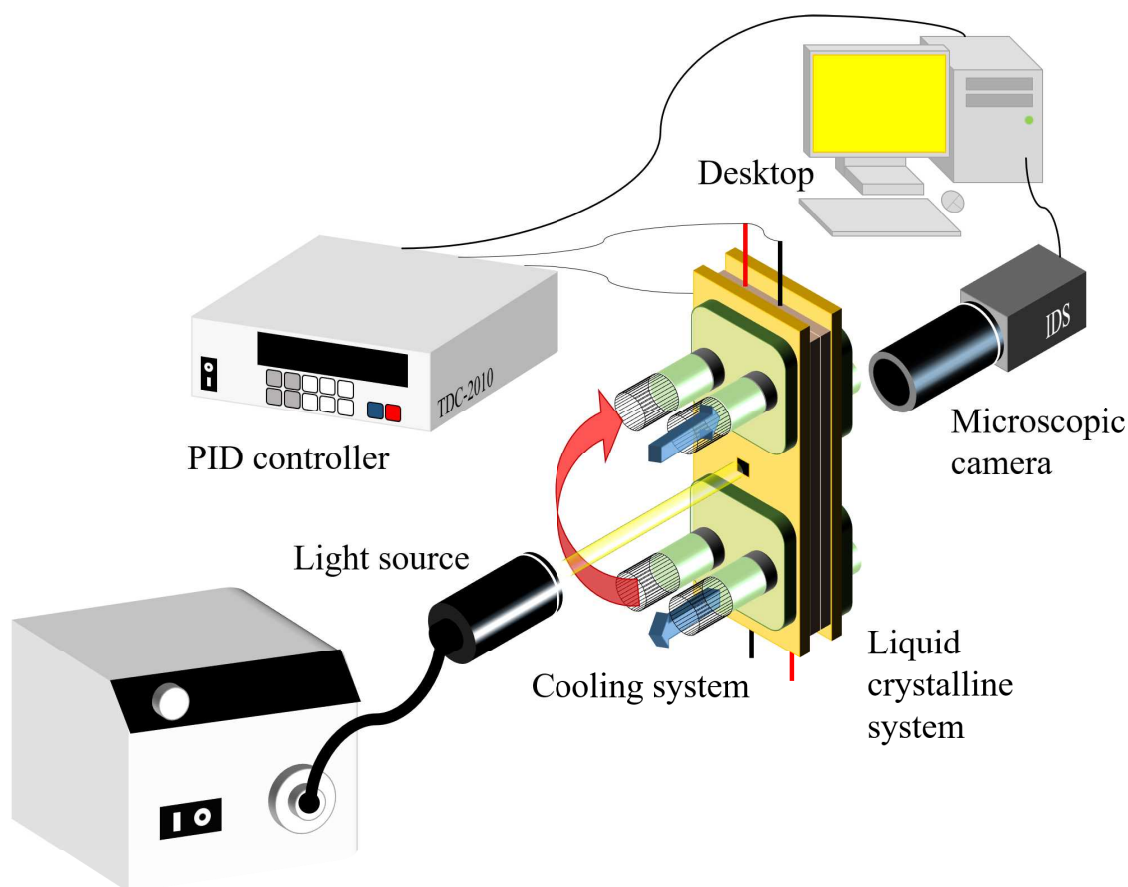
Figure 3.2: Schematic of the overall experimental setup. The system includes: a liquid crystalline system attached with Peltier modules controlled by a PID controller. In addition, the liquid crystalline system is attached with a cooling flow system. The dynamics of the particle is captured by a microscopic camera.

due to an endothermic reaction from the Peltier module, the water-cooling system allows to cool down the system more efficiently.

To determine that the heat inside the Peltier modules is properly exhausted, a temperature test is attempted. Figure 3.4 shows the temperature of the upper and lower Peltier modules with respect to time. For the experimental testing, the target temperature is set to be 58.5 °C for both T_L and T_U, where T_L is the temperature of the lower part of the system and T_U is the temperature of the upper part of the system. The temperature of both Peltier modules rises to 58.5 °C and remained constant after 150 seconds. Therefore, it is confirmed that the heat in the Peltier modules
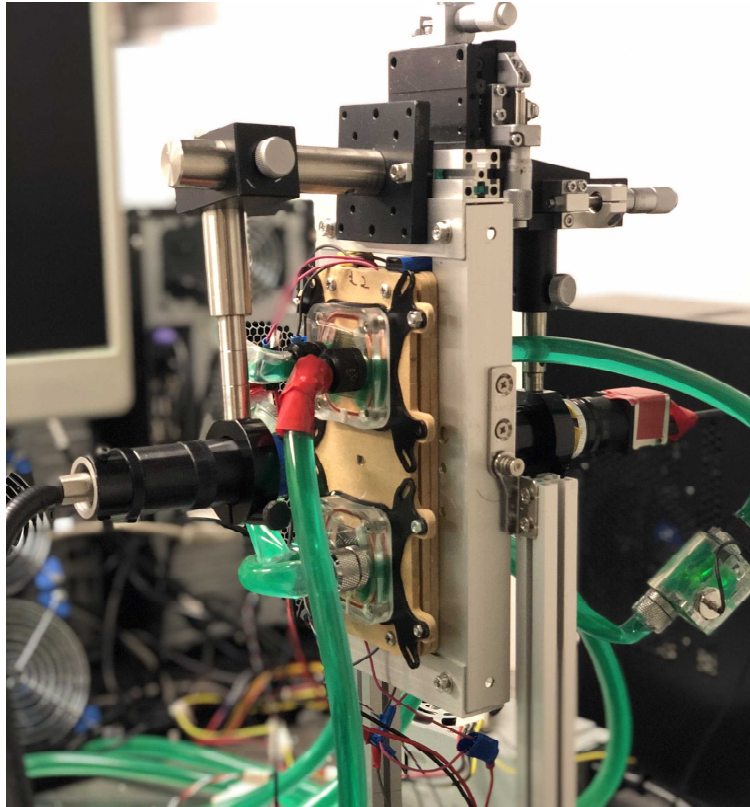
Figure 3.3: Photograph of the experimental system.

is properly exhausted and reaches a constant temperature with $\pm 0.01\ ^\circ$C temperature fluctuations inside the system. Therefore, it has been determined that the system provides very low fluctuations in temperature distribution, so a stable phase interface of the liquid crystal material can be achieved. For higher and distinct temperature conditions, we set $T_L = 58.5\ ^\circ$C and $T_U = 63.5\ ^\circ$C, and the temperature of the system reaches to a stable temperature condition after 300 seconds, as shown in Figure 3.5.

The position of the phase interface changes depending on the temperature distribution applied in the liquid crystal cell. For the purpose of creating the coexistence state of the phase interface between the liquid crystal and isotropic/liquid crystal phases, a liquid crystal cell is created and inserted inside our micromanipulator system. Experiments were conducted under room temperature (25 $^\circ$C). The experimental liquid crystal cell consists of two $26 \times 76 \times 0.7$mm rectangular
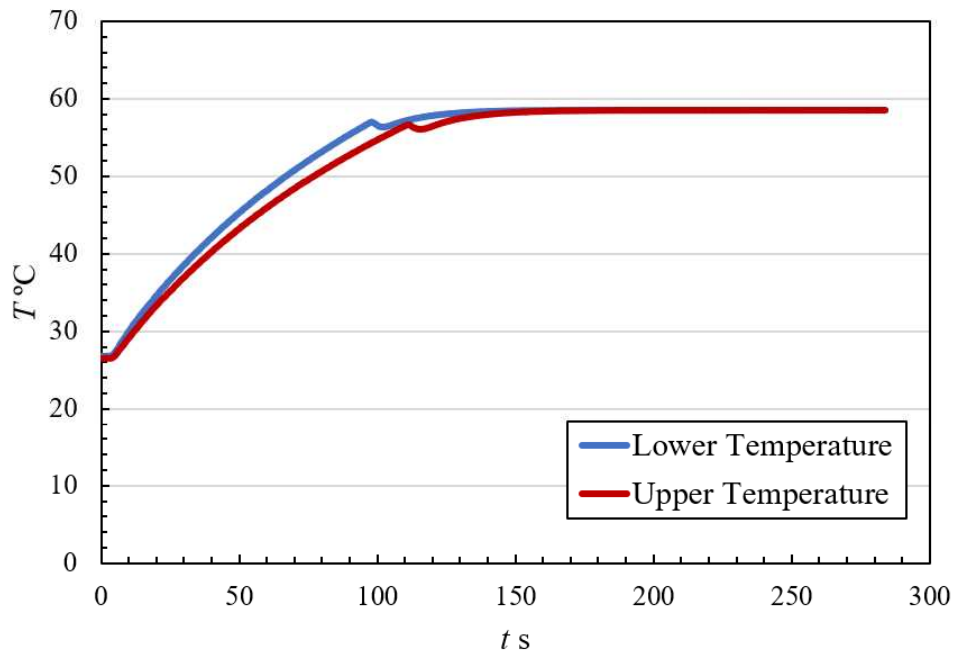
Figure 3.4: For calibration purposes, both the Peltier modules, T_U and T_L, were set to be 58.5 °C.
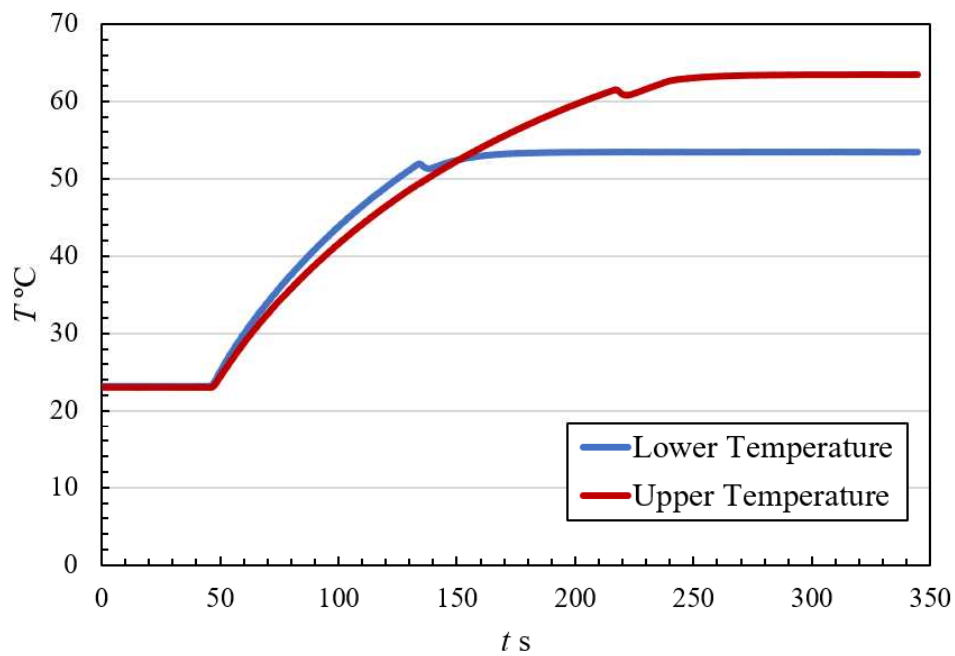
Figure 3.5: Temperature of the upper and lower Peltier modules at $T_U = 63.5$ °C and $T_L = 53.5$ °C.

glass plates bonded together with a 188μm spacer. A homeotropic alignment film (JSR JALS-2021-R25: AL60101) is treated on the facing surfaces of the glass plates by utilizing a spin coater (Mikasa Co. Ltd: 1H-DX2) at 3500 RPM. The alignment film on the surface of the glass plates forces the director field of the liquid crystal molecules to be perpendicular throughout the entire cell. The homeotropic alignment thin-film coated glass plates are baked for 45 minutes utilizing an electric drying oven (Advantec Co. Ltd: Electric Drying Oven DRN320DA). The liquid crystal cell is sandwiched with the copper plates, and the paired Peltier modules are attached at the upper and lower part of the copper plates. In addition, heat conduction gel sheets (Mac-Eight Co. Ltd: GC-A) are placed between the copper plates and the liquid crystal cell in order to improve the heat transfer performance. The temperature distribution of the cell is achieved by controlling the Peltier modules through the PID controller. By adjusting the temperature of the upper and lower ends of the liquid crystal cell, T_U and T_L, a stable horizontal phase interface emerges at the desired position.

We encapsulated a 5CB, 8CB, and 12CB liquid crystal inside the liquid crystal cell to create a phase interface. The experimental procedures to create the phase interface are as follows. At first, the liquid crystal cell is horizontally placed to have a homogeneous temperature gradient throughout the liquid crystal cell. Both the T_U and T_L are once set to a temperature for which the higher temperature phase is stable, and then T_L is decreased below the phase transition temperature of the liquid crystal, respectively. By setting the average of the T_U and T_L to be roughly equal to the phase transition temperature, the phase interface appears at the center of the liquid crystal cell. For example, the nematic liquid crystal inside the liquid crystal cell is heated to a temperature higher than the $T_{\text{N-I}}$ (5CB: nematic-isotropic phase transition temperature at $T_{\text{N-I}} = 35.2$ °C) so that an isotropic liquid state appears in the liquid crystal cell. The attitude of the liquid crystal cell is then positioned vertically. Then by making the temperature of the lower part of the cell lower than the $T_{\text{N-I}}$, a nematic phase is created in the lower part of the liquid crystal cell. The phase interface appears between the boundary of the nematic phase and isotropic phase, the nematic phase and smectic phase, or the smectic phase and isotropic phase, as shown in Figure 3.6, respectively.
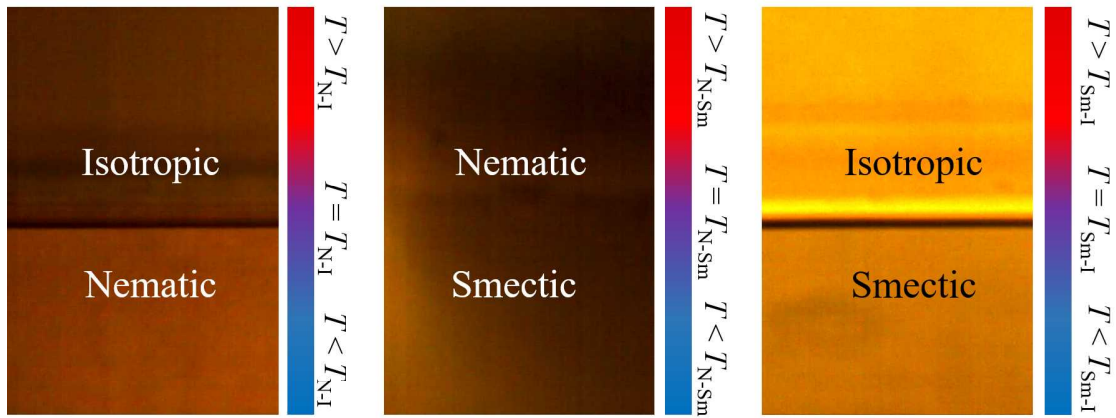
Figure 3.6: Microscopic images of the phase interface between the nematic to isotropic phases (5CB), nematic to smectic phases (8CB) and smectic to isotropic phases (12CB). Note that the 8CB liquid crystal possesses a nematic to isotropic phases as well.
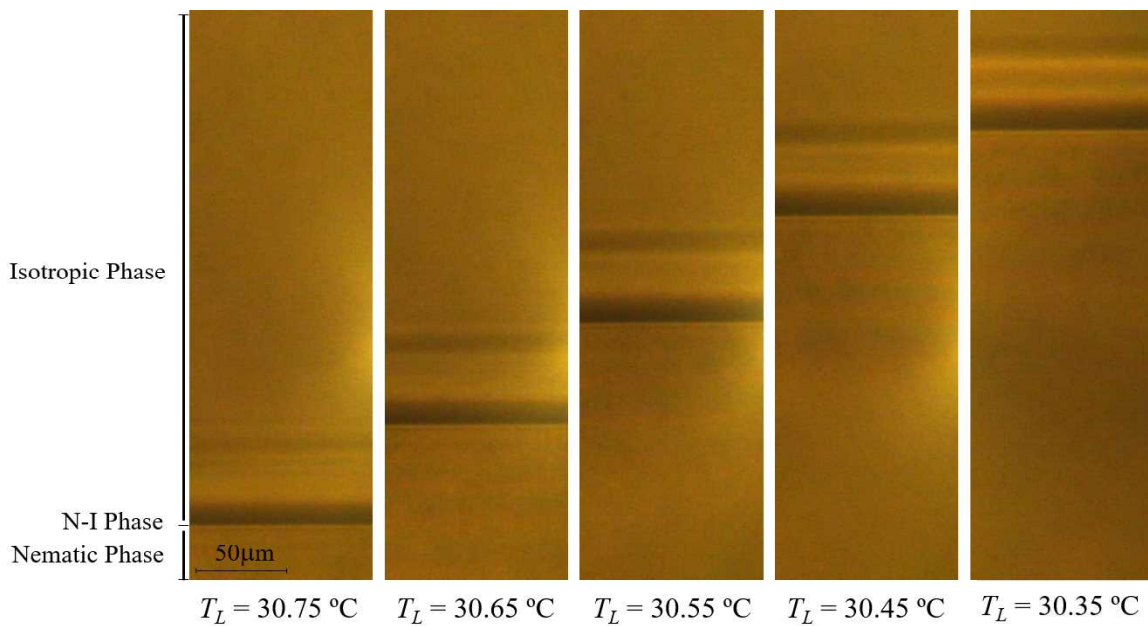
Figure 3.7: The position of the nematic-isotropic phase interface of a 5CB liquid crystal with temperature change. The upper temperature was set fixed to be $T_U = 39.5\,^\circ$C and the lower temperature decreases at a rate of 0.05 $^\circ$C.

$$h(\Delta T) = 553.6\Delta T - 4813$$
$$R^2 = 100\%$$
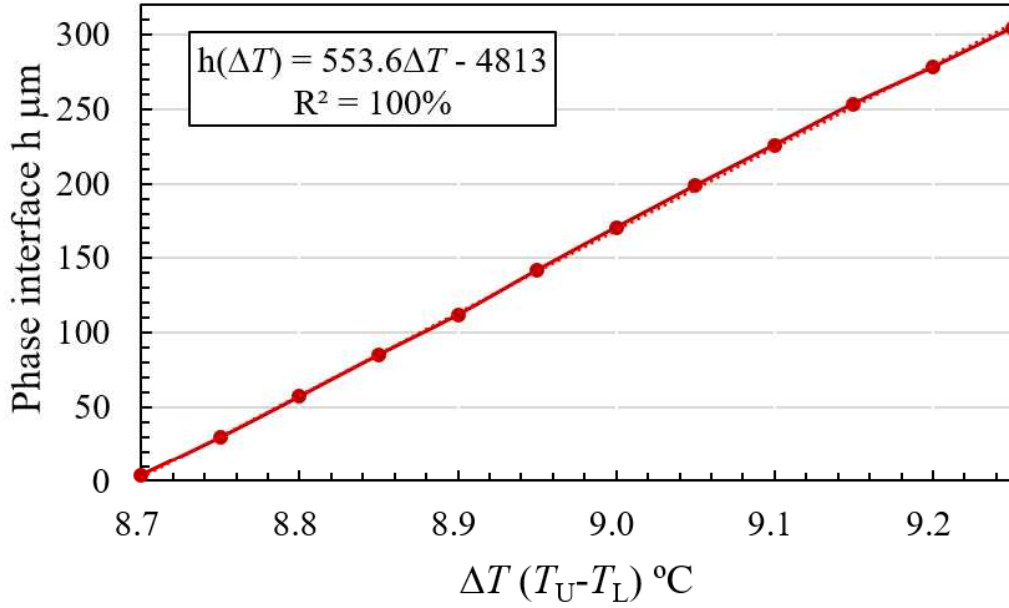
Figure 3.8: Position of the nematic-isotropic phase interface with respect to temperature change in 5CB.

To understand the position of the phase interface of the liquid crystals (defined as h) to temperature change (ΔT), the temperature of the upper part of the liquid crystal cell (T_U) is set to be fixed and the temperature of the lower part of the liquid crystal cell (T_L) is decremented at 0.05 °C. Figure 3.7 shows the position of the nematic-isotropic phase interface with respect to the temperature of the lower end of the liquid crystal cell of a 5CB liquid crystal material. By changing the temperature of the lower end of the liquid crystal cell in 5CB (starting at T_L = 30.8 °C), it is observed that the nematic-isotropic phase interface is shifted up at an average rate of approximately 27.3±1.5μm for every 0.05 °C. Figure 3.8 shows a graphical representation of the position of the phase interface h with respect to temperature difference (ΔT, where T_U = 39.5 °C) of the 5CB liquid crystal. Therefore, it can be observed that the nematic-isotropic phase interface can have fluctuations in the position of the phase interface of 5.4±0.3μm for every 0.01 °C.

In the same manner, the position of the phase interface with respect to temperature difference for 8CB liquid crystal (nematic-isotropic phase interface and nematic-smectic phase interface)

$$h(\Delta T) = 459.6\Delta T - 4930$$
$$R^2 = 99\%$$
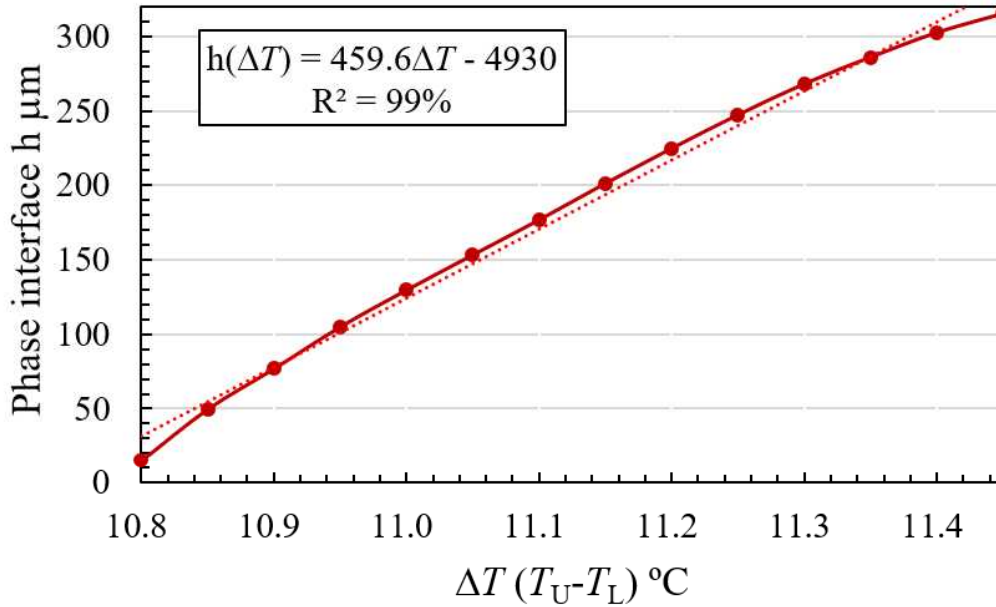
Figure 3.9: Position of the nematic-isotropic phase interface with respect to temperature change in 8CB.

and 12CB liquid crystal (smectic-isotropic phase interface) is conducted. The experiments were conducted similar to the 5CB liquid crystal, T_U remained fixed, and T_L is decremented at a rate of 0.05 °C. Figure 3.9 shows the change of position with temperature change for a nematic-isotropic phase interface in 8CB liquid crystal ($T_U = 46.0$ °C and the starting at $T_L = 35.2$ °C) and it has been estimated that the nematic-phase interface changes approximately $23\pm5.5\mu$m for every 0.05 °C. Figure 3.10 shows the position of the nematic-smectic phase interface of 8CB liquid crystal with temperature change ($T_U = 37.5$ °C and starting at $T_L = 28.2$ °C) and it has been estimated that the nematic-smectic phase interface changes at a rate of $33\pm6.5\mu$m for every 0.05 °C.

The 12CB smectic liquid crystal requires high temperatures to create a coexistence state of the smectic and isotropic phases. Therefore, T_U is set to be fixed at 63.0 °C and T_L, which starts at 53.7 °C, decrements 0.05 °C. Figure 3.11 shows the position of the smectic-isotropic phase interface with respect to temperature change, and it has been estimated that the position of the smectic-isotropic phase interface changes at approximately $16.9\pm4.7\mu$m for every 0.05 °C.

25
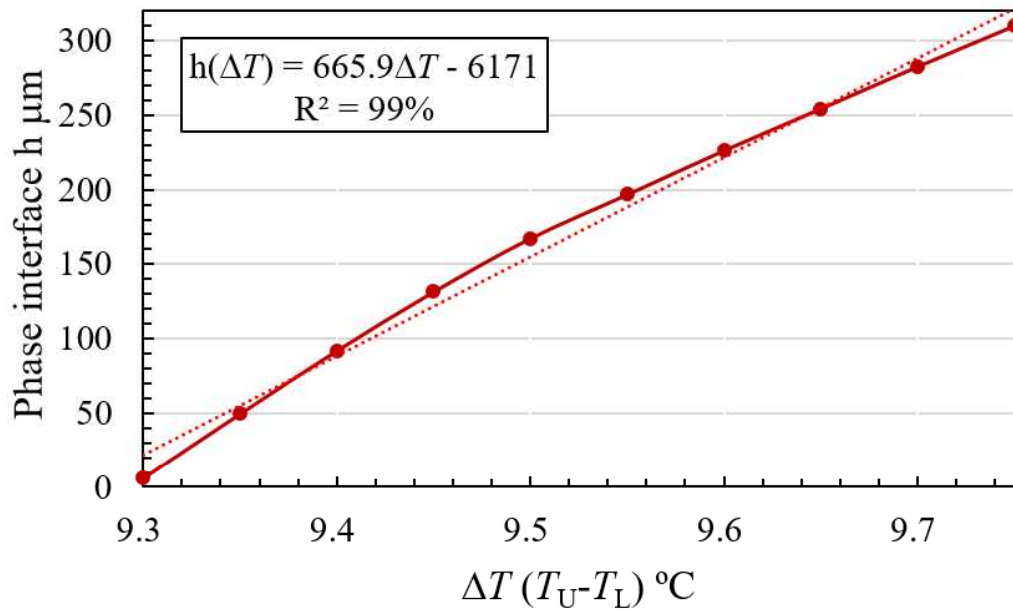
Figure 3.10: Position of the nematic-smectic phase interface with respect to temperature change in 8CB.
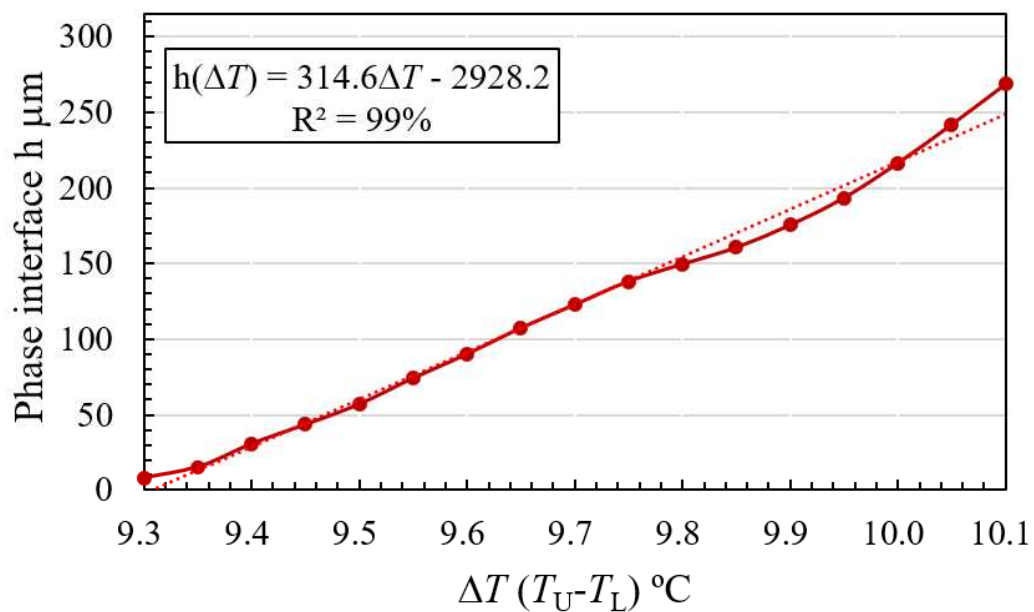
Figure 3.11: Position of the smectic-isotropic phase interface with respect to temperature change in 12CB.

3.2.2 Overview of the experimental system

The micromanipulator system shows that a phase interface between the liquid crystal and isotropic phases can be created, and the fluctuation in temperature distribution is minimal. Therefore, the main factors of this micromanipulator system are considered as follows.

1. The sensitivity of the control system. A slight change in the temperature distribution changes the position of the phase interface. The system must stay steady (positioned horizontally or vertically) to reach a homogeneous temperature condition.

2. The system must be sealed tightly to keep the temperature stable. The thermocouples (temperature sensors) are pasted with thermal grease for better thermal conductivity and precise measurements. Experiments have demonstrated a ± 0.01 °C temperature fluctuations within our system.

3. A thermally conductive sheet should be attached to the liquid crystal glass cell for higher thermal conductivity with the copper plates.

3.2.3 Method of tracking spherical particles and phase interface in liquid crystals

The experimental procedures of measuring the interfacial force in liquid crystals will be discussed. Similar to the first part of the experimental methods, we encapsulated a 5CB, 8CB, and 12CB liquid crystals since the selected liquid crystals provide the phases of nematic-isotropic, nematic-smectic, and smectic-isotropic. By utilizing our developed experimental system, the liquid crystal cell is sandwiched between copper plates and heat conductive sheets, as shown in Figure 3.12. We used several kinds of different spherical particles with different weight depending on the strength of the interfacial force, so we have chosen micropearl polystyrene (diameter $\approx 100 \mu$m, density 1.19 g/cm^3), glass bead (diameter $\approx 100 \mu$m, density 2.5 g/cm^3), and tungsten carbide (diameter $\approx 100 \mu$m, density 15.63 g/cm^3) for this study. The typical densities and viscosities for each phase of the liquid crystal materials are shown in Table 3.3.
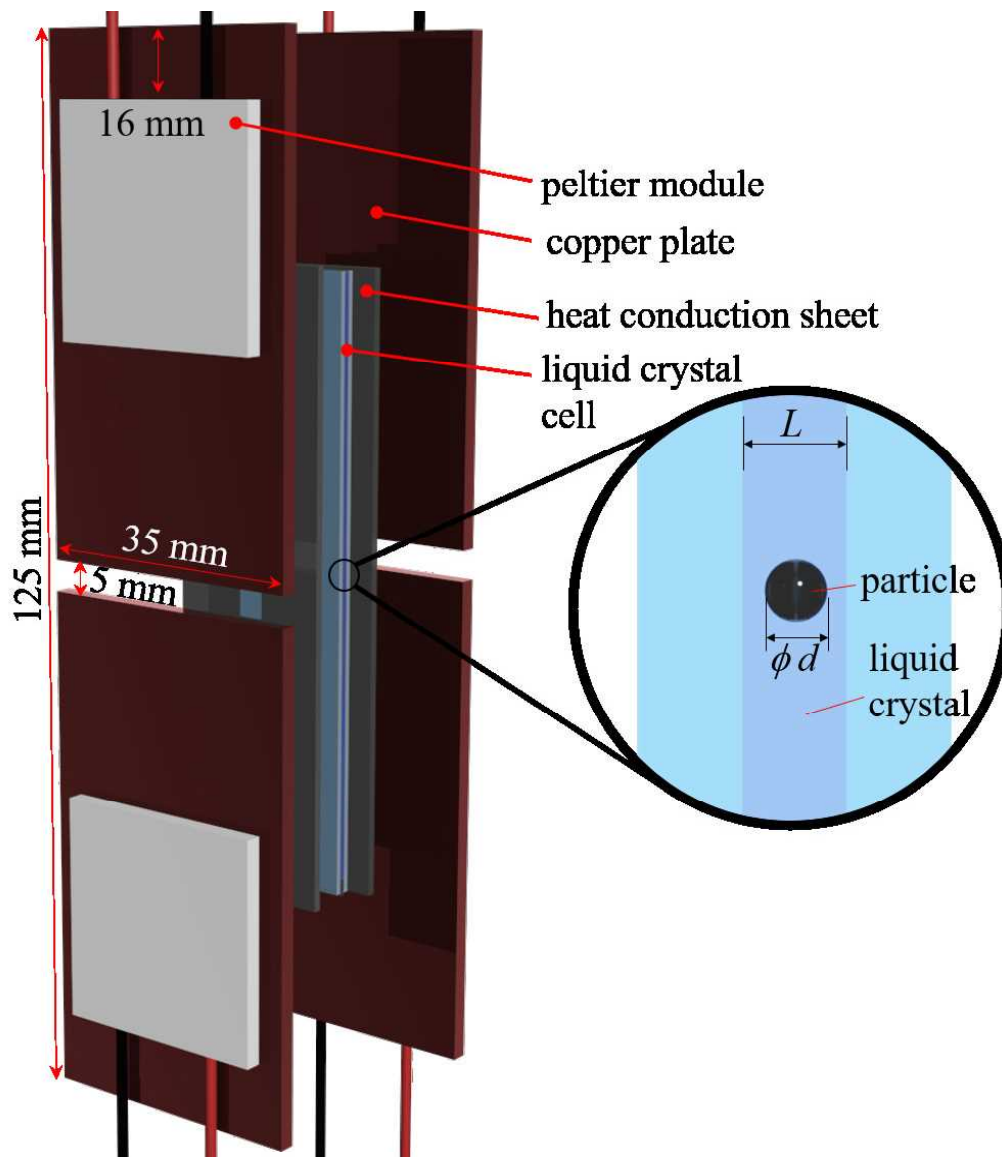
Figure 3.12: Device schematic diagram for the manipulation of particles inside a liquid crystal cell.

Table 3.3: Summary of the densities and viscosities of the thermotropic liquid crystalline materials

Material	Phases	Density [kg/m^3]	Viscosity [Pa·s]
5CB	Nematic-Isotropic	1008	0.023
8CB	Nematic-Isotropic	978	0.024
	Nematic-Smectic	989	0.10
12CB	Smectic-Isotropic	1000	0.02

The experimental procedures are as follows. At first, the liquid crystal cell is horizontally placed to keep the position of the spherical particles mixed in the liquid crystalline materials stable. Both of the T_U and T_L are once set to the temperature for which the higher temperature phase is stable, and then T_L is decreased below the phase transition temperature. By setting the average of the T_U and T_L to be roughly equal to the phase transition temperature, the phase interface appears at the center of the liquid crystal cell. Then, the attitude of the liquid crystal cell changes vertically, and spherical particles start to fall by gravity. The motions of the spherical particles are recorded with a video camera attached on a polarized light microscopic lens and an image analysis software (imageJ [43]) allows us to obtain the position, velocity and acceleration of the spherical particles and the phase interface.

3.3 Experimental Results

This section will discuss the experimentation observations of the thermotropic liquid crystals (5CB, 8CB and 12CB) and spherical particles (polystyrene, glass bead and tungsten carbide). The interfacial force between these thermotropic liquid crystals will be presented.

3.3.1 Nematic-isotropic phase interface and polystyrene particle in 5CB liquid crystal

Figure 3.13 shows the experimental results of the 4-cyano-4'-pentylbiphenyl liquid crystal (5CB) and the polystyrene particle under a polarized light microscope. In order to keep the position of the nematic-isotropic phase interface stable, the temperature on both the upper and lower Peltier modules remain unchanged. We set the upper Peltier module to be $T_U = 39.5°C$ and the lower Peltier module to be $T_L = 30.6°C$. The dark and bright areas in the images correspond to the isotropic and the nematic phase regions, and the horizontal boundary between the areas is the phase interface. The time when the polystyrene particle contacts the phase interface is defined at $t = 0s$. Before the polystyrene particle contacts the phase interface at (a) $t = $ -9.5s, the polystyrene particle settles in the isotropic phase region at a constant rate due to gravity. After the polystyrene particle contacts the phase interface, as shown in (b), it can be observed that the position of the polystyrene particle is kept constant above the phase interface. It is confirmed that the nematic-isotropic phase interface is deformed along the shape of the polystyrene particle, as shown in (c), but it is retained into the isotropic phase region above the phase interface.

The trajectories of the center of gravity of the polystyrene spherical particle and the phase interface is shown Figure 3.14. The positional origin ($h = $ 0mm) is defined as the position of the center of gravity at $t = $ 0s. The polystyrene spherical particle falls in the isotropic phase region with a terminal velocity. Then, the polystyrene spherical particle decelerates subjected to the phase interfacial force of the nematic liquid crystal and finally stops moving. The downward displacement of the phase interface occurs at the same time due to the reaction of the phase interfacial force. Although the profile of the phase interface in the liquid crystal cell gap is not as flat, the focusing position of the microscope is set at the center of the liquid crystal gap and the profile

30

Isotropic
phase

N-I phase
interface

Nematic
phase

50μm

$T > T_{NI}$

$T = T_{NI}$

$T < T_{NI}$

(a) $t = $ -9.5s   (b) $t = $ 0s   (c) $t = $ 11.8s
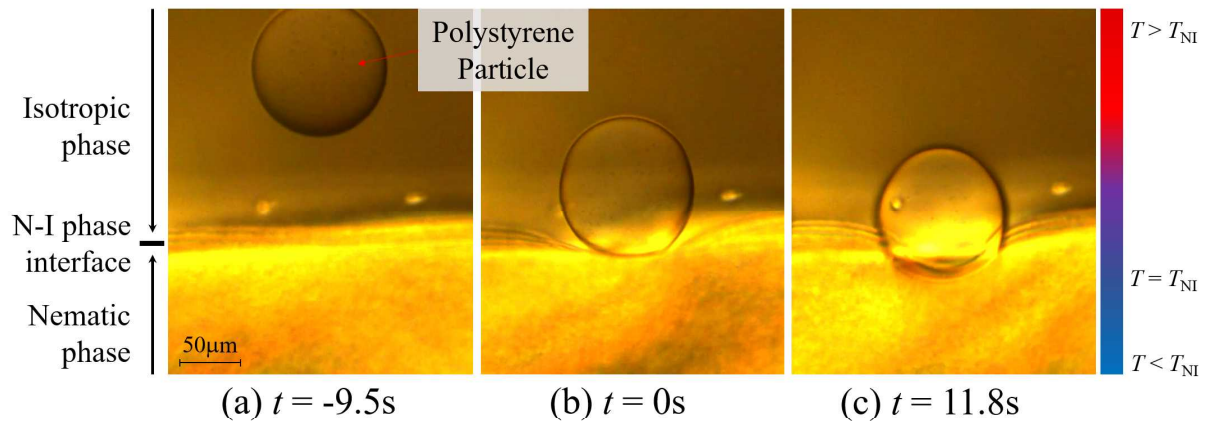
Figure 3.13: A sequence of microscopic images of the nematic-isotropic phase interface ($T_U = $ 39.5°C, $T_L = $ 30.6°C) in 5CB liquid crystal.

Figure 3.14: Displacement of the nematic-isotropic phase interface and the polystyrene particle in 5CB liquid crystal.

31

(a) $t = -1.14\text{s}$ (b) $t = 0\text{s}$ (c) $t = 1.14\text{s}$

Figure 3.15: A sequence of microscopic images of the nematic-isotropic phase interface and glass bead spherical particle in 5CB liquid crystal.

is not taken into account for the definition of the origin of the time and position. In addition, it can be observed from the image analysis data of the spherical particle and phase interface that the deformation of the nematic-isotropic phase interface, which is defined as the maximum deviation of the phase interface, is about 36.7μm at $t = 11.8$s.

3.3.2 Nematic-isotropic phase interface and glass bead particle in 5CB liquid crystal

Figure 3.15 shows the time series of a glass bead spherical particle falling in the nematic liquid crystal (5CB) under a polarized light microscope. The sequential microscopic images show (a) the position of the glass bead spherical particle approaching to the N-I phase interface, (b) the instant contact at the phase interface and (c) after contact with the phase interface. The time $t = 0$s is when the glass bead spherical particle makes contact with the phase interface. As the particle reaches the nematic-isotropic phase interface, the phase interface is slightly deformed, and the glass bead spherical particle breaks through the interface to settle into the nematic phase region. Therefore, a particle that is denser than the liquid crystal itself is unable to be captured by the phase interface of a nematic liquid crystal. Figure 3.16 shows the trajectories of the glass bead spherical particle and the nematic-isotropic phase interface.

From the molecular orientation field of molecules in the isotropic phase in the nematic liquid
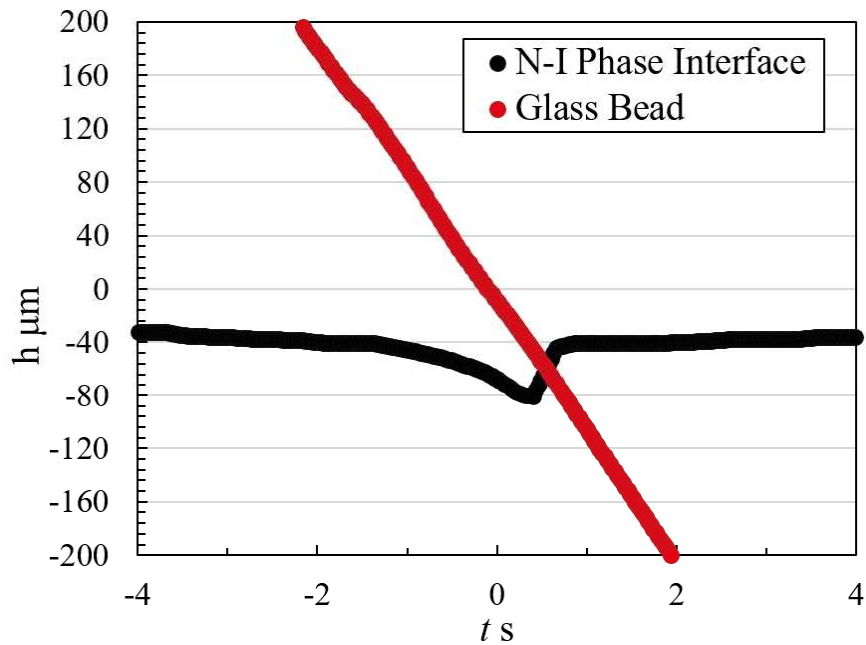
Figure 3.16: Displacement of the nematic-isotropic phase interface and the glass bead particle in 5CB liquid crystal.

crystals, the orientation and center of gravity of the liquid crystal molecules are not well ordered, so the molecules are not restricted in molecular direction. The molecular orientation field in the isotropic phase region is not disturbed by the particle due to the lack of orientation. On the other hand, in the nematic liquid crystal phase, the molecular orientation field is disturbed by the particle due to the certain order in orientation, and the distortion energy generated by the particle in the nematic bulk phase is minimized. A force from the interfacial tension is generated, and the particle is pushed up by the nematic liquid crystal phase into the isotropic phase to achieve a stable state condition, as shown with the polystyrene particle. However, the molecular orientation field is not strong enough to be able to hold the glass bead particle in the phase interface, so the particle freely passes through the phase interface. A schematic representation of the disturbance in the molecular field caused by the particle is shown in Figure 3.17.
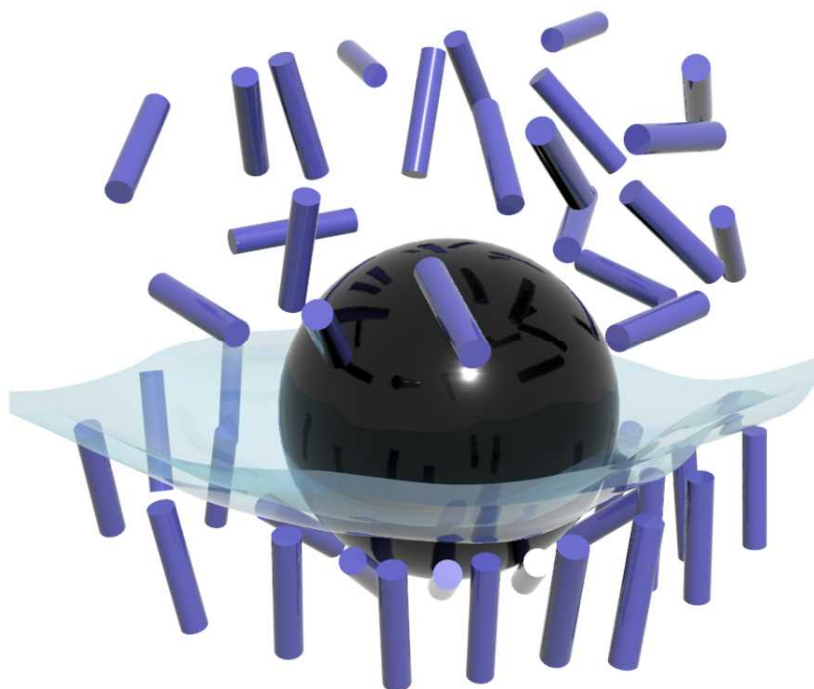
Figure 3.17: Schematic of the nematic and isotropic phases when the particle makes contact with the phase interface. Note that the size of the liquid crystal molecules is about 10^6 smaller compared to the size of the particle itself.

3.3.3 Nematic-isotropic phase interface and polystyrene particle in 8CB liquid crystal

The 4-cyano-4'-octylbiphenyl liquid crystal (8CB) provides phases of smectic to nematic and nematic to isotropic. Figure 3.18 shows the time series of the polarized light microscopic images of a polystyrene particle falling from the isotropic phase into the nematic bulk phase region with temperature difference of $T_U = 46.0°C$ and $T_L = 35.0°C$. The boundary between the isotropic and nematic phases is represented as the nematic-isotropic phase interface. The polarized light microscopic images show (a) the polystyrene particle approaching to the nematic phase region, (b) polystyrene particle making direct contact with the phase interface, and (c) the polystyrene particle remains captured by the phase interface. The disturbance of the molecular orientation field, which is represented similar to the 5CB, allows to create an interfacial force and the polystyrene particle is excluded from the nematic phase region.

The trajectories of the polystyrene particle and the phase interface is represented in Figure 3.19. The behaviors of the polystyrene spherical particle and the phase interface are similar to those for the nematic-isotropic phase interface of 5CB, while the terminal velocity is lower in comparison with that for the 5CB due to a lower viscosity in 8CB. Therefore, due to a weak phase interfacial force in the nematic-isotropic phase interface, the polystyrene particle remains settled in the phase interface after $t > 0s$ with the phase interface having a deformation along the outer shape of the particle.

(a) $t = -7.4$s   (b) $t = 0$s   (c) $t = 15.4$s
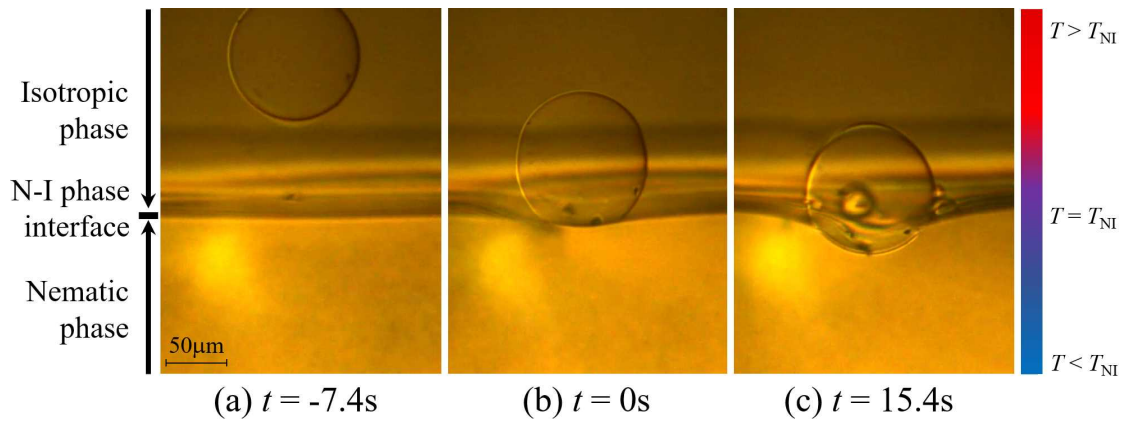
Figure 3.18: A sequence of microscopic images of the nematic-isotropic phase interface ($T_U = 46.0°$C, $T_L = 35.0°$C) of 8CB liquid crystal.
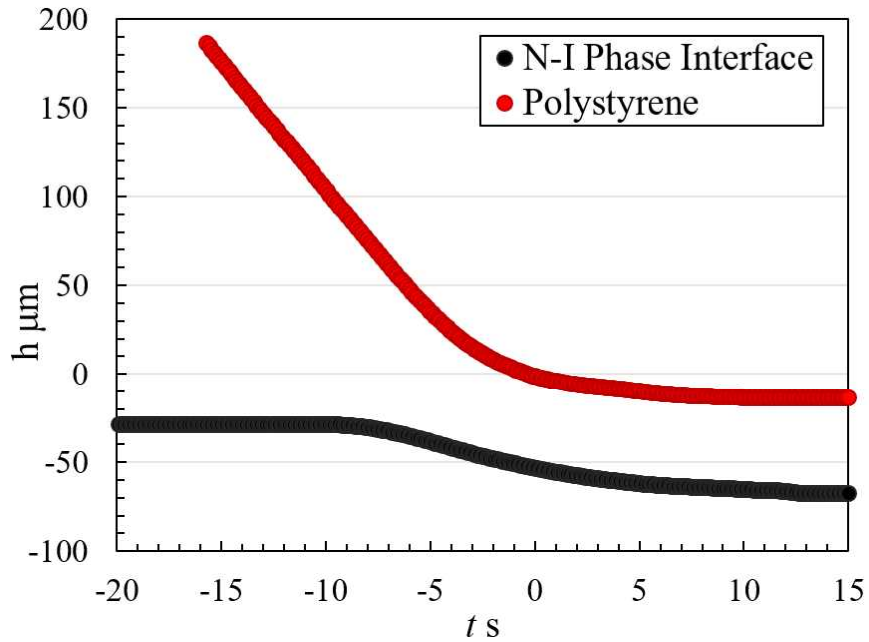

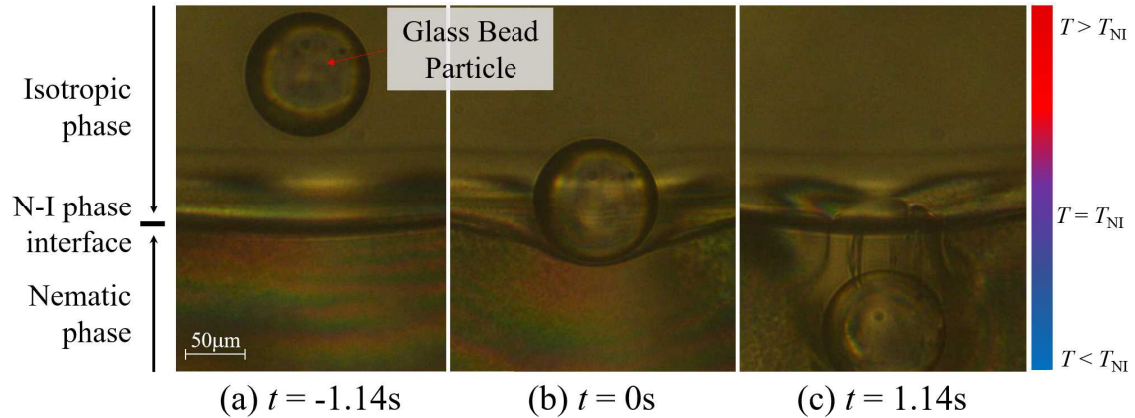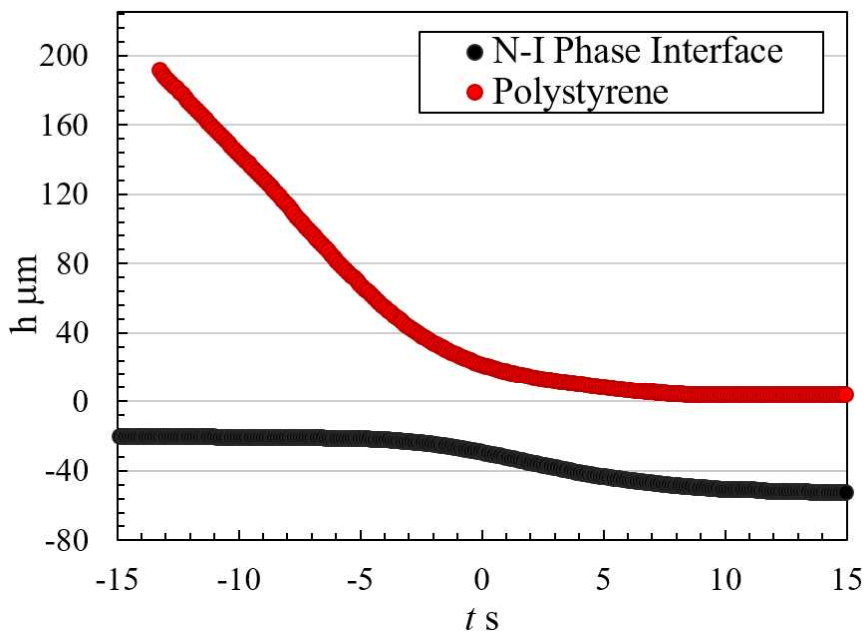Figure 3.19: Displacement of the nematic-isotropic phase interface and the polystyrene particle of 8CB liquid crystal.

3.3.4 Nematic-isotropic phase interface and glass bead particle in 8CB liquid crystal

Figure 3.20 shows the time series of the experimental results of the 8CB liquid crystal material and the glass bead spherical particle. Similar to the temperature conditions from the falling polystyrene particle in 8CB, the temperatures were set $T_U = 46.0\,^\circ\text{C}$ and $T_L = 35.0\,^\circ\text{C}$. The phase interface remains fixed with temperature fluctuation of $\pm 0.01\,^\circ\text{C}$, so the position of the phase interface remaines constant. The polarized light microscopic images show (a) the glass bead particle falling in the isotropic phase region, (b) the particle contacting the nematic-isotropic phase interface, and (c) the particle breaks through the phase interface due to gravity and settles in the nematic phase region. It is observed from the microscopic images that the glass bead spherical particle reaches to a terminal velocity in the isotropic phase region, then insignificant decelerates when approaching to the deformed nematic-isotropic phase interface, and freely passes through the nematic-isotropic phase interface. The nematic-isotropic phase interface is not strong enough to sustain the glass bead particle.

Figure 3.21 shows the trajectories of the nematic-isotropic phase interface and the position of the center of gravity of the glass bead spherical particle obtained from image analysis. The glass bead spherical particle slightly decelerates due to the phase interfacial force from the phase interface, and due to low interfacial force, the particle breaks through the interface. It can be also observed that the position of the phase interfaces changes according to the contact shape of the particle. The glass bead particle passes entirely through the phase interface after $t = 1\text{s}$ at a constant rate. Later, the position of the phase interface is restored after the particle is in the nematic phase.
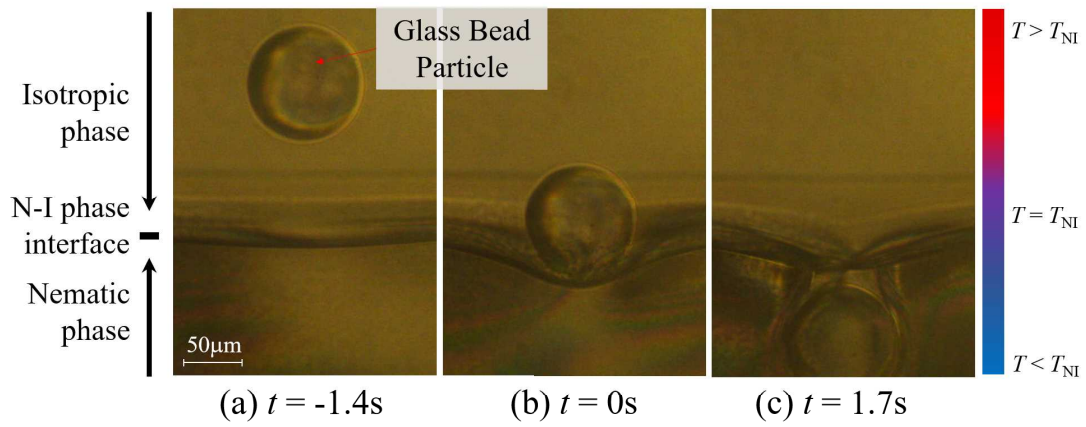
Figure 3.20: A sequence of microscopic images of the nematic-isotropic phase interface ($T_U = 46.0°$ C, $T_L = 35.0°$C) of 8CB liquid crystal.
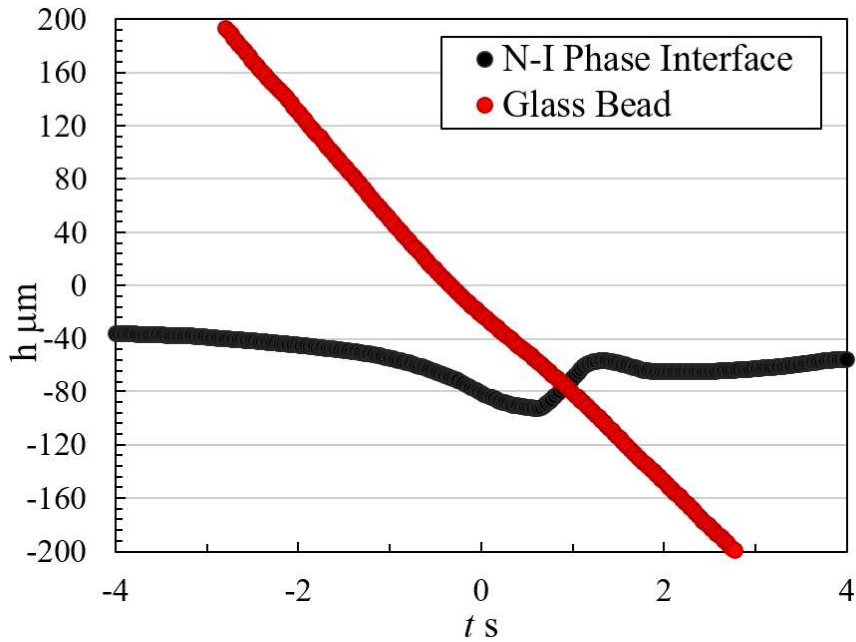
Figure 3.21: Displacement of the nematic-isotropic phase interface and the glass bead spherical particle of 8CB liquid crystal.

3.3.5 Nematic-smectic phase interface and polystyrene particle in 8CB liquid crystal

Figure 3.22 shows the time series of the polarized light microscopic images of a polystyrene spherical particle and the nematic-smectic phase interface of an 8CB liquid crystal. The nematic-smectic phase interface of the 8CB liquid crystal is achieved for $T_U = 37.5$ °C and $T_L = 28.0$ °C. Although the difference in the brightness for the nematic and smectic phase regions are slight, the nematic phase region is identified as the darker region and the nematic-smectic phase interface is at the boundary between the darker nematic and brighter smectic phase regions. Specifically, since the molecules from the molecular orientation structure in 8CB are aligned in both the nematic and smectic phases, the phase interface between the nematic and smectic phases is almost indistinguishable. Therefore, a crossed polarized lens is utilized to distinguish both liquid crystal phases. When the polystyrene spherical particle falls in the nematic phase region, as shown in (a), the distortion in the molecular orientation in the molecular orientation field is confirmed at the surrounded area of the spherical particle. As the spherical particle approaches to the phase interface, the orientationally distorted area shrinks and the spherical particle directly contacts the phase interface at $t < 0$s. Furthermore, since both the nematic and smectic phases are simultaneously pushing the particle up, the smectic bulk phase region is unable to attain the particle at the nematic-smectic phase interface. As a result, the polystyrene particle invades the nematic-smectic phase interface, and breaks through the phase interface due to a weak nematic-smectic phase interfacial force.

Figure 3.23 shows the trajectories of the nematic-smectic phase interface and the polystyrene particle. The spherical particle decelerates due to the interfacial force until it completely falls into the smectic phase region at $t > 81.9$s. Then, the polystyrene particle accelerates to the terminal velocity in the smectic phase region. When the polystyrene particle passes through the nematic-smectic phase interface, a temporal displacement of the phase interface is observed.

Nematic
phase

N-Sm phase
interface

Smectic
phase

50μm

P

A

$T > T_{NSm}$

$T = T_{NSm}$

$T < T_{NSm}$

(a) t = -32.2s (b) t = 0.0s (c) t = 81.9s (d) t = 142.8s
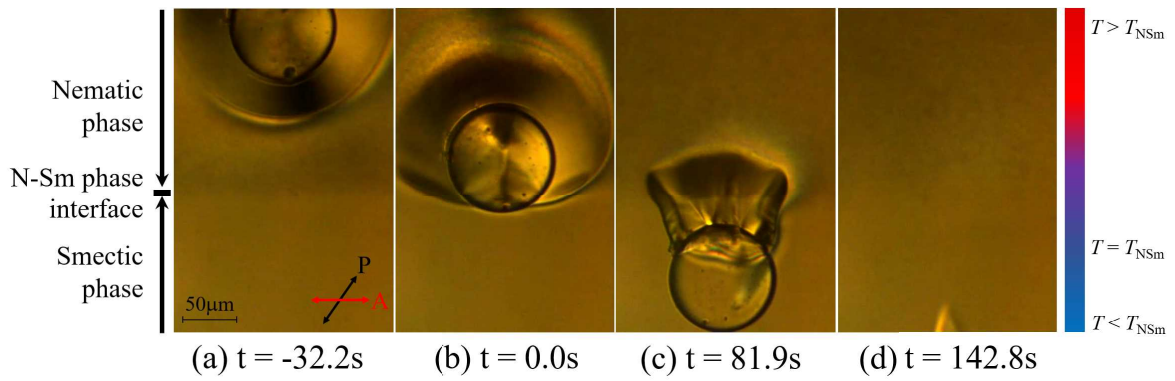
Figure 3.22: Microscopic images of the smectic-nematic phase interface ($T_U = 37.5°$C, $T_L = 28.0°$C) of 8CB liquid crystal.
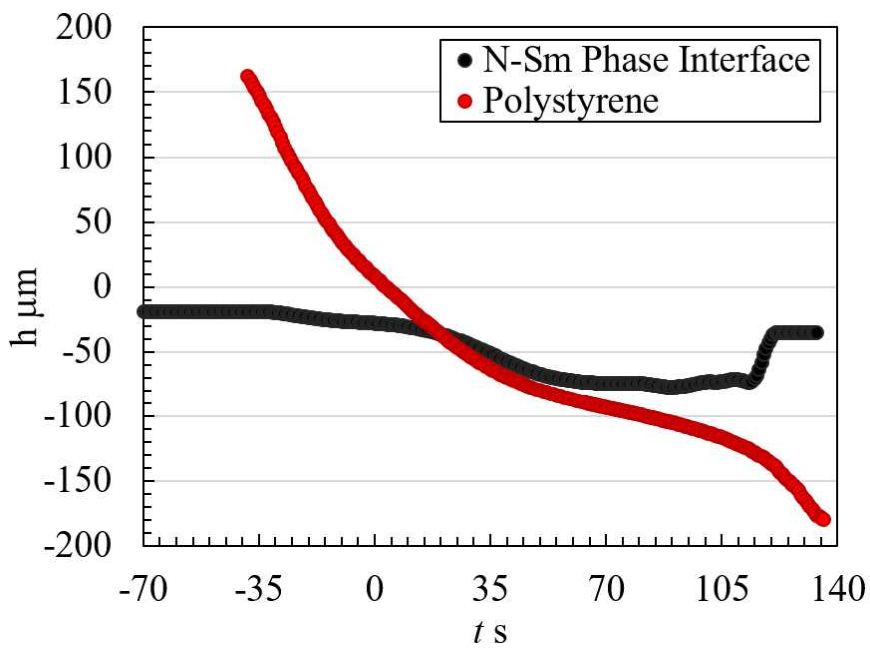
Figure 3.23: Displacement of the nematic-smectic phase interface and the polystyrene spherical particle of 8CB liquid crystal.

40

3.3.6 Nematic-smectic phase interface and glass bead particle in 8CB liquid crystal

Figure 3.24 shows the time series of the nematic-smectic phase interface and a falling glass bead spherical particle with temperature conditions of $T_U = 37.5\ °C$ and $T_L = 28.0\ °C$ of the 8CB liquid crystal. The difference between the nematic phase region and smectic phase region is slightly distinguishable, the nematic phase is identified as the bright region, and the smectic phase is identified as darker phase region. The nematic-smectic phase interface is at the boundary between the bright nematic phase and darker smectic phase region. Note that the analyzer is positioned horizontally and the polarizer is positioned approximately $60°$ counterclockwise. As shown in (a), the glass bead falls in the nematic phase and it is observed from the surrounded area of the particle that the molecular orientation field of the nematic phase region is disturbed. The nematic phase tries to drag the spherical particle after contacting the nematic-smectic phase interface at $t > 0s$. The particle decelerates while trying to break through the phase interface. Although the nematic-smectic phase interface was able to slowly sustain the particle, the particle settles in the smectic phase after $t > 9.8s$. It is observed that the glass bead particle is able to break through the phase interface faster than the polystyrene particle due to higher density.

Figure 3.25 shows the trajectories of the nematic-smectic phase interface and the center of gravity of the glass bead particle. It is observed that the particle accelerates to a terminal velocity once the particle passes entirely to the smectic phase region. The deformed phase interface is restored to a stable nematic-smectic phase interface after $t > 15s$.

(a) t = -3.8s   (b) t = 0.0s   (c) t = 9.8s   (d) t = 43.9s
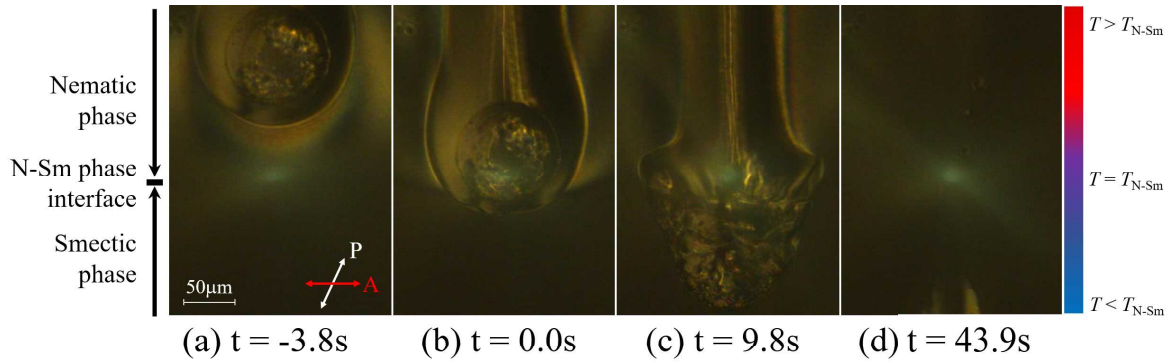
Figure 3.24: Microscopic images of the smectic-nematic phase interface ($T_U = 37.5°C$, $T_L = 28.0°C$) of 8CB liquid crystal.
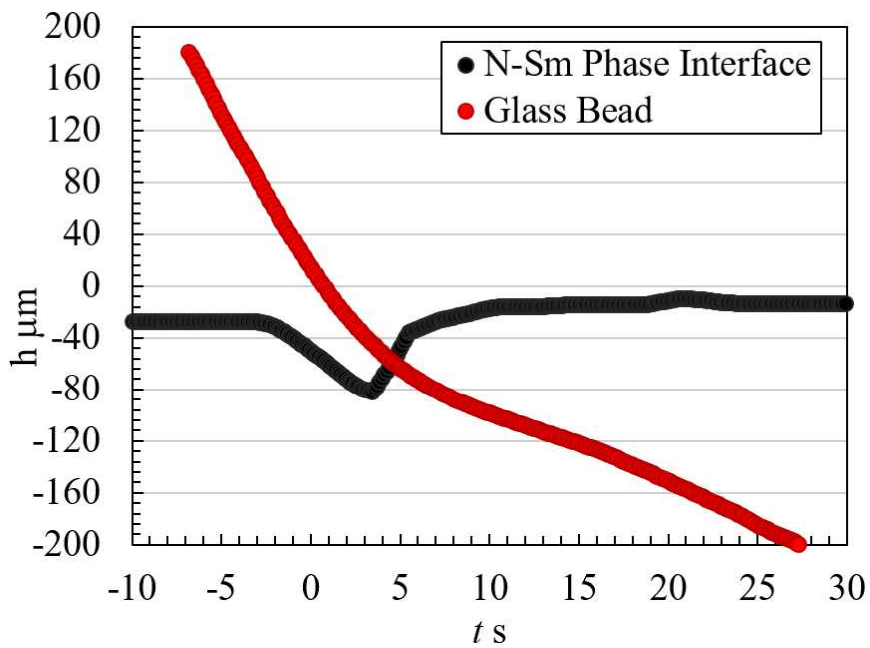
Figure 3.25: Displacement of the nematic-smectic phase interface and the glass bead spherical particle of 8CB liquid crystal.

3.3.7 Smectic-isotropic phase interface and tungsten carbide particle in 12CB liquid crystal

Smectic liquid crystals have been studied due to their high-layered molecular orientational structure properties. Since the smectic liquid crystal molecules have a preferred direction normal to the smectic layers, the distortion energy generated from the disorder of the layered structure in addition to the alignment field of the smectic liquid crystal molecules is eliminated. Therefore, a larger smectic-isotropic phase interfacial force is expected than that for the nematic-isotropic phase interface. The temperature conditions to create the phase interface between the smectic and isotropic phases are $T_U = 63.0$ °C and $T_L = 53.5$ °C. A tungsten carbide particle, with density of 15.93 g/cm^3, is used in our experiments to estimate the phase interfacial force of a 12CB liquid crystal. Figure 3.26 shows the time series of the smectic-isotropic phase interface and a falling tungsten carbide particle, and it demonstrates that the capture of the tungsten carbide spherical particle by the smectic-isotropic phase interface is successfully achieved. Because of the high density of the tungsten carbide spherical particle, the particle rapidly approaches to the phase interface. Even for the high density and high terminal velocity of the particle, the smectic-isotropic phase interfacial force possesses enough strength to decelerate and hold the particle on the phase interface. Since the smectic-isotropic phase interface is the only interface which can stop and capture the tungsten carbide particle, it is obvious that the smectic-isotropic phase interfacial force is greater than the other liquid crystalline phase interfaces.

The time-dependency changes of the tungsten carbide particle and the displacement of the smectic and isotropic phase interface obtained from the light microscopic image analysis is shown in Figure 3.27. The particle is immediately stopped by the phase interface after $t > 0$s with a deformation of the smectic-isotropic phase interface of approximately 80μm at $t = 1.2$s. From the molecular orientation field in the isotropic phase region of the 12CB liquid crystal, the orientation and center of gravity of the liquid crystal molecules are not well ordered, so the molecules are not restricted in molecular direction. Moreover, the molecular orientation in the isotropic phase region is not disturbed by the particle due to the lack of orientation structure. Because of a well-defined layered structure, the disturbance of the smectic phase region is small, and the particle is attained in

43

(a) t = -0.2s   (b) t = 0s   (c) t = 1.2s
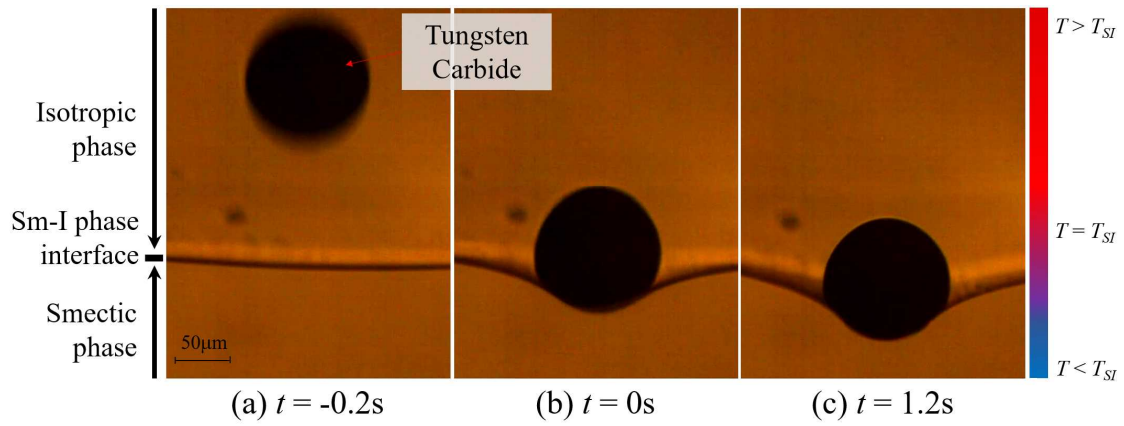
Figure 3.26: Microscopic images of the smectic-isotropic phase interface ($T_U = 63.0°C$, $T_L = 53.5°C$) of 12CB liquid crystal.
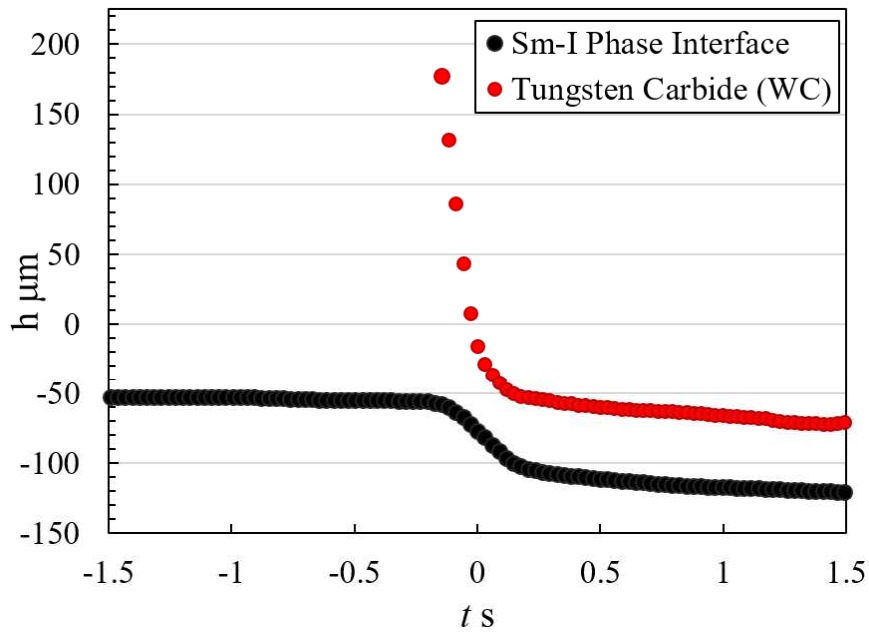
Figure 3.27: Displacement of the smectic-isotropic phase interface and the tungsten carbide particle of 12CB liquid crystal.
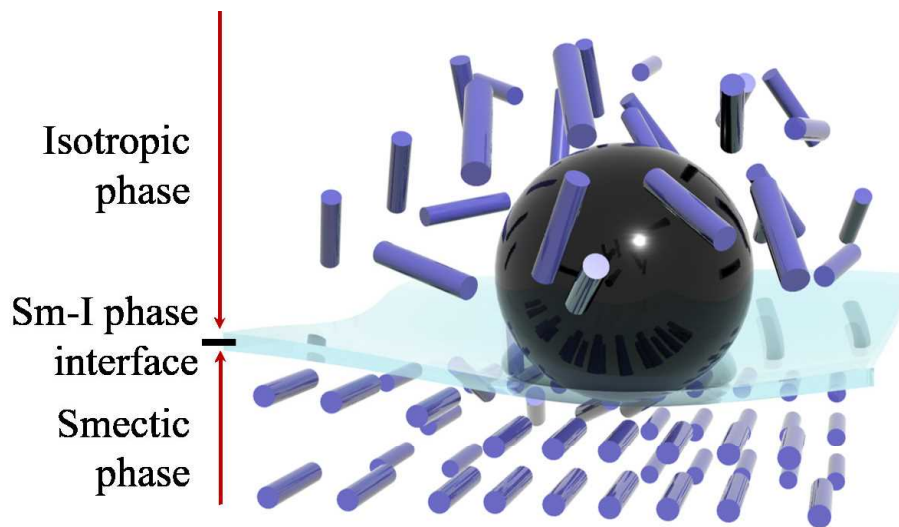
Figure 3.28: Schematic of the smectic and isotropic phases when the particle makes contact with the phase interface. The smectic liquid crystal has higher alignment order of molecules compared to that for the nematic liquid crystal

the isotropic region, detailed shown in Figure 3.28. Therefore, a force from the interfacial tension is generated, and the particle is pushed up by the smectic liquid crystal phase into the isotropic phase to achieve a stable state condition. In reality, while the particle size is approximately 100μm, the length of the liquid crystal molecules is about 10^6 times smaller compared to the size of the particle.

3.4 Numerical Calculations
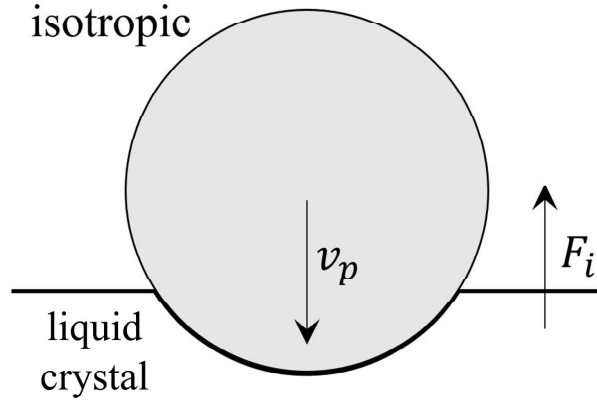
Figure 3.29: Schematic of the particle with acting forces on the particle and the phase interface.

To support the analysis of the interfacial force from the experimental results, the force acting on the particle and the phase interface is considered, as shown in Figure 3.29. The interfacial force between the liquid crystal and isotropic phases is estimated through the evaluation of forces acting on the particle based on experimental results. The forces acting on the particle are the gravitational acceleration force F_g, the buoyancy force F_b, the drag force F_d, and the phase interfacial force F_i, respectively. Therefore, the equation of motion is expressed as

$$m\frac{dv_p}{dt} = F_i - F_g + F_b - F_d. \tag{3.1}$$

Here, m is the mass of the particle, and v_p is the velocity due to gravity of the particle. The fluid resistance force is applied based on the Stoke's resistance law acting on the particle falling from the isotropic viscous fluid to the liquid crystal phase. It is noted that the velocity of the captured particle is constant at the phase interface. Since the Reynold's number is relatively small for both nematic and smectic, the Stoke's drag force is applicable. Therefore, the equation to determine the phase interfacial force of liquid crystals is written as follows,

$$F_i = \left(\rho_P \frac{dv_p}{dt} + (\rho_P - \rho)g\right) \frac{\pi d^3}{6} + 3\pi d\mu v_p. \tag{3.2}$$

Here, ρ_p is the density of the particle, ρ is the density of the liquid crystal material, d is the diameter of the particle, g is the gravitational acceleration of the particle, and μ is the viscosity of the liquid crystal material.

From the phase interfacial force equation, the acceleration, dv_p/dt, and velocity, v_p, of the particle are numerically obtained and derived by the finite difference technique and Savitzky-Golay from the numerical data of the particle. The Savitzky-Golay [44] is defined as a filter to optimize and smooth a set of data points to a local least-squared polynomial approximation without distortion in the signal tendency. The Savitzky-Golay filter is expressed as

$$y_j = \sum_{i=\frac{1-k}{2}}^{\frac{k-1}{2}} a_i x_{j+i}, \tag{3.3}$$

where k is the set of number of data points, and a_i is the convolution coefficients. Figure 3.30 shows the trajectories of the particle and nematic-isotropic phase interface using the Savitzky-Golay filter technique. The red line depicts the original position of a falling polystyrene particle, and the blue line depicts the Savitzky-Golay filter technique imposed to the trajectories of the falling particle. It is obvious that the line is smoothed without affecting the extracted signals. Due to smoothing of the trajectories of the falling particle, the results for the acceleration a of the particle is enhanced, as shown in Figure 3.31. The red line shows the distorted acceleration from the results utilizing the finite difference technique and the black line shows the imposed Savitzky-Golay filter. It is found that the highest acceleration of the particle can easily be determined through the use of the filter.

For the case of 5CB liquid crystal, the following material properties were used: $\rho = 1008$ kg/m^3 and $\mu = 0.023$ Pa·s [45, 46]. The polystyrene particle falling in the isotropic phase region falls with a maximum acceleration of 1.6μm/s^2. The phase interfacial force for the nematic-isotropic phase interface is able to stop the particle from breaking through the phase interface. However, the maximum interfacial force cannot be determined for the case of the polystyrene particle in 5CB since the interfacial force becomes the maximum when the position of the phase interface
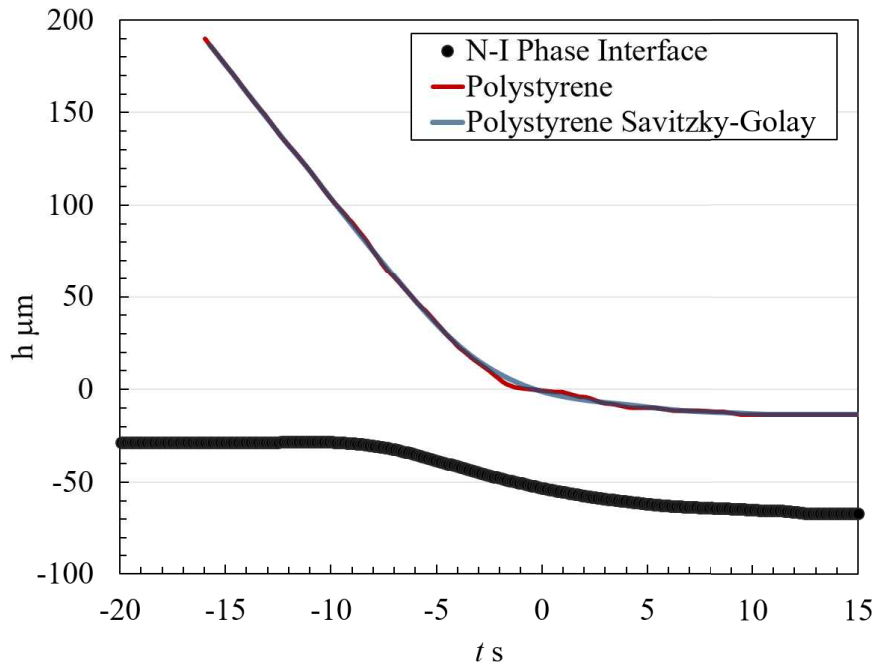
Figure 3.30: Trajectories of the nematic-isotropic phase interface and polystyrene particle with and without the use of the Savitzky-Golay technique.
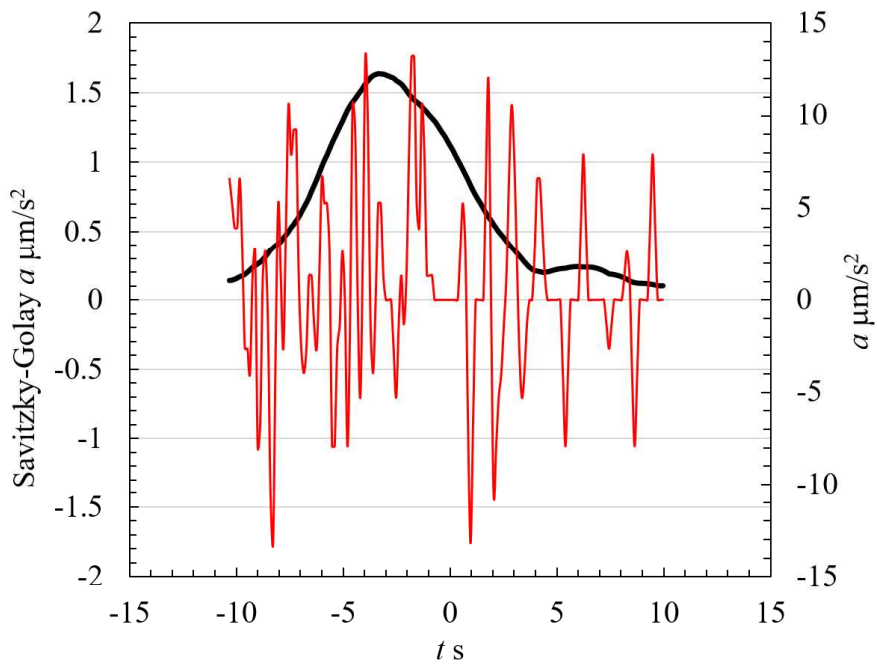
Figure 3.31: Results of the acceleration of the falling particle using the finite difference technique (red) and Savitzky-Golay technique (black).

coincides with the center of the spherical particle. For the case of the glass bead particle, the particle reaches to a maximum acceleration of 23.3μm/s^2, and starts to decelerate while breaking through the nematic-isotropic phase interface. Since the glass bead particle was able to break through the phase interface, it is calculated that the maximum average interfacial force for the nematic-isotropic phase interface is approximately 5.5±0.8nN.

For the 8CB liquid crystal, the following material properties were used: ρ = 978 kg/m^3 for the nematic-isotropic [47] and ρ = 989 kg/m^3 for the nematic-smectic [19], and μ = 0.024 Pa·s for the nematic-isotropic [46] and μ = 0.111 Pa·s for the nematic-smectic [48]. We can observe that the polystyrene particle falls from the isotropic phase region to the nematic phase region with a maximum acceleration of 1.69μm/s^2. Similar to the 5CB liquid crystal, the 8CB liquid crystal is able to hold the particle on the nematic-isotropic phase interface. Since the maximum interfacial force can only be determined when the center of the particle and the phase interface coincides, the maximum interfacial force cannot be determined with the polystyrene particle. Therefore, a glass bead particle is used in order to determine the maximum interfacial force. It is observed that the glass bead particle reaches to a maximum acceleration of 17.2μm/s^2 and it starts to decelerate while passing through the nematic-isotropic phase interface. It is calculated that the maximum interfacial force for the 8CB nematic-isotropic phase interface is approximately 5.9±0.7nN.

For the nematic and smectic phases in the 8CB liquid crystal, both the nematic and smectic phases are pushing the particle simultaneously, and the particle invades the high-layered molecular structure of the smectic liquid crystal with a maximum acceleration of 0.11μm/s^2. The polystyrene particle is dragged by the nematic phase region, but the phase interfacial force is not strong enough to hold the particle. As a result, the polystyrene particle invades the nematic-smectic phase interface and passes through the nematic-smectic phase interface with a maximum interfacial force of 1.04±0.1nN. For comparison purposes, we used a spherical glass bead to determine the maximum interfacial force of the nematic-smectic phase interface in 8CB liquid crystal. Similar to the polystyrene particle, the particle travels through the nematic phase region and reaches to a maximum acceleration at 1.93μm/s^2 while breaking through the smectic phase region at $t = 2.7$s.

49

Therefore, the distortion in the molecular orientation field is confirmed at the surrounded area of the spherical particle while it shrinks when approaching to the phase interface. The glass bead particle breaks slowly through the nematic-smectic phase interface and it is determined that the maximum phase interfacial force is approximately 1.3 ± 0.1nN.

Now we focus on the interaction between a tungsten carbide particle and the phase interface of a 12CB liquid crystal with material properties of ρ = 1000 kg/m^3 and μ = 0.01752 P·s [49]. The density of the tungsten carbide particle is approximately 15 times more than the density of the 12CB liquid crystal, and the particle is able to reach stationary state after contact with the phase interface with a maximum acceleration of $13660.6\pm388.2\mu$m/s^2. Since the smectic-isotropic phase interface is the only interface in which can stop and capture the tungsten carbide spherical particle, it is obvious that the smectic-isotropic phase interfacial force is greater than the other liquid crystalline phase interfaces. From the developed program, it is determined that the smectic-isotropic phase interfacial force for the 12CB liquid crystal is approximately 76.1 ± 1.1nN, which is about 13 times stronger than the recently calculated 5CB liquid crystal maximum phase interfacial force (utilizing the glass bead particle). However, the smectic-isotropic phase interfacial force is not the maximum interfacial force since the tungsten carbide particle could not break through the phase interface.

A detailed summary of the interfacial force of the 5CB, 8CB and 12CB is demonstrated in Table 3.4. Based on the current experimental results, the interfacial force of the 12CB liquid crystal is the strongest of all the liquid crystalline materials tested. Therefore, the potential development of better micromanipulator systems can be utilized for a better and stronger driving source by utilizing the phase interface of a 12CB liquid crystal.

Table 3.4: Experimental values of the interfacial force of different liquid crystal materials

Liquid Crystal Material	Phases	Particle	Force [nN]
5CB	Nematic-Isotropic	Glass Bead	5.5 ± 0.8
8CB	Nematic-Isotropic	Glass Bead	5.9 ± 0.7
	Nematic-Smectic	Glass Bead	1.3 ± 0.1
12CB	Smectic-Isotropic	Tungsten Carbide	$> 76.1 \pm 1.1$

3.5 Theoretical Models

The energy densities due to the disturbance of the molecular alignment fields, which are represented by the director $\mathbf{n}$ and/or layer normal to $\nabla \phi$, for the isotropic, nematic, and smectic-A phase regions are described as [21]

$$\text{Isotropic phase: } f_I = f_0 \tag{3.4}$$

$$\text{Nematic phase: } f_N = f_0 + \frac{1}{2}\left(K_1(\nabla \cdot \mathbf{n})^2 + K_2(\mathbf{n} \cdot \nabla \times \mathbf{n})^2 + K_3|\mathbf{n} \times \nabla \times \mathbf{n}|^2\right) \tag{3.5}$$

$$\text{Smectic-A phase: } f_S = f_0 + \frac{1}{2}\left(K_1(\nabla \cdot \mathbf{n})^2 + K_2(\mathbf{n} \cdot \nabla \times \mathbf{n})^2 + K_3|\mathbf{n} \times \nabla \times \mathbf{n}|^2\right)$$
$$+ \frac{1}{2}(\mathbf{n} - \nabla \phi)^T \mathbf{B}(\mathbf{n} - \nabla \phi) \tag{3.6}$$

where f_0 is the energy associated with the equilibrium condition of the liquid crystal material, and $\mathbf{B} = B_\perp \mathbf{I} + (B_\parallel - B_\perp)\mathbf{nn}$. The scalar function ϕ is parametrized by iso-surfaces of the smectic layers. From these equations, the energy caused by the disturbance of the spherical particle in the liquid crystal phases has the relationship of $f_S > f_N > f_I$, leading to the relationship of $P_S > P_N > P_I$, where P_S, P_N, and P_I are the stresses at the surface of the particle exerted by the smectic-A, nematic, and isotropic phases, respectively.

Figure 3.32 shows the schematic of the particle at the nematic-isotropic phase interface. The origin O of the coordinate x is positioned at the center of the particle and x_i is defined as the position of the nematic-isotropic phase interface. The direction of the stress is normal to the surface of the particle, and the total force acting on the particle is the sum of the forces exerted by the isotropic
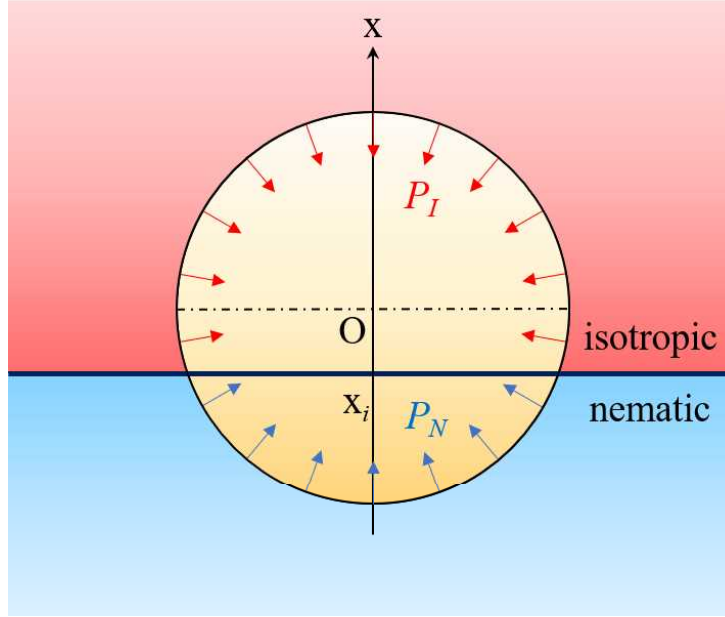
Figure 3.32: Schematic of the particle and interface with stresses acting on the surface of the particle by the nematic and isotropic phases, respectively.

and nematic phases, which are derived by integrating the stress over the surface immersed in each phase as follows,

$$F_{IN}^{\text{total}} = F_I + F_N = \int_{x_i}^{R} 2\pi \sqrt{R^2 - x^2} \frac{x}{R} P_N dx + \int_{-R}^{x_i} 2\pi \sqrt{R^2 - x^2} \frac{x}{R} P_I dx. \qquad (3.7)$$

Since the stress in the $|x| < |x_i|$ region is eliminated and has no contribution on the total force, the above equation is simplified as

$$F_{NI}^{\text{total}} = 2\frac{\pi}{R}(P_N - P_I)\int_{|x_i|}^{R} x\sqrt{R^2 - x^2}dx = \frac{2\pi}{3R}(P_N - P_I)\sqrt{(R^2 - x_i^2)^3}. \qquad (3.8)$$

In the same manner, the total forces acting on the particle at the nematic-smectic-A and the
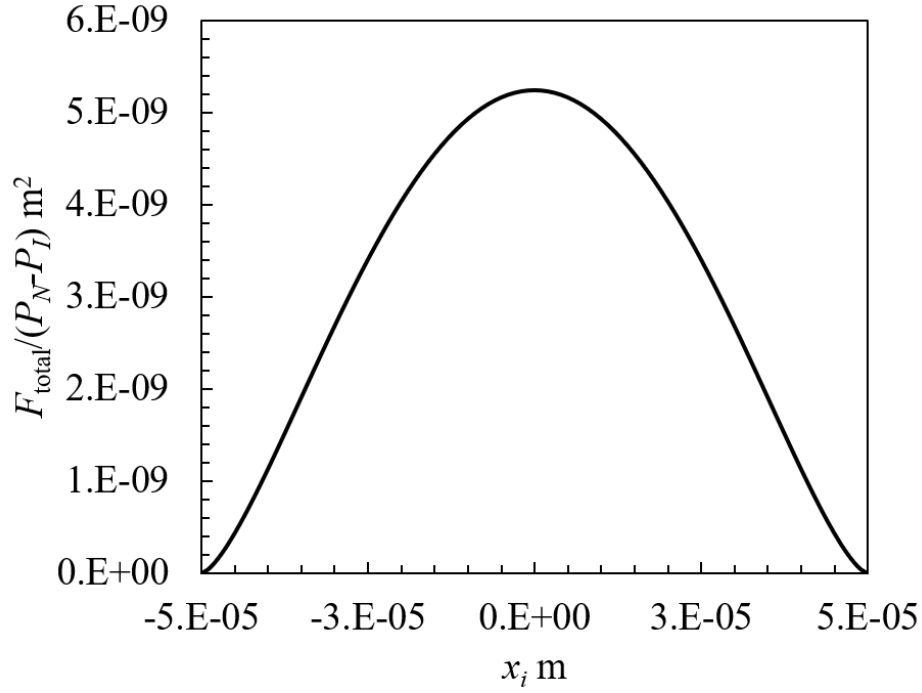
Figure 3.33: The effect of the position of the interface based on the force acting on the particle.

isotropic-smectic-A phase interfaces are derived as

$$F_{SN}^{\text{total}} = \frac{2\pi}{3R}(P_S - P_N)\sqrt{(R^2 - x_i^2)^3},$$
$$F_{SI}^{\text{total}} = \frac{2\pi}{3R}(P_S - P_I)\sqrt{(R^2 - x_i^2)^3}.$$

(3.9)

Figure 3.33 shows the effect of the position of the interface on the force acting on the particle obtained from Equation 3.8. The interfacial force becomes the maximum when the position of the interface coincides with the center of the spherical particle with a maximum value of $5.2 \times 10^{-9} \text{m}^2$ at $x_i = 0$. The maximum forces for the phase interfaces are then simplified as follows,

$$F_{NI}^{\max} = \frac{2\pi}{3}(P_N - P_I)R^2,$$
$$F_{SN}^{\max} = \frac{2\pi}{3}(P_S - P_N)R^2,$$
$$F_{SI}^{\max} = \frac{2\pi}{3}(P_S - P_I)R^2.$$

(3.10)

Therefore, only the spherical particles breaking through the phase interface of the liquid crystals

53

can be utilized to determine the maximum interfacial force. As explained before, the interfacial force becomes the maximum when the position of the phase interface coincides with the center of the spherical particle. The glass bead particles are the only particles in our experiments that can determine the maximum interfacial force for 5CB and 8CB liquid crystals.

3.6 Normal stresses

By utilizing the phase interfacial force results from Table 3.4 with the Equations (3.10), the normal stresses are evaluated as shown in Table 3.5. Based on the results of the normal stress, the maximum force of the interfacial force is suitable regardless of shape and size of the particle. Note that for the case of P_S for the 12CB liquid crystal, the particle could not pass through the smectic-isotropic phase interface, since the particle is captured by the interface before the interfacial force reaches its maximum value.

Table 3.5: Normal stress values of different liquid crystal materials

Material	Phase	Normal Stress [N/m^2]
5CB	Nematic	1.06 ± 0.15
8CB	Nematic	1.13 ± 0.13
	Smectic-A	1.37 ± 0.15
12CB	Smectic-A	>14.5

3.7 The phase interfaces of a 6CB, 7CB, 9CB and 11CB, and a falling spherical particle

To expand the phase interfacial forces of other liquid crystal materials, four distinctive thermotropic liquid crystals materials have been chosen (4-cyano-4'-hexylbiphenyl (6CB), 4-cyano-4'-heptylbiphenyl (7CB), 4-cyano-4'-nonylbiphenyl (9CB), and 4-cyano-4'-undecylbiphenyl (11CB)), as shown in Table 3.6, respectively. The nematic-isotropic phase interface appears at temperature of $T = 30.1\,^{\circ}\text{C}$ in 6CB, $T = 42.8\,^{\circ}\text{C}$ in 7CB, and $T = 49.5\,^{\circ}\text{C}$ in 9CB, the smectic-isotropic phase interface at $T = 57.5\,^{\circ}\text{C}$ in 11CB. The stable phase interfaces are created by controlling the temperature distribution of the liquid crystal materials. For this case, a polystyrene particle of diameter

100μm and a tungsten carbide particle of diameter 100μm are chosen for this study.

Table 3.6: Summary of the thermotropic liquid crystal phases with a phase transition temperature [1]

Thermotropic liquid crystals	Phase transitions [°C]			
4-cyano-4'-hexylbiphenyl (6CB)	Crystal		$\xrightarrow{14.3}$ Nematic	$\xrightarrow{30.1}$ Isotropic
4-cyano-4'- heptylbiphenyl (7CB)	Crystal		$\xrightarrow{30.0}$ Nematic	$\xrightarrow{42.8}$ Isotropic
4-cyano-4'-nonylbiphenyl (9CB)	Crystal	$\xrightarrow{42.0}$ Smectic	$\xrightarrow{48.0}$ Nematic	$\xrightarrow{49.5}$ Isotropic
4-cyano-4'-undecylbiphenyl (11CB)	Crystal	$\xrightarrow{53.0}$ Smectic		$\xrightarrow{57.5}$ Isotropic

3.7.1 Nematic-isotropic phase interface and polystyrene particle in 6CB liquid crystal

Figure 3.34 shows the time series of the polarized light microscopic images of a polystyrene particle and the nematic-isotropic phase interface of a 6CB liquid crystal, for temperatures of $T_U = 42.0$ °C and $T_L = 16.0$ °C. The polystyrene particle falls in the isotropic phase region with a terminal velocity towards the phase interface for $t < 0$s until it contacts the phase interface. After the polystyrene particle contacts the nematic-isotropic phase interface, the particle is captured by the phase interface and remain settled for $t > 0$s. It is observed that the nematic-isotropic phase interfacial force for the 6CB is strong enough to hold the particle from passing through the phase interface. The trajectories of the center of gravity of the polystyrene particle and the phase interface of 6CB is shown in Figure 3.35. The horizontal axis h is the displacement of the particle and the phase interface, and its origin is defined as the position of the center of gravity at $t = 0$s. Similar to the 5CB liquid crystal, the downward displacement of the phase interface occurs apparently at the same time due to the skew of the interface.
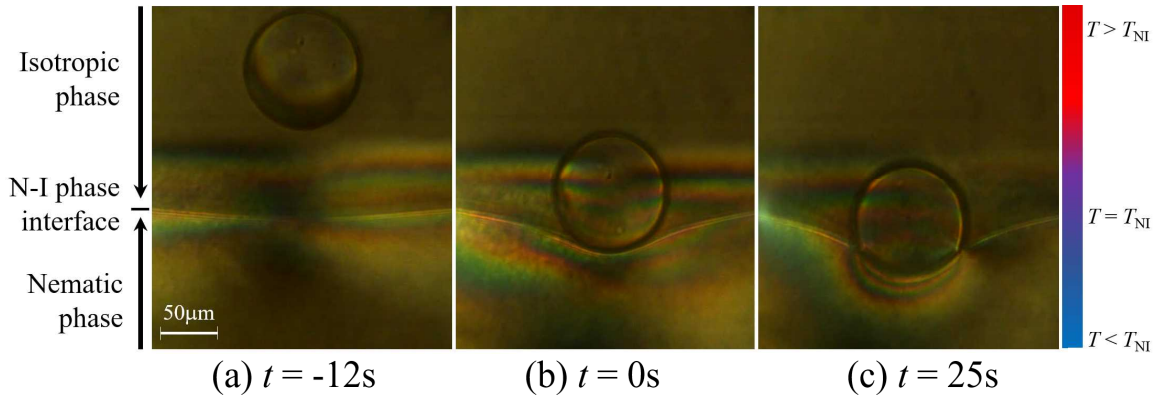
Figure 3.34:   A sequence of microscopic images of the nematic-isotropic phase interface ($T_U = 42.0°C$, $T_L = 16.0°C$) of 6CB liquid crystal.

Figure 3.35:   Displacement of the nematic-isotropic phase interface and the polystyrene particle of 6CB liquid crystal.

3.7.2 Nematic-isotropic phase interface and polystyrene particle in 7CB liquid crystal

Figure 3.36 shows the time series of the polarized light microscopic images of a polystyrene particle and the nematic-isotropic phase interface of a 7CB liquid crystal, for temperatures of $T_U = 55.0\,°C$ and $T_L = 34.0\,°C$. The bright and dark areas in the images correspond to the isotropic and nematic phases, and the horizontal line between the phases is the nematic-isotropic phase interface. From the images, the polystyrene particles fall towards the phase interface with a terminal velocity. When the particle contacts the phase interface, the particle remains settle on the phase interface. After $t > 23.8$s, it is observed that the phase interfacial force is not strong enough to hold the polystyrene particle; thus, the particle breaks through the phase interface. In addition, the deformation of the phase interface is minimal. The trajectories of the nematic-isotropic phase interface and the polystyrene particle for 7CB is shown in Figure 3.37. From the figure, it is observed that the polystyrene spherical particle reaches to a terminal velocity for $t < 0$s. Then the velocity of the particle decreases and is temporarily trapped on the phase interface. At $t = 23.0$s, it is observed that the particle slowly passes through the phase interface. It has been proven that the phase interfacial force for the 7CB is the weakest in comparison to the other thermotropic liquid crystals.

3.7.3 Nematic-isotropic phase interface and polystyrene particle in 9CB liquid crystal

Figure 3.38 shows the time series of the polarized light microscopic images of a polystyrene spherical particle and the nematic-isotropic phase interface of a 9CB liquid crystal material, for temperatures of $T_U = 55.0\,°C$ and $T_L = 46.0\,°C$. It is observed from the images that the polystyrene particle starts falling from the isotropic phase region towards the nematic-isotropic phase interface. After the polystyrene particle makes contact to the phase interface, at $t > 0$s, the particle remains captured on the phase interface. It is observed that the disturbance of the nematic phase region caused by the polystyrene spherical particle is minimal. The phase interfacial force for the 9CB liquid crystal is strong enough to capture the polystyrene particle. The trajectories of the nematic-isotropic phase interface of a 9CB and the falling polystyrene spherical particle is shown
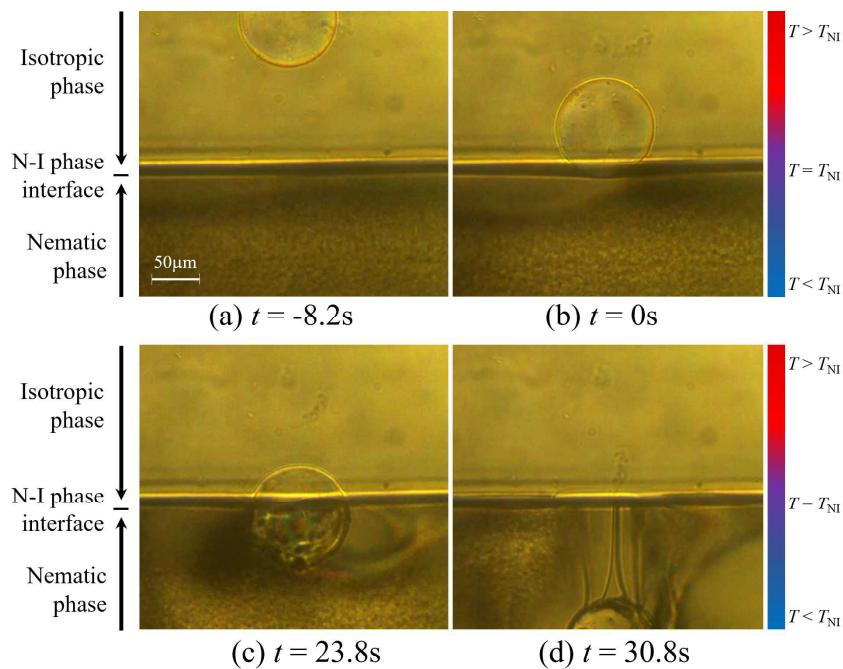
Figure 3.36: A sequence of microscopic images of the nematic-isotropic phase interface ($T_U = 55.0°C$, $T_L = 34.0°C$) of 7CB liquid crystal.

Figure 3.37: Displacement of the nematic-isotropic phase interface and the polystyrene particle of 7CB liquid crystal.

Isotropic phase

N-I phase interface

Nematic phase

50μm

$T > T_{NI}$

$T = T_{NI}$

$T < T_{NI}$

(a) $t = -6.7$s   (b) $t = 0$s   (c) $t = 5.0$s
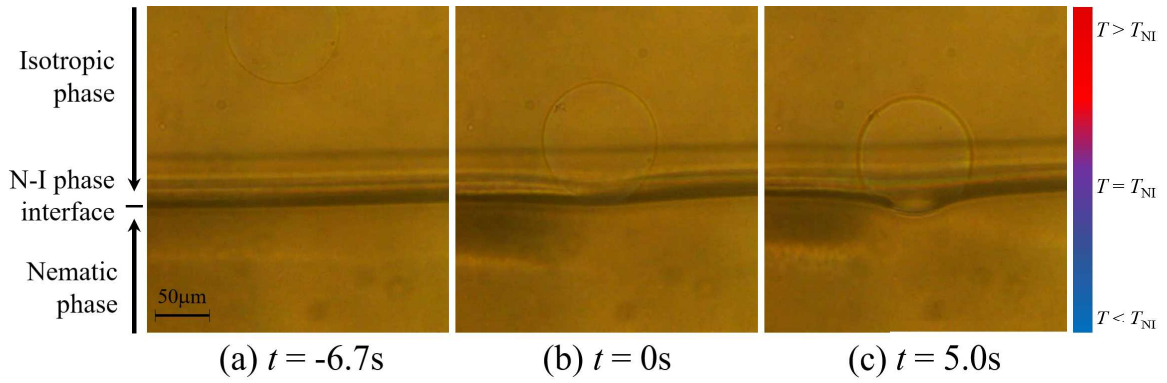
Figure 3.38:   A sequence of microscopic images of the nematic-isotropic phase interface ($T_U = 55.0°$C, $T_L = 46.0°$C) of 9CB liquid crystal.
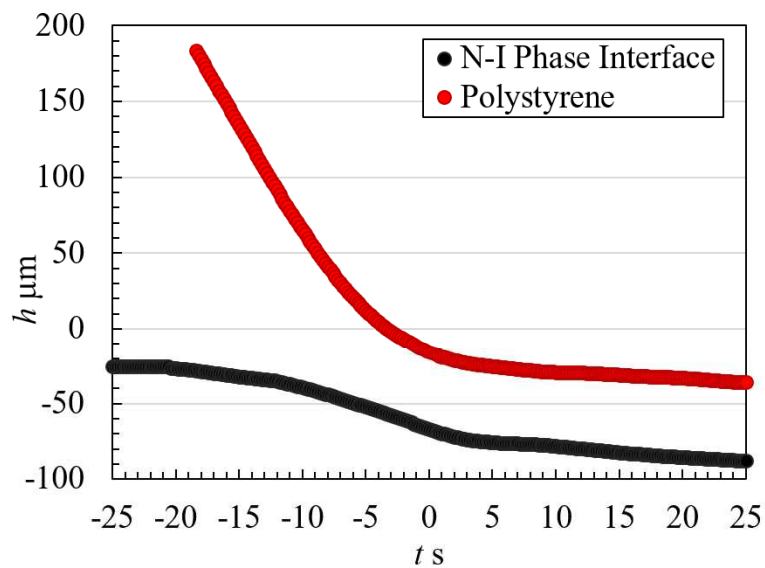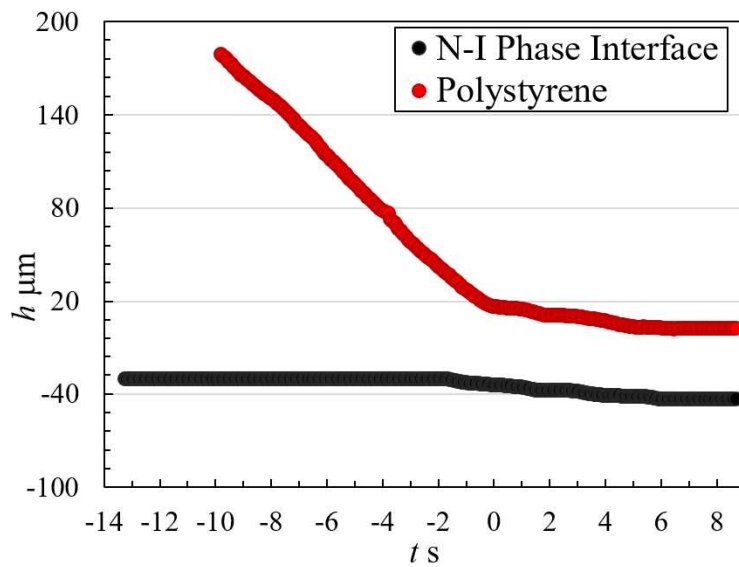

Figure 3.39:   Displacement of the nematic-isotropic phase interface and the polystyrene particle of 9CB liquid crystal.

59

in Figure 3.39. It is observed from the trajectories of the particle that the particle reaches a terminal velocity for $t < 0$s. As soon as the particle contacts the phase interface, the particle remains settled on the phase interface with minimal disturbance in the nematic phase region. It is found the deformation of the phase interface is minimal. Due to low deformation on the phase interface caused by the polystyrene particle, it is understandable that the nematic-isotropic phase interfacial force for the 9CB is stronger than the 5CB, 6CB, 7CB and 8CB.

3.7.4   Smectic-isotropic phase interface and polystyrene particle in 12CB liquid crystal

Figure 3.40 shows the time series of the polarized light microscopic images of a tungsten carbide particle and the smectic-isotropic phase interface of an 11CB liquid crystal, for temperatures of $T_U = 63.0$ °C and $T_L = 54.0$ °C. From the figure, the smectic-isotropic phase interface can be observed as a dark horizontal line, and the upper and lower areas correspond to the smectic and isotropic phase interfaces. Due to the high density of the tungsten carbide particle, the particle falls with a terminal velocity from the isotropic phase region and the particle is captured by the smectic-isotropic phase interface. Furthermore, the tungsten carbide particle remains settled on the smectic-isotropic phase interface at $t > 1.08$s.

The trajectories of the smectic-isotropic phase interface of an 11CB and the tungsten carbide particle is shown in Figure 3.41. It is observed that the tungsten carbide particle rapidly approaches to the phase interface with a terminal velocity. It is found that the 11CB smectic-isotropic phase interfacial force possesses enough strength to decelerate and capture the tungsten carbide particle on the phase interface. Therefore, it is found that only the 11CB and 12CB liquid crystals in our study are able to capture the tungsten carbide particle, and the phase interfacial force for the 11CB and 12CB is extremely large and applicable for future micromanipulator systems.
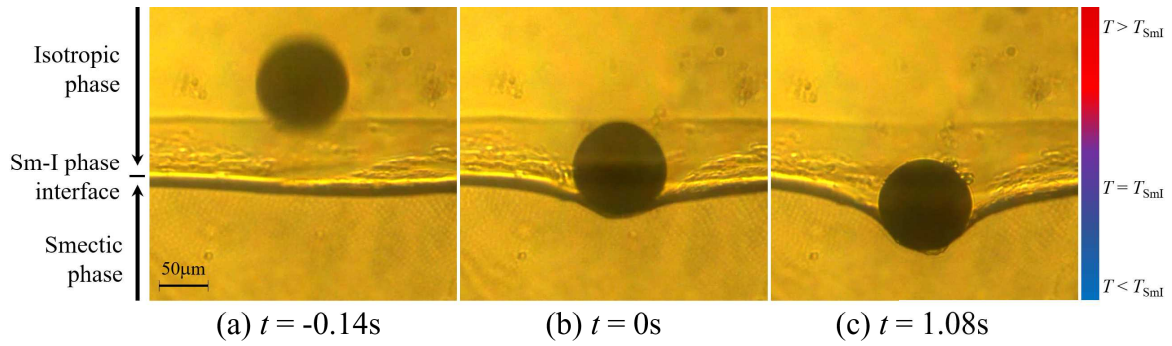
Figure 3.40: A sequence of microscopic images of the nematic-isotropic phase interface ($T_U = 63.0°C$, $T_L = 54.0°C$) of 11CB liquid crystal.
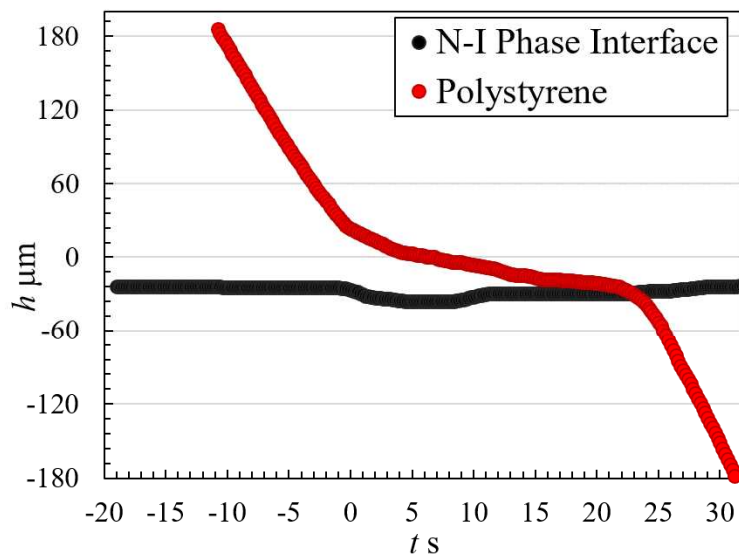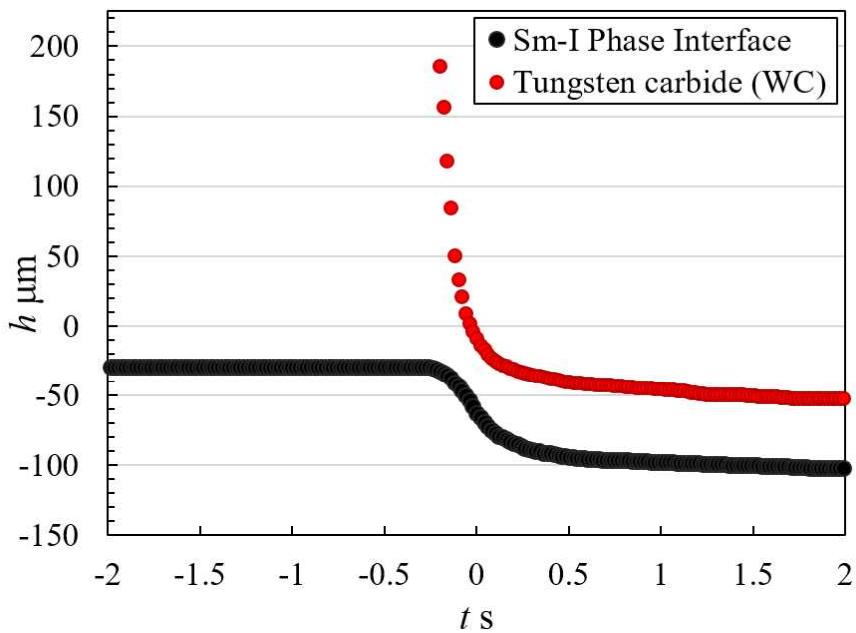

Figure 3.41: Displacement of the smectic-isotropic phase interface and the tungsten carbide particle of 11CB liquid crystal.

3.8 Conclusion

In this study, for the purpose of developing better manipulator systems utilizing the phase interfacial force of liquid crystals and expanding the application of a liquid crystal micromanipulators, we have demonstrated experimental results of the phase interfacial force of distinctive thermotropic liquid crystal materials (5CB, 8CB, and 12CB). Stable phase interfaces are created by controlling the temperature distribution of the liquid crystal material and microscale particles were tracked by an image analysis software. By utilizing the phase interfacial force of a 12CB liquid crystal, we have demonstrated that particles with density 15 times more than the liquid crystal itself can be captured by the phase interface. Therefore, the smectic liquid crystal material (12CB) reveals a stronger interfacial force compared to the nematic liquid crystal materials. It is possible to develop a micromanipulator with a significant driving force that can drag heavier microscale objects utilizing the 12CB liquid crystal. It has been experimentally and theoretically demonstrated that the normal stress acting on the particle is suitable regardless of shape and size of the particle. In addition, the capturing of spherical particles utilizing another four distinctive thermotropic liquid crystal materials (6CB, 7CB, 9CB, and 12CB) is attempted, respectively.

4. Fundamental study on the development of a mechanical device by utilizing the elasticity of the molecular orientation field of nematic liquid crystals

In this section, a 4-cyano-4'-pentylbiphenyl nematic liquid crystal (5CB) is filled between two circular glass plates that are subjected to a rubbing treatment. Then, by making the rubbing directions of the upper and lower glass plates orthogonal to each other, the twist distortion occurs in the director field of the nematic liquid crystal. Consequently, the upper glass plate needs to rotate to eliminate the twist distortion occurred in the director field in the nematic liquid crystal, as shown in Figure 4.1. We observe the motion of the upper glass plate after being released on the nematic liquid crystal and examine how the distortion energy of the director field is then converted into kinetic energy. Finally, we compared our experimental results with a postulated theoretical model based on the director profile between the two glass plates to quantify the rotational angle of an upper glass plate in our experiments. Additionally, we consider the possibility of new mechanical elements using this principle of utilizing the elasticity of the molecular orientation field of nematic liquid crystals.

4.1 Experimental methods

Figure 4.2 demonstrates an outline of the experimental setup used for this study. Experiments were performed at room temperature (21 - 22 °C) on top of an optical table to prevent unnecessary noise coming to the system. Glass plates of several diameter sizes (manufactured by Toshinriko, Co., Ltd), detailly explained in Table 4.1, are subjected to a planar alignment treatment (AL3046, manufactured by JSR Corporation and γ-Butyrolactone, Wako Pure Chemical Industries, Ltd.) and baked for approximately 20min. Each glass plates are marked with an arrow to show the rubbing direction on the surface of the glass plate. The principle role of the alignment layer on the surface of each cell is to manipulate the direction of the director profile of the liquid crystal molecules so that the molecules in the orientational field are parallel to the rubbing direction with a small pre-tilt angle, as shown in Figure 4.3. The open system cell is performed between a polarizer and analyzer
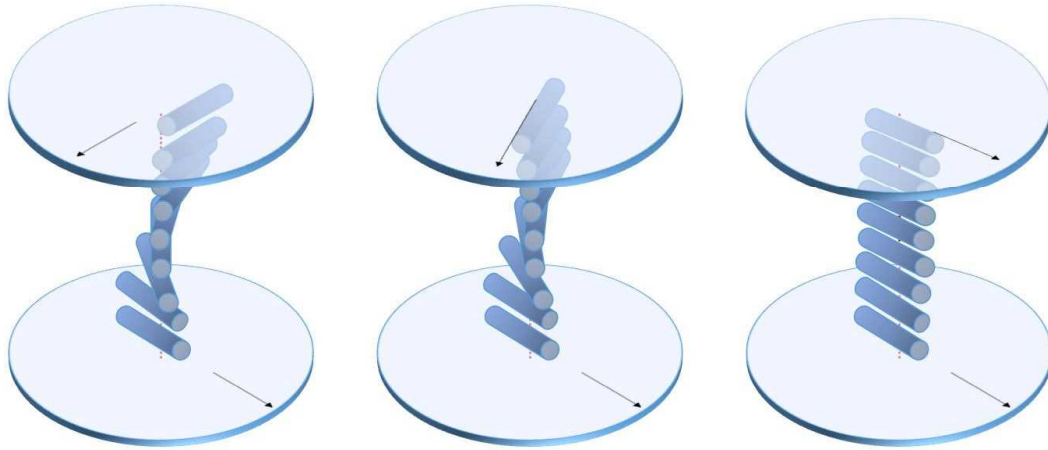
Figure 4.1: Schematic diagram of a twisted nematic orientation molecular field. The rod-like cylinders represent the direction of the director alignment through anchoring in the cell.

Table 4.1: Summary of the circular glass plates.

diameter size (mm)	mass (mg)	thickness (mm)	inertia (mg· mm^2)
5.0	8.99	0.16~0.19	28.09
5.5	9.60	0.16~0.19	36.30
6.0	11.45	0.16~0.19	51.53

(Edmund Industrial Optics) and the cell is optical recorded with Full HD 1080P video camera.

The experimental procedure follows by placing a droplet of 5CB on the rubbing treated lower glass plate. The liquid crystal is heated to a temperature of more than 35.2 °C to reach to isotropic phase change transition state and then kept at room temperature to minimize the defects in the liquid crystal material. The upper plate is stacked so that the rubbing direction of the upper glass plate is orthogonal to the rubbing direction of the lower glass plate. The difference between the anchoring directions at the lower and upper glass plates is defined as the rotational angle Θ of the upper plate, as shown in Figure 4.4.
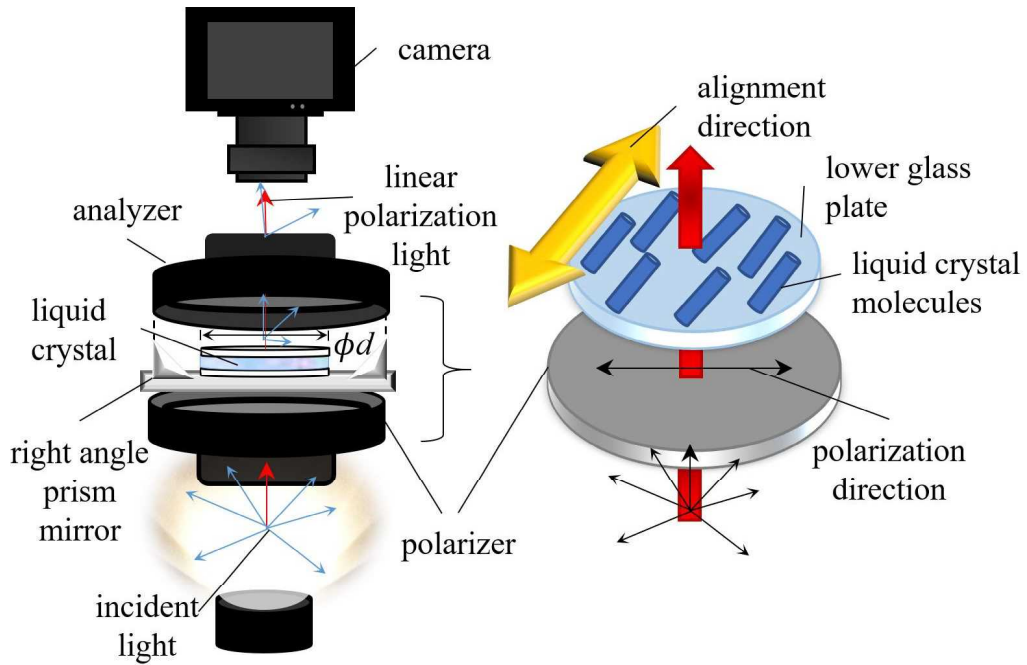
Figure 4.2: Schematic of the experimental setup and alignment of the liquid crystal molecules.
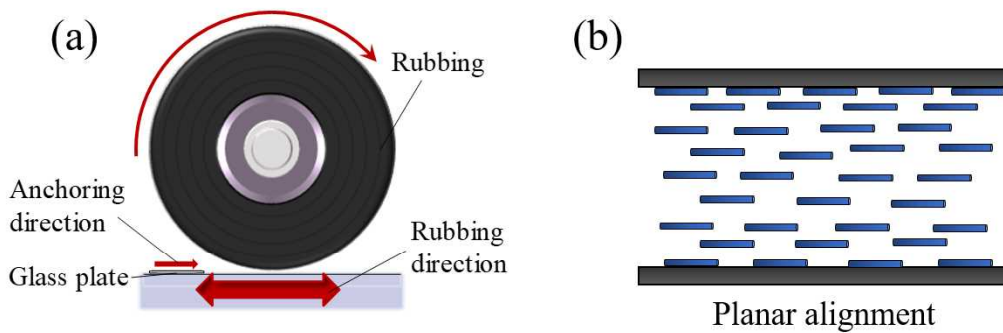
Figure 4.3: (a) Schematic of the rubbing technique to align the molecules from the molecular orientation field at the rubbing direction. (b) Planar alignment anchoring condition.
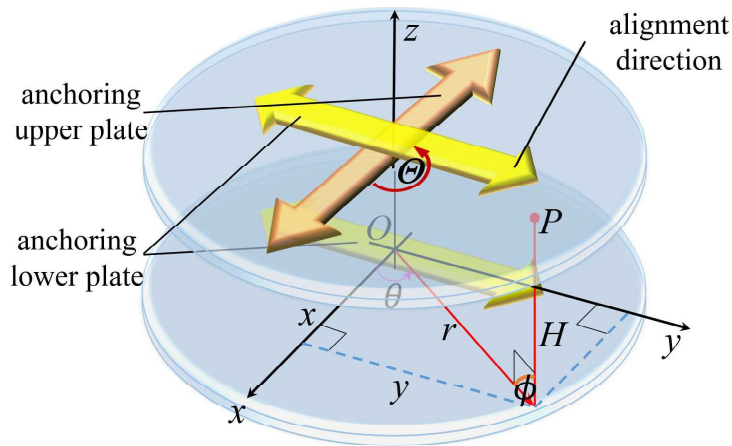
Figure 4.4: Schematic that represents the alignment direction in the liquid crystal cell.

4.2 Experimental Results

Figure 4.5 shows a sequential images of a rotating upper glass plate of diameter 5.0mm under a polarized light optical video camera. The arrow marked on the glass plate represents the anchoring direction, and the anchoring direction of the lower glass plate is fixed in the vertical direction. A 12μl 5CB liquid crystal droplet is placed on top of the bottom glass plate, and the gap between the lower and upper glass plate is approximately 0.61mm. In the image (a), the rubbing direction of the upper glass plate is placed roughly orthogonal to the lower glass plate at $t = 0$s. As time t elapses, as shown in image (b), the arrow indicating the rubbing direction of the upper glass plate rotates counterclockwise. In image (c), the upper glass plate come to rest at which the rubbing direction of the upper and lower glass plate coincides at $t = 21$s. When the molecules in the nematic molecular orientation field become parallel to each other, the twist distortion energy is eliminated when the upper glass plate comes to rest. Figure 4.6 demonstrates the time variation of the rotational angle Θ (black line) and the angular velocity ω (red line) of the rotating upper glass plate. As we observe from the polarized light optical image analysis, the Θ smoothly decreases from approximately 81° and reaches a constant value of 0°. The angular velocity of the upper glass plate increases more rapidly immediately after the release of the upper glass plate and continues to decrease to 0 rad/s after reaching a peak value of 0.12 rad/s at $t = 11.5$s.

66

(a) $t = 0$ s   (b) $t = 11.5$ s   (c) $t = 21$ s

Figure 4.5: A sequence of images of the upper plate rotating to the direction of the bottom plate with time t. The diameter of the glass plates is 5.0mm with a 12μl 5CB liquid crystal droplet.

Figure 4.6: Rotational angle Θ and angular velocity ω with time t of 5.0mm diameter glass plates with 12μl liquid crystal droplet.

Figure 4.7 shows the sequential optical images of the rotating upper plate (diameter 5.5mm) under a polarizing light video camera. As previously described, the arrow marked on the glass plate represents the anchoring direction, the direction where the rubbing treatment is performed, and the anchoring direction of the lower glass plate is fixed in the vertical direction. Since the diameter of the glass plates is increased to 5.5mm, higher volume of liquid crystal material is required to keep the same gap conditions for the rotational upper glass plate experiments. A 15μl 5CB liquid crystal droplet is placed on top of the lower glass plate and the gap between the upper and lower glass plate is approximately 0.63mm. In image (a), the rubbing direction of the upper and lower glass plates are orthogonal to each other. As time t elapses, as shown in image (b), the upper glass plate rotates towards the rubbing direction of the lower glass plate. In image (c), the upper glass plate come to rest at $t = 26$s where the rubbing anchoring direction of both the upper and lower glass plates coincides to each other. It is observed that there is no light transmitted through the liquid crystal cell since the molecules in the molecular orientation field are aligned to the rubbing direction. Figure 4.8 shows the time variation of the rotational angle and angular velocity of the rotating 5.5mm upper glass plate. As shown in the figure, the upper glass plates rapidly rotates from $\Theta = 90°$ until reaching an angular velocity peak value of 0.13 rad/s at $t = 13.9$s, then the upper glass plate starts to decelerate from $t > 13.9$s until coming to rest.

(a) $t = 0$ s   (b) $t = 12.5$ s   (c) $t = 26$ s

Figure 4.7: A sequence of images of the upper plate rotating to the direction of the bottom plate with time t. The diameter of the glass plates is 5.5mm with a 15μl 5CB liquid crystal droplet.
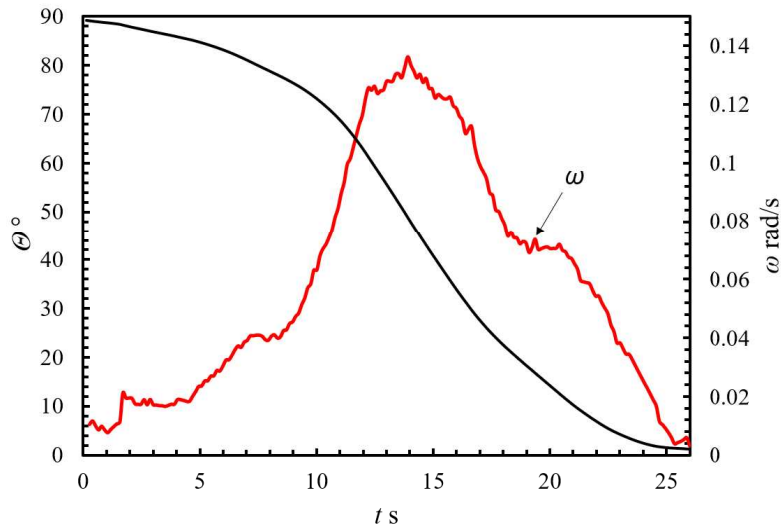
Figure 4.8: Rotational angle Θ and angular velocity ω with time t of 5.5mm diameter glass plates with 15μl liquid crystal droplet.

Figure 4.9 shows the sequential optical images of a 6.0mm rotating glass plate under a polarized light video camera. An 18μl liquid crystal droplet is placed on top of the lower glass plate, and the gap between the upper and lower glass plates is approximately 0.64mm. In image (a), the upper glass plate is placed orthogonally to the lower glass plate (positioned vertically). As t elapses, the upper glass plate starts to slowly rotate counterclockwise, as shown in image (b). The upper glass plate come to rest and positioned parallel to the lower glass plate at $t = 56$s. It is confirmed that the glass plates with higher diameter rotate much lower than the smaller glass plates. Figure 4.10 shows the time variation of the rotational angle and angular velocity of the rotating 6.0mm upper glass plate. It is observed that the upper glass plate rotates rapidly until reaching an angular velocity peak value of 0.06 rad/s at $t = 15.7$s, and the upper glass plate starts to decelerate until it comes to rest.

With increasing the diameter of the glass plates, the weight of the glass plates also increases, in which reduces the angular velocity. In Figure 4.11, while keeping the gap constant for different glass plates size, the highest angular velocity decreases as the gap between the upper and lower glass plates increases. However, while increasing the gap of the experiments from 0.61mm to

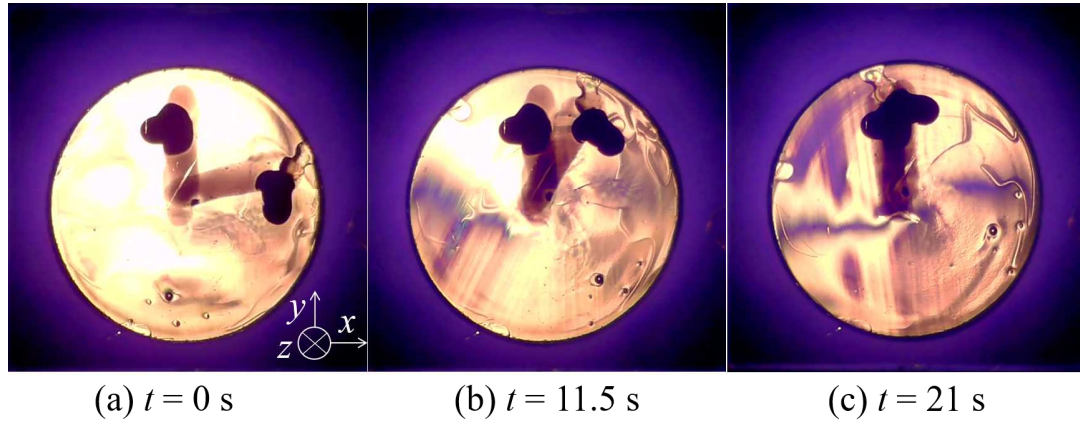(a) $t = 0$ s   (b) $t = 15.7$ s   (c) $t = 56$ s
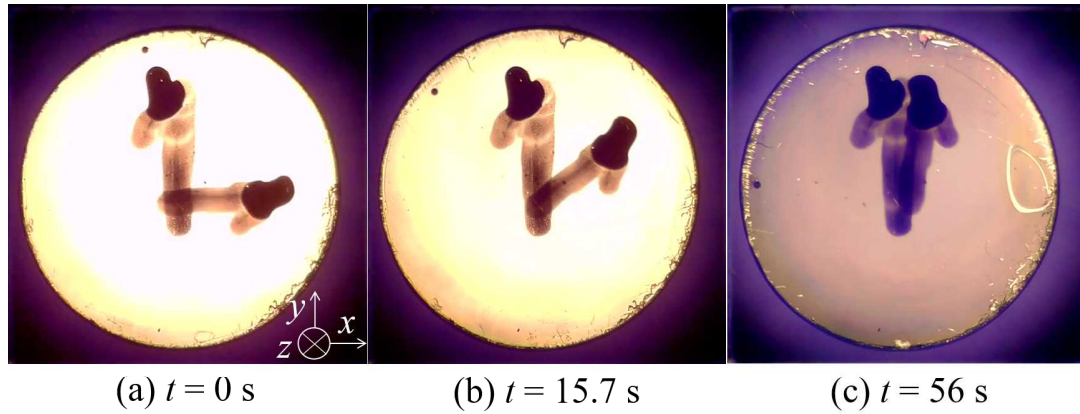
Figure 4.9: A sequence of images of the upper plate rotating to the direction of the bottom plate with time t. The diameter of the glass plates is 6.0mm with a 18μl 5CB liquid crystal droplet.
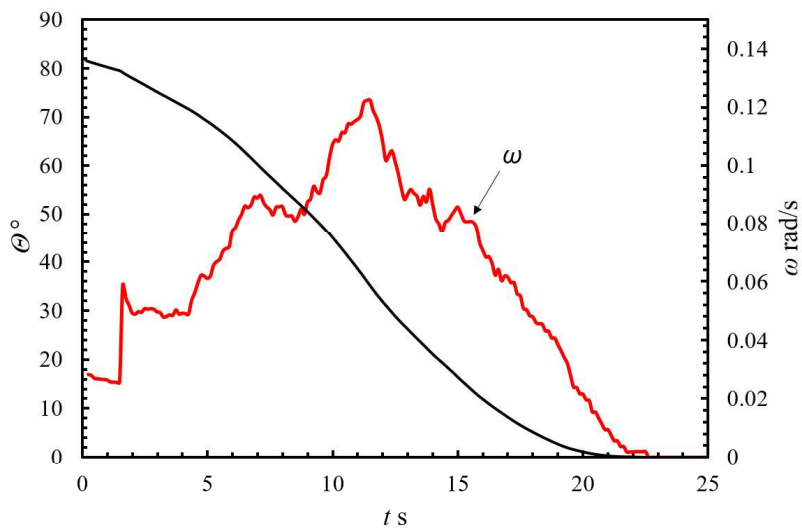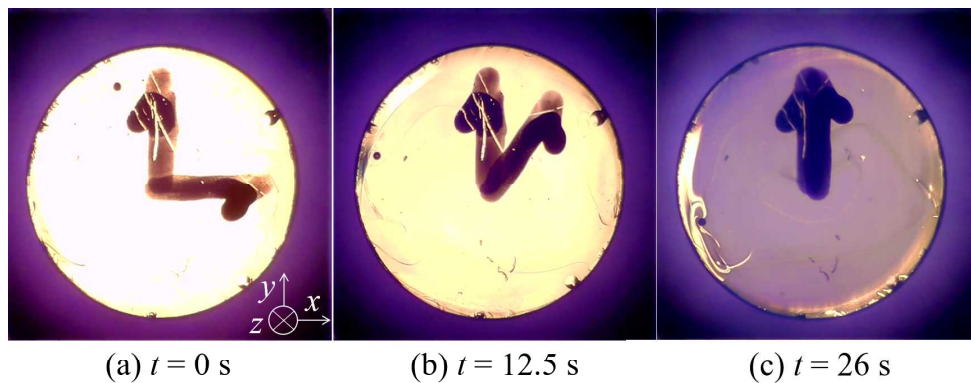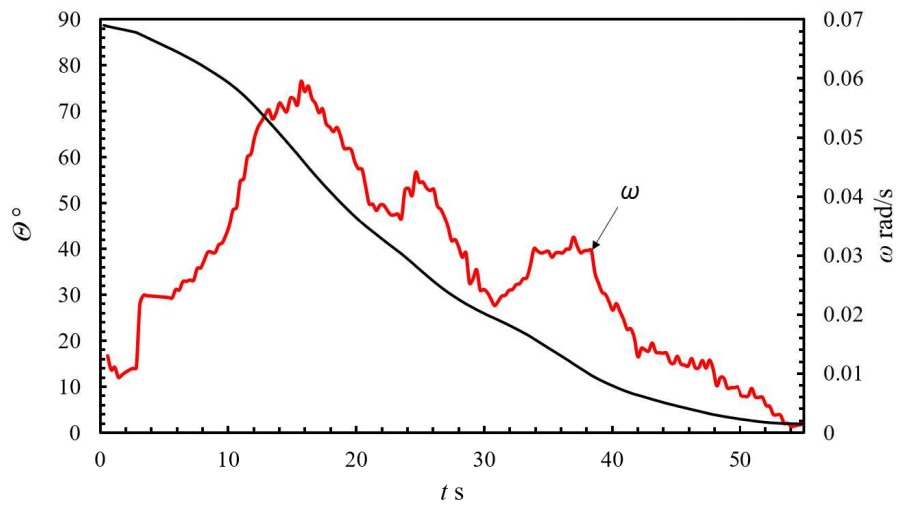

Figure 4.10: Rotational angle Θ and angular velocity ω with time t of 6.0mm diameter glass plates with 18μl liquid crystal droplet.
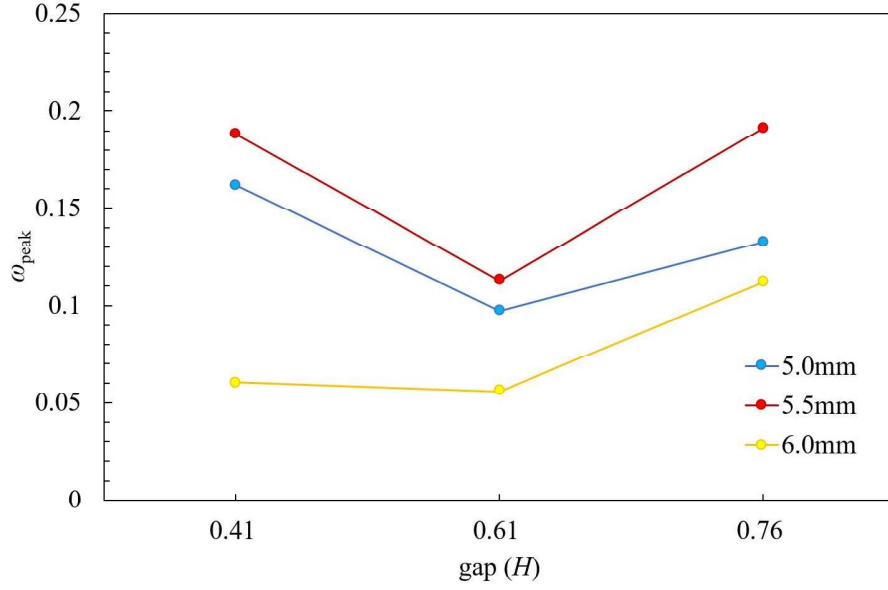
Figure 4.11: Experimental results of the gap (H) and the highest angular velocity ω_{peak}.

0.76mm, the highest angular velocity increases as well. In addition to that, the effect of inertia on the rotational motion of the upper glass plate shows lower angular velocity when R increases. The data in-details of comparison for the rotational angles utilizing the nematic liquid crystal with different gaps and glass plate sizes are given in Table 4.2.

Assuming that the distortion energy of the director field is the driving source of the upper glass plate, the maximum driving torque is generated at $t = 0$s, where the difference in the anchoring direction between the upper and lower glass plates is the greatest. While the angular velocity of the upper glass plate is increasing, the resistance due to the viscosity of the liquid crystal also increases. However, while the upper glass plate rotates, the driving torque decreases as the difference in the anchoring direction decreases. Furthermore, when the effect of the viscous drag becomes dominant, the angular velocity of the upper glass plate tends to decline, and the upper glass plate comes to rest. Due to the increase of the mass of the glass plate, it can be observed that the inertia momentum of the glass plate declines. The behavior of this phenomena is explored to understand the effects of elasticity of the molecular orientation field in the nematic liquid crystal (5CB).

71

Table 4.2: Summary of the rotational angles utilizing the nematic liquid crystal (5CB).

size [mm]	gap [mm]	$\Theta_{initial}$ [°]	Θ_{final} [°]	t_{final} [s]	$\omega_{average}$ [1/s]
5.0	0.41	86.4($\pm$3.2)	15.6($\pm$2.3)	15.4($\pm$1.9)	0.098($\pm$0.012)
5.0	0.61	82.9($\pm$1.6)	0.54($\pm$1.2)	24.7($\pm$2.7)	0.059($\pm$0.006)
5.0	0.76	88.1($\pm$0.8)	2.89($\pm$2.4)	19.3($\pm$1.1)	0.080($\pm$0.047)
5.5	0.42	88.5($\pm$0.3)	4.11($\pm$1.6)	19.3($\pm$1.2)	0.080($\pm$0.010)
5.5	0.63	85.4($\pm$3.8)	2.27($\pm$2.0)	24.8($\pm$4.1)	0.061($\pm$0.008)
5.5	0.76	86.4($\pm$2.9)	4.34($\pm$1.2)	14.3($\pm$1.4)	0.106($\pm$0.008)
6.0	0.42	83.1($\pm$1.0)	1.09($\pm$1.3)	34.7($\pm$3.8)	0.042($\pm$0.004)
6.0	0.64	87.5($\pm$2.2)	3.59($\pm$2.9)	45.3($\pm$8.8)	0.034($\pm$0.006)
6.0	0.78	79.6($\pm$9.9)	12.8($\pm$3.7)	19.8($\pm$1.7)	0.066($\pm$0.013)

4.3 Theoretical derivation of the elasticity of the molecular orientation field in nematic liquid crystals

To understand the dynamics which confirms the rotation of an upper glass plate with the relaxation of the distortion energy, a theoretical model is developed to quantify the twist distortion energy. We consider a nematic liquid crystal placed between two circular glass plates whose radius and gap are R and H. The theoretical model is performed by utilizing Frank's elasticity energy, and Leslie-Ericksen theory[10]. For $R \gg H$, the director profile between the plates is assumed as

$$\mathbf{n} = (n_r, n_\theta, n_z) \tag{4.1}$$

$$\mathbf{n}(r, \theta, 0) = (\cos\theta\cos\phi, -\sin\theta\cos\phi, \sin\phi) \tag{4.2}$$

$$\mathbf{n}(r, \theta, H) = (\cos(\Theta - \theta)\cos\phi, \sin(\Theta - \theta)\cos\phi, \sin\phi) \tag{4.3}$$

Then, the director profile of the liquid crystal molecules in the encapsulated cell can be described as

$$\mathbf{n}(r, \theta, z) = \left(\cos\left(\frac{\Theta z}{H} - \theta\right)\cos\phi, \sin\left(\frac{\Theta z}{H} - \theta\right)\cos\phi, \sin\phi \right). \tag{4.4}$$

By applying the director profile conditions, the Frank energy F is derived as

$$F = \frac{\Theta^2 \cos^2\phi((K_2 - K_3)\cos 2\phi + K_2 + K_3)}{4H^2}. \tag{4.5}$$

72

The total energy in the cylindrical liquid cell is

$$F_{\text{total}} = \int_0^{2\pi} \int_0^R \int_0^H F(r,\theta,z) dz r dr d\theta = \frac{\pi \Theta^2 R^2 \cos^2 \phi ((K_2 - K_3) \cos 2\phi + K_2 + K_3)}{4H}, \quad (4.6)$$

where F is the local energy density, K_2 and K_3 are the curvature elastic constants. The elastic torque on the upper glass plate due to the inhomogeneity in the molecular orientation field is

$$\Gamma^e = -\frac{\partial F_{\text{total}}}{\partial \Theta} \approx -\frac{\pi \Theta R^2 \cos^2 \phi ((K_2 - K_3) \cos 2\phi + K_2 + K_3)}{2H}. \quad (4.7)$$

The viscous torque on the upper plate due to the shearing of the liquid crystal material (at $\mathbf{v} = (0, v_\theta(z), 0)$ in the gap direction is written as

$$\Gamma^v = -\frac{R^4 \omega \pi (4\eta_1 - 2\sin^2 \phi (\alpha_2 - \alpha_5))}{8H} - \frac{R^4 \omega \pi (\cos^2 \phi (\alpha_1 - 2\eta_1 + 2\eta_3 - \alpha_1 \cos 2\phi))}{8H}. \quad (4.8)$$

Here, ω is the angular velocity of the plate. The Miesowicz coefficients are defined as

$$\eta_1 = \frac{1}{2}(\alpha_4 + \alpha_5 - \alpha_2), \quad (4.9)$$

$$\eta_2 = \frac{1}{2}(\alpha_3 + \alpha_4 + \alpha_6), \quad (4.10)$$

$$\eta_3 = \frac{1}{2}\alpha_4. \quad (4.11)$$

Finally, the angular momentum equation for the plate is

$$I\frac{\partial \omega}{\partial t} = \Gamma^e + \Gamma^v = -\frac{\pi \Theta R^2 \cos^2 \phi ((K_2 - K_3) \cos 2\phi + K_2 + K_3)}{2H}$$
$$-\frac{R^4 \omega \pi (4\eta_1 - 2\sin^2 \phi (\alpha_2 - \alpha_5)) + R^4 \omega \pi (\cos^2 \phi (\alpha_1 - 2\eta_1 + 2\eta_3 - \alpha_1 \cos 2\phi))}{8H}. \quad (4.12)$$

As a result, the angular momentum equation for the upper glass plate, for the case that there is no tilt angle (i.e., $\phi = 0$), reduces to

$$I\frac{\partial \omega}{\partial t} = \Gamma^e + \Gamma^v = -\frac{\pi R^2}{H}\left(\Theta K_2 + \frac{R^2 \omega}{4}(\eta_1 + \eta_3)\right), \quad (4.13)$$

where I is the inertia of the upper plate. Thus, the general solution for this equation is

$$\Theta(t) = \frac{1}{2}\Theta_0 \left(\frac{\sqrt{\pi}R^2\eta}{\sqrt{\pi R^4\eta^2 - 16HK_2m}} + 1 \right) \exp\frac{-\eta\pi R^2 + \sqrt{\eta^2\pi^2R^4 - 16\pi mHK_2}}{4mH}t$$

$$+\frac{1}{2}\Theta_0 \left(1 - \frac{\sqrt{\pi}R^2\eta}{\sqrt{\pi R^4\eta^2 - 16HK_2m}} \right) \exp\frac{-\eta\pi R^2 - \sqrt{\eta^2\pi^2R^4 - 16\pi mHK_2}}{4mH}t, \qquad (4.14)$$

where m is the mass of the glass plate, $\eta = (\eta_1 + \eta_3)$ and given for the conditions $\Theta(0) = \Theta_0$ and $\omega(0) = 0$.

For equation 4.14, we use the available values of 5CB [50]: $K_2 = 3.81 \times 10^{-12}$ Pa·s, $\eta_1 = 2.04 \times 10^{-2}$ Pa·s, $\eta_3 = 3.26 \times 10^{-2}$ Pa·s. According to the theoretical results (as shown in Figure 4.12), Θ comes to rest at $\approx 100,000$s, in which does not satisfy to our experimental results. Therefore, the rotation of the upper glass plate is much faster than expected from the developed theory. The upper glass plate tries to minimize the distortion energy when released to become parallel to the lower glass plate. However, the theoretical model shows that the driving source of the upper glass plate is much lower compared with experimental results.
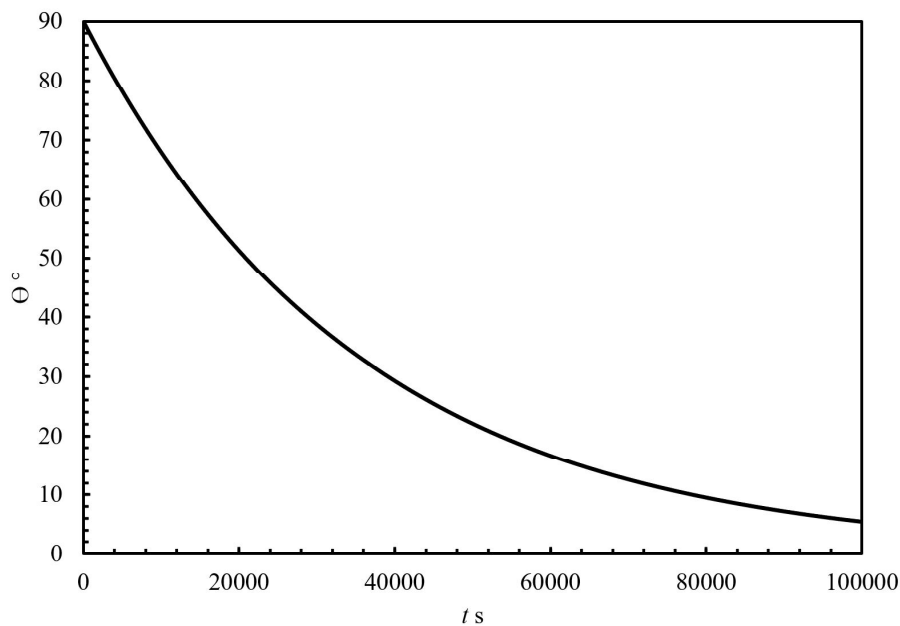
Figure 4.12: Theoretical results of the rotational upper glass plate Θ with respect to time. The theoretical results disagree with experimental results; thus, an additional energy besides the Frank's elasticity energy is expected and should be explored.

4.4 Conclusion

To summarize this section, we try to develop future liquid crystal micro-manipulator systems by utilizing the elasticity of the molecular orientation field in nematic liquid crystal materials. By distorting the molecular orientation field through anchoring, the rotation of an upper glass plate is confirmed at a rapid speed with different glass plate sizes and gap. We proposed a theoretical model to explore more the phenomena that causes the rotational of the upper glass plate, in which the relaxation of the director field must determine the rotation of the upper glass plate. Although the theoretical model predicts that the time elapse for the upper glass plate to come to rest is much longer compared to the experimental results, it has been discovered that additional energy besides the free distortion energy density is expected and should be explored.

75

5. SUMMARY AND CONCLUSIONS

We aim to develop the soft microactuator device that allows the capturing and manipulation of microscale objects by the interfacial force between the liquid crystal and isotropic phases. In previous work, the interfacial force between the nematic and isotropic phases is 1.4nN. To extend the application of the device, we focus on the interfacial force between the smectic and isotropic phases. From the experiments, the smectic-isotropic interfacial force is found to be more than 13 times stronger than the nematic-isotropic interfacial forces of 5CB and 8CB. The results show that potential usage of this microactuator device that enables the manipulation of biological cells without damage. To summarize:

1. We introduced a micromanipulator system capable of capturing heavy objects by the smectic-isotropic phase interface.

2. The smectic liquid crystal material reveals a stronger interfacial force compared to the nematic liquid crystal material while using a tungsten carbide particle.

3. Thus, the smectic-isotropic phase interfacial force is much stronger than the nematic-isotropic phase interfacial forces of the 8CB and 5CB.

4. The normal stresses acting on the surface of the particle is demonstrated to be $P_S(12CB) \gg P_S(8CB) > P_N(8CB) > P_N(5CB)$.

5. The interfacial forces and stresses depend on the material and the liquid crystalline material.

6. By utilizing the phase interface of the smectic liquid crystal, it is possible to develop a micromanipulator with a significant driving force that can drag microscale objects, not limited to only biological cells, but for transport of heavier particles.

7. The capturing of spherical particles utilizing another four distinctive thermotropic liquid crystal materials (6CB, 7CB, 9CB, and 12CB) is attempted.

Secondly, we aimed to develop a mechanical device by utilizing the elasticity of the molecular orientation field of nematic liquid crystals. To summarize the second section:

1. We developed mechanical elements by utilizing the elasticity of the molecular field of the nematic liquid crystals.

2. By utilizing the energy when the molecular orientation field of the liquid crystal filled between two circular glass plates is distorted through anchoring, the rotation of the object is attempted.

3. Our experiment results confirm that the object rotates with the relaxation of not only the distortion energy but with another internal energy.

4. However, the postulated theoretical model does not satisfy our experimental results, and we assume another internal energy besides the free energy density should be expected and explored.

6. Future Work

The dissertation focuses on evaluating the phase interfacial forces of various thermotropic liquid crystalline materials and evaluating the normal stresses from the maximum phase interfacial force of the thermotropic liquid crystals. The 5CB, 8CB, and 12CB liquid crystals were chosen for the systematic investigation for their phase interfacial forces since these liquid crystal materials provide phases of nematic, smectic, and isotropic. However, there are several inquiries required to enhance the phase interfacial force research work.

In this dissertation, we only focused on the phase interfacial force of the 5CB, 8CB and 12CB liquid crystal through the use of different spherical particles with different densities. It is suggested that the phase interfacial forces for the 4-cyano-4-hexylbiphenyl (6CB), 4-cyano-4-heptylbiphenyl (7CB), 4-cyano-4-nonylbiphenyl (9CB), and 4-cyano-4-undecylbiphenyl (11CB) should be evaluated to expand the applications of liquid crystals. Thus, it will be helpful in the future to know the phase interfacial forces of these thermotropic liquid crystal materials. Knowing the maximum interfacial forces from the listed liquid crystal materials, the normal stresses can also be evaluated.

Since the indium tin oxide (ITO) shows high conductivity properties, good adherence on the glass, and easy to be etched, the ITO layer should be implemented to glass plates for the purpose of miniaturization. Figure 6.1 shows an example of the microactuator system utilizing the ITO layer as an electrode material to supply electrodes to the glass plate to create a thermal source. A more precise photolithography technique should be considered for a more stable phase interface of the liquid crystal materials. In addition, the microfabrication pattern on the bulk of the substrate should be considered in order to create a moving phase interface for the purpose of dragging microscale particles. Therefore, by miniaturizing the manipulator, it is highly possible to transfer or transport biological cells freely applicable such as in pathological examinations without damaging the cells. Since the phase interface in nematic liquid crystals can be moved by μm/s through a temperature source, it is expected to lead to more accurate diagnosis in the biomedical applications.

DSC experiments to determine the enthalpies of the liquid crystal materials during phase tran-
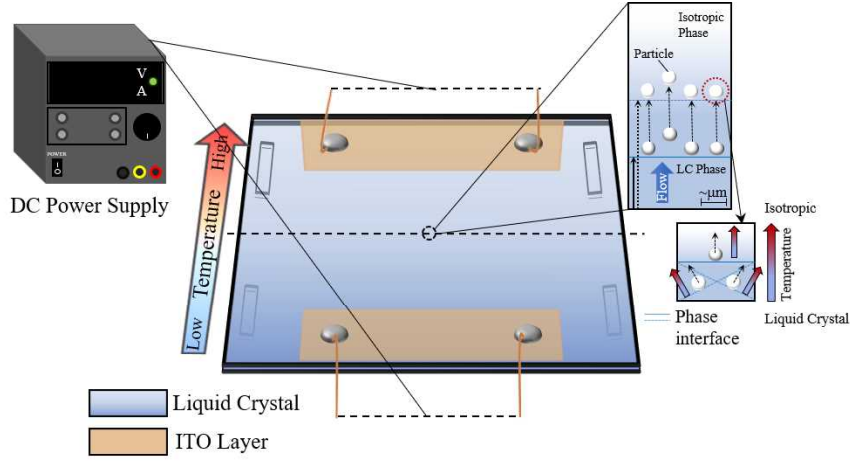
Figure 6.1: Future micromanipulator system

sition forces should be correlated with the maximum phase interfacial forces. The heat flow of the liquid crystal materials should be explored and theoretical explanations should be developed corresponding to the measured DSC data. The relationship between the DSC data of the liquid crystals and the curvature energy of the molecular orientation field should be explored.

In chapter 4, the theoretical results do not satisfy with experimental results. The additional energy besides the Frank's energy should be explored and considered. A possibility should be focused on the total energy in the cylindrical liquid crystal cell such that an additional force is experienced during the rotation of the upper glass plate. Therefore, the total energy and the additional energy is considered as follows,

$$\Gamma^e = -\frac{\partial F_{\text{total}}}{\partial \Theta} = -\frac{\pi \Theta R^2 \cos^2 \phi \left((K_2 - K_3) \cos 2\phi + K_2 + K_3 \right)}{2H} + F_d, \qquad (6.1)$$

where F_d is the additional energy besides the Frank's free energy density.

Also, it is observed from the experimental results that the defects are continuously connected between the upper and lower plates forming line-defects, and the length of the line-defects increases as Θ increases. To take the energy of the line-defects into account for the energy of the system, we should assume that the defects positions at the upper and lower plates are $(R - \delta, \Theta \pm \pi/2, H)$ and $(R - \delta, \Theta \pm \pi/2, 0)$, where δ is the distance between the plate edge and the defect

79

core, and the total length of two line-defects, where a line-defect is straight line connecting the upper and lower plates, and the other line-defect is curved along the cylindrical surface of the liquid crystal cell.

7. Publication List

7.1 Journals

1. J.E. Mejia, T. Tsuji, S. Chono, "Capture of microscale objects utilizing the smectic-isotropic phase interfacial force for the development of soft-manipulation devices", submitted to the Journal of Sensors and Actuators A: Physical - ELSEVIER (Q1)

2. J.E. Mejia, T. Tsuji, S. Chono, "Manipulation of microscale objects utilizing the smectic-isotropic phase interface force by a liquid crystalline microactuator device", Micro Electro Mechanical Systems, IEEE Proceeding paper, 2020. (Published)

7.2 Conferences

1. J.E. Mejia, J. Takasawa, T. Tsuji, S. Chono, "Trap of microparticles utilizing the interfacial force between the smectic-isotropic phases", Proceedings of the 2019 Multiphase Flow Symposium of the Japan Multiphase Flow Society, Fukuoka, August 2019. Received Best Presentation Award.

2. J.E. Mejia, T. Tsuji, S. Chono, "Development of a mechanical device utilizing the elasticity of molecular orientation field of nematic liquid crystals", Liquid Crystal Society of Japan Conference, Tsukuba, Ibaraki, September 2019.

3. J.E. Mejia, T. Tsuji, S. Chono, "Manipulation of microscale objects utilizing the smectic-isotropic phase interface force by a liquid crystalline microactuator device", MEMS, Vancouver, Canada, January 2020.

REFERENCES

[1] J. Thiem, ed., *Transition Temperatures and Related Properties of One-Ring Systems and Two-Ring Systems without Bridging Groups*. Springer-Verlag, 1992.

[2] M. Ozkan, M. Wang, C. Ozkan, R. Flynn, and S. Esener *Biomedical Microdevices*, vol. 5, no. 1, pp. 61–67, 2003.

[3] C. Yi, C.-W. Li, S. Ji, and M. Yang, "Microfluidics technology for manipulation and analysis of biological cells," *Analytica Chimica Acta*, vol. 560, pp. 1–23, feb 2006.

[4] K. Dholakia and T. Čižmár, "Shaping the future of manipulation," *Nature Photonics*, vol. 5, pp. 335–342, may 2011.

[5] T. Deng, G. M. Whitesides, M. Radhakrishnan, G. Zabow, and M. Prentiss, "Manipulation of magnetic microbeads in suspension using micromagnetic systems fabricated with soft lithography," *Applied Physics Letters*, vol. 78, pp. 1775–1777, mar 2001.

[6] S. Martel, C. C. Tremblay, S. Ngakeng, and G. Langlois, "Controlled manipulation and actuation of micro-objects with magnetotactic bacteria," *Applied Physics Letters*, vol. 89, p. 233904, dec 2006.

[7] J. Fröhlich, "New techniques for isolation of single prokaryotic cells," *FEMS Microbiology Reviews*, vol. 24, pp. 567–572, dec 2000.

[8] J. L. West, A. Glushchenko, G. Liao, Y. Reznikov, D. Andrienko, and M. P. Allen, "Drag on particles in a nematic suspension by a moving nematic-isotropic interface," *Physical Review E*, vol. 66, no. 1, p. 012702, 2002.

[9] J. L. West, K. Zhang, A. Glushchenko, D. Andrienko, M. Tasinkevych, and Y. Reznikov, "Colloidal particles at a nematic-isotropic interface: Effects of confinement," *The European Physical Journal E*, vol. 20, pp. 237–242, jun 2006.

[10] S. Chandrasekhar, *Liquid Crystals*. Cambridge University Press, 2 ed., 1992.

[11] I. W. Stewart, *The Static and Dynamic Continuum Theory of Liquid Crystals*. CRC Press, jan 2019.

[12] K. KAMEI, T. TSUJI, and S. CHONO, "Development of micromanipulators utilizing a phase interface between nematic and isotropic phases in liquid crystals," *Transactions of the JSME (in Japanese)*, vol. 81, no. 823, pp. 14–00628–14–00628, 2015.

[13] F. Beyeler, A. Neild, S. Oberti, D. J. Bell, Y. Sun, J. Dual, and B. J. Nelson, "Monolithically fabricated microgripper with integrated force sensor for manipulating microobjects and biological cells aligned in an ultrasonic field," *Journal of Microelectromechanical Systems*, vol. 16, pp. 7–15, feb 2007.

[14] J. Arlt, V. Garces-Chavez, W. Sibbett, and K. Dholakia, "Optical micromanipulation using a bessel light beam," *Optics Communications*, vol. 197, pp. 239–245, oct 2001.

[15] Y. Harada, D. Koyama, M. Fukui, A. Emoto, K. Nakamura, and M. Matsukawa, "Molecular orientation in a variable-focus liquid crystal lens induced by ultrasound vibration," *Scientific Reports*, vol. 10, apr 2020.

[16] P. A. Penz and G. W. Ford, "Electromagnetic hydrodynamics of liquid crystals," *Physical Review A*, vol. 6, pp. 414–425, jul 1972.

[17] M. V. Gorkunov, F. Giesselmann, J. P. F. Lagerwall, T. J. Sluckin, and M. A. Osipov, "Molecular model for de vries type smectic-a–smectic-cphase transition in liquid crystals," *Physical Review E*, vol. 75, jun 2007.

[18] M. Sadati, H. Ramezani-Dakhel, W. Bu, E. Sevgen, Z. Liang, C. Erol, M. Rahimi, N. T. Qazvini, B. Lin, N. L. Abbott, B. Roux, M. L. Schlossman, and J. J. de Pablo, "Molecular structure of canonical liquid crystal interfaces," *Journal of the American Chemical Society*, vol. 139, pp. 3841–3850, mar 2017.

[19] G. A. Oweimreen, "On the nature of the smectic a-to-nematic phase transition of 8cb," *The Journal of Physical Chemistry B*, vol. 105, pp. 8417–8419, sep 2001.

[20] D. Sharma, J. C. MacDonald, and G. S. Iannacchione, "Thermodynamics of activated phase transitions of 8cb: DSC and MC calorimetry," *The Journal of Physical Chemistry B*, vol. 110, pp. 16679–16684, aug 2006.

[21] E. Weinan, "Nonlinear continuum theory of smectic-a liquid crystals," *Archive for Rational Mechanics and Analysis*, vol. 137, pp. 159–175, jun 1997.

[22] H. Stark, "Director field configurations around a spherical particle in a nematic liquid crystal," *The European Physical Journal B*, vol. 10, pp. 311–321, aug 1999.

[23] D. Andrienko, M. Tasinkevych, P. Patrício, and M. M. T. da Gama, "Interaction of colloids with a nematic-isotropic interface," *Physical Review E*, vol. 69, feb 2004.

[24] O. D. Lavrentovich, "Transport of particles in liquid crystals," *Soft Matter*, vol. 10, no. 9, pp. 1264–1283, 2014.

[25] E. M. Terentjev, "Disclination loops, standing alone and around solid particles, in nematic liquid crystals," *Physical Review E*, vol. 51, pp. 1330–1337, feb 1995.

[26] M. Škarabot, M. Ravnik, S. Žumer, U. Tkalec, I. Poberaj, D. Babič, N. Osterman, and I. Muševič, "Interactions of quadrupolar nematic colloids," *Physical Review E*, vol. 77, mar 2008.

[27] O. V. Kuksenok, R. W. Ruhwandl, S. V. Shiyanovskii, and E. M. Terentjev, "Director structure around a colloid particle suspended in a nematic liquid crystal," *Physical Review E*, vol. 54, pp. 5198–5203, nov 1996.

[28] M. Vilfan and M. Čopič, "Azimuthal and zenithal anchoring of nematic liquid crystals," *Physical Review E*, vol. 68, no. 3, p. 031704, 2003.

[29] T. Tsuji, S. Chono, and T. Matsumi, "Velocity profiles of electric-field-induced backflows in liquid crystals confined between parallel plates," *Journal of Applied Physics*, vol. 117, no. 5, p. 054501, 2015.

[30] A. Sunarso, T. Tsuji, and S. Chono, "Three-dimensional molecular dynamics simulations of reorientation process and backflow generation in nematic liquid crystals under application of electric fields," *Journal of Applied Physics*, vol. 110, no. 4, p. 044911, 2011.

[31] B. Jerome, "Surface effects and anchoring in liquid crystals," *Reports on Progress in Physics*, vol. 54, pp. 391–451, mar 1991.

[32] M. Inoue, K. Yoshino, H. Moritake, and K. Toda, "Evaluation of nematic liquid-crystal director-orientation using shear horizontal wave propagation," *Journal of applied physics*, vol. 91, no. 5, pp. 2798–2802, 2002.

[33] A. Pizzirusso, R. Berardi, L. Muccioli, M. Ricci, and C. Zannoni, "Predicting surface anchoring: molecular organization across a thin film of 5cb liquid crystal on silicon," *Chemical Science*, vol. 3, no. 2, pp. 573–579, 2012.

[34] P. J. Rodrigo, R. L. Eriksen, V. R. Daria, and J. Glückstad, "Interactive light-driven and parallel manipulation of inhomogeneous particles," *Optics Express*, vol. 10, p. 1550, dec 2002.

[35] K. Sasaki, M. Koshioka, H. Misawa, N. Kitamura, and H. Masuhara, "Pattern formation and flow control of fine particles by laser-scanning micromanipulation," *Optics Letters*, vol. 16, p. 1463, oct 1991.

[36] A. Haake and J. Dual, "Contactless micromanipulation of small particles by an ultrasound field excited by a vibrating body," *The Journal of the Acoustical Society of America*, vol. 117, pp. 2752–2760, may 2005.

[37] T. Kozuka, K. Yasui, S. ichi Hatanaka, K. Eguchi, and K. Kamijo, "Control of a particle flow in a microchannel using ultrasound," in *2012 International Symposium on Micro-NanoMechatronics and Human Science (MHS)*, IEEE, apr 2012.

[38] G. R. Goddard, G. Kaduchak, J. H. Jett, and S. W. Graves, "Method for non-contact particle manipulation and control of particle spacing along an axis," 1 2015.

[39] J. E. Mejia, T. Tsuji, and S. Chono, "Manipulation of microscale objects utilizing the smectic-isotropic phase interface force by a liquid crystalline microactuator device," in *2020 IEEE 33rd International Conference on Micro Electro Mechanical Systems (MEMS)*, IEEE, jan 2020.

[40] R. G. Larson, *The structure and rheology of complex fluids*, vol. 150. Oxford university press New York, 1999.

[41] D. Tuckerman and R. Pease, "High-performance heat sinking for VLSI," *IEEE Electron Device Letters*, vol. 2, pp. 126–129, may 1981.

[42] A. Chan and J. Wei, "Study on alternative cooling methods beyond next generation micropro-cessors," in *2003 International Electronic Packaging Technical Conference and Exhibition, Volume 2*, ASMEDC, jan 2003.

[43] J. Schindelin, I. Arganda-Carreras, E. Frise, V. Kaynig, M. Longair, T. Pietzsch, S. Preibisch, C. Rueden, S. Saalfeld, B. Schmid, J.-Y. Tinevez, D. J. White, V. Hartenstein, K. Eliceiri, P. Tomancak, and A. Cardona, "Fiji: an open-source platform for biological-image analysis," *Nature Methods*, vol. 9, pp. 676–682, jun 2012.

[44] A. Savitzky and M. J. E. Golay, "Smoothing and differentiation of data by simplified least squares procedures.," *Analytical Chemistry*, vol. 36, pp. 1627–1639, jul 1964.

[45] M. J. Stephen and J. P. Straley, "Physics of liquid crystals," *Reviews of Modern Physics*, vol. 46, no. 4, p. 617, 1974.

[46] H. Kneppe, F. Schneider, and N. K. Sharma, "Rotational viscosity γ1of nematic liquid crys-tals," *The Journal of Chemical Physics*, vol. 77, pp. 3203–3208, sep 1982.

[47] A. J. Leadbetter, J. L. A. Durrant, and M. Rugman, "The density of 4 n-octyl-4-cyano-biphenyl (8cb)," *Molecular Crystals and Liquid Crystals*, vol. 34, pp. 231–235, oct 1976.

[48] K. MUKAI, F. KISHI, and T. AMARI, "Slit flow of liquid crystals," *Nihon Reoroji Gakkaishi(Journal of the Society of Rheology, Japan)*, vol. 25, no. 3, pp. 155–160, 1997.

[49] J. Jadzyn, R. Dabrowski, T. Lech, and G. Czechowski, "Viscosity of the homologous series of n-alkylcyanobiphenyls," *Journal of Chemical and Engineering Data - J CHEM ENG DATA*, vol. 46, 12 2000.

[50] P. Karat and N. Madhusudana, "Elastic and optical properties of some 4'-n-alkyl-4-cyanobiphenyls," *Molecular Crystals and Liquid Crystals*, vol. 36, no. 1-2, pp. 51–64, 1976.

DEDICATION

I would like to sincerely thank my supervisor, Dr. Tomohiro Tsuji, for his guidance and support throughout the course of this research.

Thanks also go to my friends and colleagues and the department faculty and staff for making my time at Kochi University of Technology a great experience.

I sincerely thankful for the encouragement of my family of pursuing my doctoral degree, Miriam Mejia, and Jose Refugio Mejia, for their support and love.